Sustainable
Energy & Fuels
Interdisciplinary research for the development of sustainable energy technologies

This article can be cited before page numbers have been issued, to do this please use: S. K. Yadav, V. P. Jha, D. P. Pabba and A. Thirumurugan, *Sustainable Energy Fuels*, 2026, DOI: 10.1039/D5SE01377A.

ROYAL SOCIETY
OF CHEMISTRY

rsc.li/sustainable-energy

View Article Online
DOI: 10.1039/D5SE01377A

Development of Core-Shell Nanofibers in Magnetoelectric Sensors, Fuel Cells, and Drug-Delivery Applications: A Review

Sandeep Kumar Yadav[a]*, Vishwa Prakash Jha[b], Durga Prasad Pabba[c], Arun Thirumurugan[d]

[a*]Department of Physics and Electronics, Christ (Deemed to be University), Bangalore, 560029, Karnataka, India.
[b]School of Computer Science and Engineering, IILM University, Gurugram, 122011, Haryana, India.
[c]Departamento de Electricidad, Facultad de Ingenieria, Universidad Tecnologica Metropolitana, Santiago, Chile.
[d]Sede Vallenar, Universidad de Atacama, Costanera #105, 1612178, Vallenar, Chile

*Corresponding author- sandeeplumar.yadav@christuniversity.in

Abstract

Core–shell nanofibers have emerged as a versatile class of nanostructured materials due to their unique ability to integrate multiple functionalities within a single architecture. Their coaxial geometry, which combines core and shell domains, allows for precise control over composition, interfacial interactions, and surface characteristics, making them highly attractive for advanced electronic and biomedical applications. This review highlights recent advancements in the design, synthesis, and application of core–shell nanofibers, with a focus on their roles in magnetoelectric devices and drug delivery systems. For magnetoelectric devices, core–shell nanofibers provide efficient coupling between magnetic and electric order parameters, enabling the development of miniaturized, flexible, high-sensitivity sensors, energy harvesters, and transducers. Their high aspect ratio, tunable interfacial stress transfer, and enhanced magnetoelectric coupling open new opportunities for next-generation spintronic and wearable technologies. In parallel, the unique core–shell morphology offers distinct advantages in drug delivery, such as high loading efficiency, sequential or sustained release, and protection of bioactive agents, which are crucial for wound healing, tissue engineering, and targeted therapies. Also, this review highlights recent progress in core–shell nanofiber-based electrodes for HT-PEMFCs, DEFCs, and IT-SOFCs, emphasizing their role in enhancing catalytic activity, stability, and ionic conductivity. These advancements pave the way for high-efficiency and durable fuel cell technologies for next-generation, efficient, and sustainable fuel cell systems. We further summarize the progress in electrospinning and other fabrication techniques that enable scalable production of uniform core–shell nanofibers, along with critical insights into structure–property relationships, challenges, and future perspectives. This review highlights the multifunctional potential of core–shell nanofibers as a transformative platform for next-generation devices and healthcare solutions, bridging developments in the electronic and biomedical domains.

Keywords: Core–shell nanofibers; Electrospinning; Magnetoelectric; Fuel Cells, Drug-delivery.

Abbreviation:

ME, Magnetoelectric; 1D, One-dimensional; CNTs, Carbon Nanotubes; nT, Nano-Tesla; PZT, $PbZr_{0.52}Ti_{0.48}O_3$; PMN–PT, $(1–x)Pb(Mg_{1/3}Nb_{2/3})O_3$-$xPbTiO_3$; AIN, Aluminum nitride, Terfenol-D, $TbxDy_{1-x}Fe_2$; PCL, Polycaprolactone; PVA, Polyvinyl Alcohol; PCL, Polycaprolactone; Col, Collagen; PVDF, Polyvinylidene fluoride; DOX, Doxorubicin; N-CMCS, N-carboxymethyl chitosan; SF, Silk fibroin; cP, Centipoise; CNCs, Cellulose nanocrystals, PMMA, poly(methyl methacrylate); PAN, Polyacrylonitrile; PLA, Poly(lactic acid), PLGA, Poly(lactic-co-glycolic acid), PEG, Polyethylene glycol, PEO, polyethylene oxide; nm, Nanometer; μm, Micrometer; FITC, Fluorescein Isothiocyanate; PGS, Poly(glycerol sebacate); GelMA, Gelatin methacryloyl; PDLLA, Poly (d, l-lactic acid); CTG, Centella total glucoside; CIP, Ciprofloxacin; PIO-Nes, Pioglitazone Nanoemulsions; GEM, Gemcitabine; PQT-12, Poly(3,3‴-didodecyl quarter thiophene);. NSMM, Near field scanning microwave microscope, MFM, Magnetic force microscope.

View Article Online
DOI: 10.1039/D5SE01377A

1. Introduction

1. 1 Nanotechnology and Nanofibers

The fundamental principle of nanotechnology is reducing the size of materials to nanometer dimensions, which alters their physicochemical properties due to quantum confinement, increased surface-to-volume ratios, and modified electronic and interfacial behaviors. In semiconductors, size confinement can induce quantum effects that significantly change their optoelectronic characteristics, while magnetic materials transition to superparamagnetic behavior below a critical size. In catalytic metal nanoparticles, decreasing the particle diameter to a few nanometers can alter the crystal structure, surface topology, and electronic properties, including shifts in the Fermi level and reduction, which can potentially influence adsorption behavior and catalytic activity [1-4]. These nanoscale phenomena underpin the broad utility of nanostructured systems in various applications, including nanoelectromechanical systems (NEMS) sensors, targeted drug delivery, tissue engineering, implant surface modification, and wound healing [5-8]. One-dimensional (1D) nanofibers are fiber structures characterized by diameters in the nanometer range. Recent advancements have broadened the definition of nanofibers; according to Horne et al. [9], fibers with diameters ranging from 0 to 500 nm are nanofibers. Prabu et al. [10] extended this definition, reporting that fibers with diameters between 50 and 1000 nm are also categorized as nanofibers, while their lengths can extend to several centimeters. The 1D nanofibers exhibit a high surface area-to-volume ratio, tunable surface functionalities, and enhanced mechanical properties as the polymer fiber diameter decreases to submicron or nanometer scales. For instance, a nanofiber is 2 cm long and 400 nm in diameter, corresponding to an aspect ratio of approximately 5,000, which significantly increases the available surface area for interactions while maintaining a low total volume [11,12].

View Article Online
DOI: 10.1039/D5SE01377A

The nanoscale holds particular significance for biological systems, as the characteristic dimensions of viruses, bacteria, biomolecules, carbon nanotubes (CNTs), and other nanostructures fall within this range. A comparison with these objects reveals that electrospun fibers can exhibit diameters across a relatively broad spectrum, as shown in **Figure 1(a).** The principal motivation for utilizing nanofiber-based systems is that materials at the micro- and nano-scale exhibit unique physical and chemical properties not observed in their bulk forms. Likewise, tailoring materials at the nanoscale can drastically alter thermal transport, for example, reducing lattice thermal conductivity in nanostructured thermoelectrics, thereby improving their energy conversion efficiency. Electrospinning is a versatile technique for fabricating continuous nanofibers by applying a high-voltage electric field to a polymer solution, inducing jet formation. In a standard laboratory electrospinning setup, a polymer solution or melt is fed through a spinneret nozzle with an inner diameter of approximately 10-100 µm (**Figure 1(b)**). This nozzle also acts as an electrode, across which a high electric field of 50–500 kV/m is applied, while the counter electrode is positioned 10–25 cm away. The fibers are usually collected on a substrate connected to the counter electrode. Electrospun fibers exhibit superior porosity, surface area, and application versatility, rendering them highly suitable for biomedical and filtration applications. CNTs excel in strength, and hair has the largest diameter, but limited surface functionality, as illustrated in **Figure 1(c)**. Electrospun fibers provide a balanced combination of biocompatibility, porosity, and practical applicability. Nanofibers, in particular, can achieve pronounced ME coupling by eliminating substrate clamping effects commonly encountered in thin film bilayers or nanopillars deposited on substrates [13-15]. Furthermore, the application of nanofibers in the medical and aerospace industries has been broadened. For example, nanofibers are being explored in the medical sector for their utility in tissue engineering scaffolds, wound dressing materials, drug delivery systems, and biosensors due to their high surface area and tunable physicochemical properties

[16, 17]. In the aerospace and space industries, nanofiber composites contribute to the development of lightweight, high-strength structural components and radiation shielding, thereby further enhancing the performance and safety of spacecraft [18,19]. The food industry benefits from utilizing nanofibers in areas such as active packaging and filtration, as well as for the controlled release of nutraceuticals and preservatives [20-22]. Overall, the multifunctional nature of nanofiber-based materials continues to expand their application landscape across various domains, including medical, space, food, environmental, and other advanced technological fields.

1.2 Core-Shell Nanofibers

Core–shell nanofibers are one-dimensional nanostructures characterized by an inner core material enveloped by an outer shell, typically fabricated through coaxial electrospinning or emulsion methods. This architecture enables the independent tuning of core and shell compositions, allowing for multifunctional properties and precise control over released profiles or surface functionalities. Core–shell nanofibers are widely recognized for their enhanced stability, tunable mechanical and electrical properties, and efficacy in drug delivery, catalysis, and sensor applications. Their structure offers protective encapsulation for sensitive molecules while maintaining nanofiber flexibility and high surface area [23]. Furthermore, with the progression of nanofiber technology, core–shell nanofibers have emerged as an advanced architecture in which a core material is encapsulated within a surrounding shell, enabling tunable physicochemical properties and multifunctionality. This configuration simplifies fabrication compared to more complex nanofiber assemblies while offering superior performance in targeted applications. In drug delivery, core–shell nanofibers facilitate controlled release kinetics and site-specific transport of therapeutics. As catalytic supports, their high surface-to-volume ratio and dual-compartment design enhance reaction efficiency and stability. The distinct core–shell interface improves coupling efficiency and sensitivity in

View Article Online
DOI: 10.1039/D5SE01377A

ME sensing. Additionally, they have been employed in the food industry for active preservation and innovative packaging, in tissue engineering as biocompatible scaffolds promoting cell adhesion and proliferation, and in water purification systems for efficient adsorption and removal of contaminants. A schematic illustrating the applications of core–shell nanofibers in drug delivery, catalysis, sensors, the food industry, tissue engineering, and water purification is presented in **Figure 2**.

1.3 Development in Core-Shell Nanofibers

Core-shell nanofibers offer distinct advantages over traditional and bulk composites due to their high surface-to-volume ratio, enabling enhanced functionality and efficiency. Their unique structure allows precise control over core and shell material properties, facilitating tailored applications such as ME coupling and drug delivery. Unlike bulk composites, they offer flexibility, a lightweight design, and enhanced interfacial interactions, which are crucial for advanced devices. Scalable fabrication methods, such as coaxial electrospinning, surpass traditional composites in producing uniform, multifunctional nanostructures. These features make core-shell nanofibers ideal for next-generation biomedical, energy, and environmental technologies. However, the roots of core-shell nanofibers lie in the development of electrospinning, a technique pioneered in the 1990s for producing micro- and nanofibers using electrostatic forces [24]. Early works by Reneker and Doshi (1995) laid the groundwork for electrospinning, demonstrating the ability to develop ultrafine fibers from polymer solutions [14]. Initial electrospinning focused on monolithic (single-component) nanofibers; however, researchers soon recognized the potential for more complex structures to enhance functionality. Core-shell nanofibers were introduced with the advent of coaxial electrospinning, which occurred around 2002–2003. Loscertales et al. (2002) and others demonstrated the use of a coaxial nozzle to simultaneously spin two different materials, forming a core-shell structure [25]. This allowed for the encapsulation of one material (the core) within another (the shell),

View Article Online
DOI: 10.1039/D5SE01377A

enabling the tailoring of properties [26-28]. Early studies, such as those by Zhang et al. (2004), investigated core-shell nanofibers composed of polymers like PCL and gelatin, highlighting their potential in biomedical applications [29]. By the late 2000s, coaxial electrospinning was refined to improve control over fiber morphology, diameter, and composition. Innovations included emulsion electrospinning and modified coaxial/triaxial electrospinning, which enabled the use of unspinnable core materials (e.g., drug solutions or lipids) by leveraging spinnable shell polymers. Alternative methods, such as self-assembly and phase-separation electrospinning, have emerged for producing core-shell-like structures without the need for coaxial setups [30]. For instance, Jiang et al. (2013) utilized vapor-induced phase separation to create core-shell nanofibers, thereby expanding the versatility of fabrication [31]. The period also saw the integration of non-polymeric materials, such as ceramics and metal oxides, into core-shell nanofibers, broadening their applications beyond biomedicine [32].

Since the 2010s, core-shell nanofibers have gained traction due to their improved scalability and functionalization capabilities. Techniques like coaxial centrifugal spinning address the limitations of coaxial electrospinning, such as low production rates and high energy consumption, thereby enabling commercialization potential. Recent advancements include multiaxial electrospinning for producing multi-layered fibers and needleless electrospinning for achieving higher yields, particularly for chitosan-based nanofibers [33-35]. Furthermore, coaxial electrospinning remains the cornerstone for fabricating ME core-shell nanofibers due to its ability to precisely control the composition of both the core and shell. By 2015-2025, researchers had optimized parameters such as solution viscosity, flow rates, and electric field strength to achieve uniform fiber diameters (50–500 nm) and enhance interfacial strain transfer, which is crucial for ME coupling. ME-based core-shell nanofibers have evolved from niche research to a versatile platform for advanced devices, driven by innovations in coaxial, multiaxial, and needleless electrospinning, as well as novel material combinations.

Although several reviews have discussed ME composites, electrospun nanofibers, or polymer–ceramic multifunctional systems, these works have primarily focused on bulk laminates, thin films, or general fiber fabrication techniques, without examining core–shell nanofibers as an integrated materials platform. Furthermore, recent advances from 2022 to 2025—including coaxial electrospinning optimization, self-assembled core–shell structures, and newly reported ME fiber systems such as $CoFe_2O_4$–$Ba_{0.95}Ca_{0.05}Ti_{0.89}Sn_{0.11}O_3$, $Ba_2Zn_2Fe_{12}O_{22}$–PZT, and $NdFeO_3$–PZT—have not been consolidated in any existing review. To the best of our knowledge, no comprehensive article has simultaneously examined (i) the structure–property relationships of core–shell nanofibers, (ii) their strain-mediated ME coupling mechanisms, and (iii) their emerging roles in fuel cells and drug-delivery technologies. This review uniquely integrates these interdisciplinary developments, highlighting material design principles, fabrication strategies, and application-specific performance metrics. Likewise, recent progress in core–shell nanofiber-based drug carriers—including dual-drug systems, stimuli-responsive release, and coaxial fibers for tissue regeneration—remains fragmented in the literature. In addition to their roles in magnetoelectric sensing and biomedical delivery systems, core–shell nanofibers have recently emerged as promising materials for fuel cell technologies due to their tunable nanoarchitecture, enhanced surface area, and ability to integrate multifunctional components within a single fiber. By synthesizing the most recent findings across these domains and identifying the critical knowledge gaps, this work provides a timely and distinctive perspective that complements and extends previously published reviews.

2. Materials and Application

2.1 Magnetoelectrics

In recent years, there has been increased scientific focus on multiferroic materials exhibiting magnetoelectric (ME) phenomena, which are characterized by the correlation between the applied magnetic field and the corresponding electric voltage [36-41]. The intrinsic coupling between electric and magnetic orders in ME materials enables wirelessly induced electric charge generation, facilitating the less-invasive incorporation of these materials into next-generation electronic devices. Recent literature [42-49] reports the notable progress in the fundamental understanding and development of advanced ME materials. These innovations have established ME materials as a promising candidate for applications in microelectronics and engineering, such as high-speed memory devices [50,51], advanced ME antennas [52-54], and ME sensors [55-57], among others. Additionally, ME materials enable the detection of low-intensity magnetic fields in MEMS sensor technologies for navigation and automotive applications, operating effectively at room temperature (RT). In contrast, highly complex SQUIDs need low-temperature environments [58-60]. Furthermore, ME materials enable the harvesting of energy from ambient magnetic fields for Internet of Things (IoT) applications, the realization of non-volatile ME random-access memory (ME-RAM) for data storage devices, and the development of highly compact, tunable antennas for radio-frequency communication in space, demonstrating enhanced efficiency relative to conventional materials [61-63].

In ME composites, coupling occurs through mechanical strain that is generated in the magnetostrictive (ferromagnetic phase), which is transferred to the piezoelectric (ferroelectric phase), resulting in an electrical response [64-66]. In the direct ME effect, an in-plane magnetic field (H) induces strain in the magnetic component through a phenomenon known as magnetostriction. This strain is mechanically transferred to the ferroelectric component, generating dielectric polarization via the piezoelectric effect, as illustrated in **Figure 3(a).** In contrast, the converse ME effect involves an out-of-plane electric field (E) that creates strain in the ferroelectric component through the inverse piezoelectric effect. This strain is

View Article Online
DOI: 10.1039/D5SE01377A

mechanically linked to the magnetic element, resulting in changes in magnetization (ΔM) or domain reorientation due to the piezomagnetic impact, as shown in **Figure 3(b).**

As a result, extensive research has focused on exploring the micro- and nanoscale structures of heterogeneous materials and their configurations, which include: (i) 0-3 type structures [67-69], where magnetostrictive nanoparticles are dispersed within a piezoelectric matrix as shown in **Figure 2(a)**; (ii) 2-2 type structures [70-74], characterized by alternating layers of magnetostrictive and piezoelectric phases as shown in **Figure 4(b)**; (iii) 1-3 type structures [75-78], consisting of piezoelectric fibers or rods embedded in a magnetostriction matrix or fiber network, as illustrated in **Figure 4(c).**

Efficient higher-order interfaces in composite heterostructures are critical for achieving strain transfer across phase boundaries. The maximizes ME coupling, which governs the interaction between magnetic and electric order parameters. Therefore, there is significant potential to enhance ME coupling by tailoring surface interactions in these heterostructures to optimize strain transfer, ultimately facilitating ME performance [79]. The phase architectures of 0-3 and 2-2 type structures exhibit irregular spatial distributions of ferroelectric/ferromagnetic phases, which impede efficient strain transfer and consequently result in relatively weak ME coupling. In particular, 2-2 type composites, characterized by alternating layered structures of magnetostrictive and piezoelectric phases, often suffer from limited interfacial contact area and possible mechanical mismatch between layers, thereby restricting effective mechanical coupling. These factors hinder robust interactions between magnetic and electric order parameters, limiting the overall ME response.

In contrast, the 1-3 type composite structure, nanofibers or core-shell nanofibers, particularly those incorporating nanofibers as the magnetostrictive phase embedded within a piezoelectric matrix, provides a more continuous and anisotropic pathway for strain-mediated coupling.

Furthermore, core–shell nanofibers are sometimes described as hybrid or variant 1–3 type structures, and both constituent phases are continuous along the length of the fiber. They are co-located within the same one-dimensional structure. This configuration facilitates higher mechanical strain transfer across the interfaces, significantly enhancing the ME coupling strength compared to other composite structures. Most importantly, the nanoscale dimensions and high aspect ratio of the fibers contribute to an increased interfacial area and improved load transfer efficiency, further enhancing the ME performance [80,81].

The first intrinsic ME effect was experimentally demonstrated in antiferromagnetic (Chromic Oxide) Cr_2O_3 single crystals in 1961 by Folen at RT [82]. Over the past century, considering both material composition and dimensionality, ME materials have progressed from single-phase to particulate, laminated, and, more recently, micro- and nano-scale nanofibers and thin films. To date, more than ten distinct families of single-phase compounds have been extensively investigated as ME materials, including $BiFeO_3$ [83-84], $RMnO_5$ (R= Eu, Gd, Er, Y) [85,86], $RMnO_3$ (R= Gd, Tb, Dy) [87,88]. Such studies have been driven by potential applications, including metallic memories [89], Universal Memory [90], Bennett clocking [91], and resistive switching [92]. However, achieving strong intrinsic ME coupling at or above RT remains challenging, as most single-phase multiferroics possess relatively low Curie temperatures [93,94]. In general, for multiferroic crystals, the polarization (P) and magnetization (M) are coupled to the electric (E) and magnetic (H) fields through the following relations [47]: Landau theory describes the ME effect in a single-phase material through the expansion of the free energy expression as

$$F(E,H) = F_0 - P_i^S E_i - M_i^S H_i - \frac{1}{2}\varepsilon_0 \varepsilon_{ij} E_i E_j - \frac{1}{2}\mu_0 \mu_{ij} H_i H_j - \alpha_{ij} E_i E_j + \frac{\beta_{ijk}}{2} E_i H_j H_k + \frac{\gamma_{ijk}}{2} H_i E_j E_k \ \ldots\ldots \qquad (1)$$

View Article Online
DOI: 10.1039/D5SE01377A

Here, ε_0 and μ_0 Denote the dielectric permittivity and magnetic permeability of the medium, respectively, while ε_{ij} and μ_{ij} Represent the relative dielectric permittivity and magnetic permeability of the material. The second and third terms in Eq. (1) correspond to the temperature-dependent spontaneous polarization (P_i^S) and spontaneous magnetization (M_i^S). The fourth and fifth terms describe the influence of electric and magnetic fields on the electrical and magnetic responses, respectively. The sixth term, containing α_{ij}, represents the linear ME coupling. The subsequent two terms, involving $\beta_{ijk}$and γ_{ijk}, are third-rank tensors that account for higher-order coupling effects.

Differentiation of Eq. (1) concerning electric and magnetic fields, respectively, leads to polarization and magnetization, which are as follows:

$$P_i = -\frac{\partial F(E,H)}{\partial E_i} = P_i^S + \varepsilon_0\varepsilon_{ij}E_j + \alpha_{ij}H_j + \frac{1}{2}\beta_{ijk}H_jH_k + \gamma_{ijk}H_jE_k \text{..........} \ (2)$$

$$M_i = -\frac{\partial F(E,H)}{\partial H_i} = M_i^S + \mu_0\mu_{ij}H_j + \alpha_{ij}E_j + \frac{1}{2}\beta_{ijk}E_jE_k + \gamma_{ijk}E_jH_k \text{..........}(3)$$

In practice, to eliminate the influence of material electrical conductivity, ME effects are investigated dynamically by applying an alternating magnetic or electric field to the samples. The magnitude of dynamic effects is characterized by using ME coefficients:

$\alpha_E = \frac{\delta E}{\delta H}$ (V/Oe.cm) for the direct ME effect, $\alpha_B = \frac{\delta B}{\delta H}$ (Oe.cm/V) for converse ME effect

Where δE and δB are the amplitudes of the ac electric field and magnetic induction in the substance, caused by a change in the magnetic δH and electric δE fields, respectively. However, in ME crystals, the effects are small in magnitude α_E ~ 1–20 mV/(Oe.cm) and are observed in single phase materials such as $BiFeO_3$, $Y_3Fe_5O_{12}$, $SrCo_2Ti_2Fe_8O_{19}$ at low temperatures (T ≈ 4–20 K) [95,96] or under high magnetic fields (H ≈ 10–50 kOe) in $BaFe_{12}O_{19}$, $Ba_2Co_2Fe_{12}O_{22}$ [97,98] which poses challenges for their practical applications.

In composite ME, the ME coupling is primarily strain-mediated, occurring at the interface between the magnetostrictive and piezoelectric phases. This coupling arises from the interaction between magnetic and electric fields via mechanical strain transfer across the interface. To quantitatively describe this phenomenon, a mathematical formulation based on continuum mechanics and electromagnetism, incorporating key physical quantities: strain (S), displacement (D), electric field (E), magnetic field (H), permittivity (ε), and permeability (μ). For general composites, tensor notation accounts for anisotropic material properties and complex microstructures [99-101]. For the magnetostrictive and piezoelectric phases, the constitutive relations can be expressed as:

$$S_i = s_{ij} T_J + d_{ki} E_k + q_{ki} H_k \text{ ...... (4)}$$

$$D_k = d_{ki} T_i + \varepsilon_{kn} E_n + \alpha_{kn} H_n \text{ ...... (5)}$$

$$B_k = q_{ki} T_i + \alpha_{kn} E_n + \mu_{kn} H_n \text{ ...... (6)}$$

where S_i and T_J, strain and stress tensor components, respectively; E_k, D_k, H_k, and B_k the components of the electric field, electric displacement, magnetic field, and magnetic induction, respectively; s_{ij}, d_{ki}, and q_{ki}, denote the effective elastic compliance, piezoelectric, and piezomagnetic constants, respectively, while ε_{kn}, μ_{kn}, and α_{kn} correspond to the effective permittivity, permeability, and linear ME coupling tensor [102-104]. The ME coefficient can be written as by solving equations (4), (5), and (6).

$$\alpha_{ME,\,ij} = \frac{\delta E_i}{\delta H_i} \approx s_{ij} \cdot d_{ki} \cdot q_{ki} \text{ .... (7)}$$

This formulation combines the sequential coupling pathway in which an applied magnetic field induces strain in the magnetostrictive phase (q_{ki}), the strain is elastically transferred across the interface (s_{ij}), and the piezoelectric phase converts the strain into an electric polarization (d_{ki}). Under the assumptions of linear constitutive behavior, ideal interfacial strain transfer, and negligible intrinsic ME effects, this product-property relationship quantitatively explains the enhanced ME coefficients observed in engineered composites relative to single-phase materials, particularly at RT.

From Eq. (7), it is evident that the characteristics of ME effects in composites can be tuned by H and E fields and by the interfacial interaction between constituent phases. Particularly attractive for practical applications are coaxial nanofiber architectures integrating ferromagnetic and ferroelectric phases, which can be fabricated relatively easily via electrospinning. Recent advances have yielded a range of composite materials exhibiting high ME conversion efficiency. Furthermore, as indicated by Eq. (3), enhancing the ME effect in composites requires the selection of ferromagnetic components with significant piezomagnetic coefficients; q_{ki} such as metals (Ni, Co), alloys such as FeCo [105-107], FeGa [108,109], Metglas [110-112], Terfenol-D ($TbxDy_{1-x}Fe_2$) [113-115], and ferrites ($NiFe_2O_4$ [116-118], $CoFe_2O_4$ [119-121]-combined with piezoelectric materials possessing high piezoelectric constants; d_{ki}. Examples include ceramics like $PbZr_{0.52}Ti_{0.48}O_3$ (PZT) [122-124], $(1-x)Pb(Mg_{1/3}Nb_{2/3})O_3$-$xPbTiO_3$ (PMN–PT) [125-127], $LaNiO_3$ [128-130], $BaTiO_3$ [131,132], aluminum nitride (AlN) crystals [133-135], and polymers such as polyvinylidene fluoride (PVDF) [136-138], which are highly promising for device applications. The α_E typically ranges from ~1–100 mV/(Oe·cm) for bulk composites, whereas for planar structures it is about 1–50 V/(Oe·cm), increasing up to 100 V/(Oe·cm) at acoustic resonance frequencies. The capability to interconvert magnetic and electric fields enables the application of the ME effect in multiferroic materials across diverse areas of science and technology. The direct ME effect serves as the foundation for devices such as sensors for detecting static and low-frequency alternating magnetic fields with sensitivities approaching $\sim 10^{-11}$ T at RT [139], solid-state inductors and transformers tunable via electric fields [131], and energy harvesters capable of converting alternating-current (AC) magnetic fields into direct-current (DC) voltage [140],

View Article Online
DOI: 10.1039/D5SE01377A

among others. The literature highlights several advanced ME composite sensors for detecting magnetic fields. Dong et al. [141] achieved the sensing of low-frequency (10^2 Hz) AC fields down to 10^{-12} T using a Terfenol-D/PMN–PT laminate. Zhai et al. [142] achieved pico-tesla-level (10-12 T) detection across a broad 10-2–10^3 Hz range using a Terfenol-D/PZT composite. Li et al. [143] demonstrated nanoelectromechanical ME sensing using FeGaB/AlN, achieving 800 pT DC detection at 3.19 MHz. Duc et al. [144] developed a $(Fe_{80}Co_{20})_{78}Si_{12}B_{10}$/PZT laminate sensitive to micro-tesla fields at 5 kHz, while Chu et al. [145] reported PMN-PT/FeBSi composites capable of detecting ultra-low AC fields of 10^{-13} T at 23.3 kHz. Together, these examples highlight the remarkable dynamic range of ME sensors—from femto-Tesla and pico-Tesla AC detection to nano-Tesla DC measurements. The converse ME effect finds applications in electrically tunable resonators, microwave filters, and electric field-controlled data storage devices [146-149]. Several significant demonstrations of converse ME composites have been reported. Yinan et al. [150] developed a dual-drive DC magnetic sensor utilizing a Metglas/PZT composite, achieving a remarkably low detection limit of 1 nT. Chen et al. [151] explored the converse ME effect in a Metglas/PMN-PT composite structure, while Jia et al. [152] investigated a PMN-PT/Terfenol-D composite, reporting a notable electric-field-induced magnetization coefficient (α_E) of 150 mG/V at RT.

2.2 Fuel cell and drug delivery

In fuel-cell architectures, core–shell nanofibers serve multiple roles simultaneously — as catalyst supports that improve catalyst dispersion and stability, as gas-diffusion or microporous layers that regulate water management and oxygen transport, and as reinforced membrane scaffolds that maintain proton conduction under low-humidity conditions. Several recent studies demonstrate the heterogeneous ways core–shell or closely related coaxial nanofiber designs improve electrochemical performance. For example, electrospun porous carbon nanofibers bearing TiO_2 hollow structures or TiO_2–derived cores coated with conductive

View Article Online
DOI: 10.1039/D5SE01377A

carbon shells provide a high-surface-area, corrosion-resilient support that enhances methanol oxidation and oxygen-reduction activity while resisting particle agglomeration. Tailoring the core composition (e.g., metal oxide or ceramic) and the conductivity/porosity of the carbon shell enables independent control of catalytic anchoring and mass-transport pathways, a design freedom that is difficult to achieve with particulate supports [153,154]. Similarly, nitrogen-doped carbon nanofiber composites with embedded TiO_2 or other metal-oxide cores have been shown to act as robust anode/cathode scaffolds with improved durability and enhanced ORR/oxidation kinetics, particularly when thermal treatment and heteroatom-doping are used to tailor electronic structure and surface chemistry. Taken together, these advances suggest that core–shell nanofiber designs offer a materials-by-architecture route to decouple catalytic, ionic, and mass-transport functions, a critical capability for next-generation, low-Pt or Pt-free electrodes [155,156]. For example, oxide–metal core–shell structures (such as CoO_x@Pt supported on carbon) promote strong metal–oxide interactions that suppress Pt dissolution, regulate the local electronic environment, and improve the durability of oxygen-reduction catalysts—all essential for high-performance and long-lived fuel-cell electrodes as shown in **Figure 5(a)**. Such engineered interfaces enable the decoupling of catalytic activity (dominated by the noble-metal shell) from structural stability (provided by the metal-oxide core), allowing for improved mass transport and enhanced long-term operational resilience.

In drug-delivery and wound-healing contexts, coaxial and core–shell electrospun fibers provide decisive advantages for controlled release, multi-drug dosing, and local bioactivity [157-159]. The enclosed core enables high loading of fragile payloads (proteins, growth factors, or hydrophobic anticancer drugs) with reduced burst release, while the shell can be engineered for stimuli-responsiveness (pH, temperature, enzymatic degradation) or surface bioactivity (adhesion, antimicrobial coatings). Recent comprehensive reviews and studies demonstrate progress in both the fundamentals and applications of core–shell fibers for therapeutics: from design rules for coaxial electrospinning and core–shell morphology control to application-specific demonstrations such as wound dressings with separate antimicrobial and healing-promoting compartments. Notably, hybrid fabrication strategies that combine self-emulsifying cores with coaxial spinning enhance the encapsulation of poorly soluble drugs (e.g., paclitaxel) and accelerate dissolution without compromising sustained release properties [160].

Beyond performance, recent work has also emphasized translational considerations. For fuel cells, research explores how electrospun networks can be integrated into electrode laminates and how process conditions (fiber diameter, shell porosity, and post-treatment) influence both short-term activity and long-term stability under realistic operating cycles. In drug delivery, the literature emphasizes the importance of standardized release testing, cytotoxicity, and biocompatibility assays for core–shell systems, as well as strategies for scale-up, such as needleless or multi-jet electrospinning, to enhance throughput without compromising core–shell morphology [161].

Core–shell designs also provide unique advantages in biomedical and therapeutic applications, where controlled release, protection of bioactive molecules, and spatially selective drug delivery are essential. Coaxial fibers or nanoparticles with drug-loaded cores and protective or stimuli-responsive shells can transport therapeutic agents through the bloodstream, shield them from premature degradation, and release them in a controlled manner at the target site, as shown in **Figure 5(b)**. By tuning shell composition, porosity, and degradation kinetics, these systems can achieve sustained or on-demand release profiles, improved drug localization, and reduced systemic toxicity. Such multifunctional platforms have been explored for anticancer therapies, antimicrobial delivery, wound healing, and regenerative medicine, demonstrating the broader utility of core–shell architectures beyond purely physical or electrochemical applications.

View Article Online
DOI: 10.1039/D5SE01377A

3. Core–Shell Nanofibers: Advantages for magnetoelectric, fuel-cell, and drug delivery

Core–shell nanofibers represent a cutting-edge class of 1D nanostructures with unique morphological and functional characteristics. The core–shell design can spatially separate different functional materials within a single fiber geometry, leading to tunable physicochemical properties and enhanced performance in various applications, including sensors, catalysis, drug delivery, energy harvesting, and wearable electronics. Core–shell nanofibers feature a core material completely encapsulated by a concentric shell, allowing for distinct functionalities in each layer. Fabricated primarily through coaxial electrospinning, this method utilizes dual nozzles to deliver core and shell solutions simultaneously, thereby enabling precise control over fiber morphology [162]. The core typically serves as the primary functional component, while the shell provides protection, biocompatibility, or controlled environmental interaction. Coaxial nanofibers are widely used in drug delivery, where a core containing a drug (polycaprolactone-clindamycin) is encapsulated by a biodegradable shell (Silk fibroin (SF)) for sustained release [163]**.** In catalysis, coaxial nanofibers with a catalytic core (e.g., metal nanoparticles) and a porous shell enhance reaction efficiency by improving the accessibility of active sites [164]. The active pharmaceutical ingredient is loaded in the core, while the shell controls the release kinetics in a drug delivery system. Coaxial fibers enable the precise spatial separation of functional domains, making them ideal for applications that require encapsulation, sustained release, or stimuli-responsive behaviour.

Moradipour et al. [165] fabricated core-shell nanofibers based on Polycaprolactone/Polyvinyl Alcohol (PCL/PVA) and PCL/Col) for Biomedical Applications such as drug delivery and wound healing. A notable application of coaxial nanofibers is in ME materials, where the core and shell are designed to couple magnetic and electric properties. ME core–shell nanofibers typically consist of a magnetic core, such as $CoFe_2O_4$, $Ba_2Zn_2Fe_{12}O_{22}$, and a piezoelectric or ferroelectric shell, such as PVDF, $BaTiO_3$. This configuration enables the nanofibers to

View Article Online
DOI: 10.1039/D5SE01377A

generate electric polarization under magnetic fields or vice versa, making them promise for applications in sensors, actuators, and energy harvesting devices. For example, coaxial nanofibers with a $BaTiO_3$ core and $Ba_2Zn_2Fe_{12}O_{22}$ shell have been shown to exhibit strong ME coupling, suitable for flexible electronics [166]. Fabricating ME nanofibers involves carefully optimizing electrospinning parameters to achieve uniform core-shell interfaces and ensure compatibility between the magnetic and electrical phases. For instance, coaxial nanofibers with a PLA-$CoFe_2O_4$ core and a PVDF-TrFE shell have demonstrated significant ME coupling, which can be utilized for energy harvesting. Therefore, continuous research and development of core–shell nanofibers are essential to fully utilize their multifunctional potential and tailor their structural and interfacial properties for advanced applications. Core–shell nanofibers are designed to optimize interfacial interactions and enable controlled transport of charge, ions, or energy across the core–shell interface [167-170]. They combine distinct core and shell materials to achieve multifunctionality, precise surface control, and superior performance unattainable in traditional nanofibers or bulk composites. This architecture enables efficient encapsulation and controlled release of sensitive agents, while also providing enhanced mechanical strength and structural versatility. Moreover, scalable fabrication methods, such as coaxial or emulsion electrospinning, ensure energy-efficient production for applications in drug delivery, fuel cells, energy harvesting, and environmental remediation [171-173].

4. Fabrication Methods for Core–Shell Nanofibers

Core–shell nanofibers are fabricated using various techniques that allow precise control over their morphology, composition, and functionality. These methods enable the creation of nanofibers with tailored core and shell materials, making them suitable for applications in biomedical engineering, energy storage, catalysis, and ME systems. The primary fabrication methods include coaxial electrospinning, emulsion electrospinning, and self-assembly or coating. Each method offers unique advantages and challenges, with the choice of technique depending on the desired fiber properties, material compatibility, and application requirements.

4.1 Coaxial Electrospinning

The coaxial electrospinning technique has emerged as a highly versatile and efficient method for fabricating core–shell nanofibers with tunable morphology and functionality. Unlike traditional single-fluid electrospinning, coaxial electrospinning employs a concentric spinneret (also known as a nozzle spinneret) composed of two coaxial needles that allow the simultaneous flow of two different polymer solutions: one designated as the core material and the other as the shell material. When subjected to a high electric field, the combined jet undergoes stretching (Taylor cone), elongation, and solidification, ultimately forming nanofibers with a distinct core–shell structure as shown in the schematic of **Figure 6 (a)** [174-176]. The successful preparation of core–shell nanofibers via coaxial electrospinning requires careful optimization of several process parameters, including the concentration and viscosity of the polymer solutions, the applied voltage, the distance between the spinneret and the collector, and the flow rates of both the core and shell solutions [177]. Each of these factors influences the morphology, diameter, and uniformity of the resulting nanofibers, as well as the stability of the Taylor cone during electrospinning [178]. The digital image of the Taylor cone during coaxial electrospinning and the SEM image of the PVDF-PC core-shell nanofiber are shown in **Figures 6(b)** and **6(c)** [162].

4.1.1 Concentration and Properties of Polymer Solution

The concentration and viscosity of the polymer solutions play a pivotal role in determining the spinnability and morphology of the coaxial fibers. For the shell solution, sufficient chain entanglement is necessary to provide mechanical stability to the jet and to prevent jet breakup during electrospinning [179]. A solution that is too dilute tends to form beads or droplets, while an excessively viscous solution may hinder the electrospinning process due to difficulties in pumping and jet elongation. Similarly, the core solution must be optimized depending on whether it is a solid polymer, a liquid, or an active agent dispersed in a carrier. For instance, the core fluid may be a bioactive compound dissolved in a biocompatible polymer, as seen in drug delivery applications. In contrast, the shell fluid provides structural support and controlled release properties. Proper miscibility between core and shell solutions is not essential; however, interfacial tension and flow stability must be managed to maintain a distinct core–shell configuration. Fiber formation requires a polymer concentration above a critical value to ensure sufficient chain entanglement [180]. Below this threshold, beads form due to Rayleigh instability; above it, viscosity rises sharply, enabling smooth jet formation [181]. For example, in SF–based core–shell fibers, SF concentrations below 6% led to bead-like fibers, whereas at 8%, the viscosity reached ~2308 cP. Similarly, increasing the PVA concentration from 3% to 9% raised the viscosity from ~92.7 cP to ~165.1 cP. Higher polymer concentrations generally enlarge fiber diameters. In SF/PVA systems, increasing the SF in the shell from 6% to 8% resulted in thicker core–shell fibers. Changing PVA in the core had a lesser effect; however, at high shell/core concentrations, the core concentration also influenced the diameter [182]. In PVDF fibers, raising the concentration from 25 wt% % (yielding ~473 nm) to 30 wt% % increased the average diameter to ~644 nm [183]. With PAN solutions, an increasing concentration also led to an increase in fiber diameter and electrical conductivity [184]. Higher solution conductivity enables more vigorous jet stretching, resulting in smaller fiber diameters. For instance, embedding cellulose nanocrystals (CNCs) into a PMMA shell significantly increased solution conductivity, yielding finer and more uniform PMMA-CNCs/PAN core–shell fibers [185].

DOI: 10.1039/D5SE01377A

4.1.2 Applied Voltage

The applied voltage is a critical parameter that governs the initiation of the Taylor cone, jet formation, and subsequent fiber elongation [186]. In coaxial electrospinning, the voltage must be sufficiently high to overcome the surface tension of both core and shell solutions simultaneously. Typically, the required voltage ranges from 5 to 50 kV, although the exact value depends on the conductivity and viscosity of the polymer solutions. A lower voltage may result in intermittent jet formation or bead-like structures, while excessively high voltage can cause whipping instabilities, irregular fiber diameter, or even fiber breakage. Moreover, the shell solution usually dominates the jet stability in the coaxial configuration. Therefore, the applied voltage should be tuned to balance the electrostatic force acting on the shell while ensuring the smooth encapsulation of the core fluid [187]. High voltage is necessary to overcome surface tension and form a stable Taylor cone. Fiber diameter typically decreases as voltage increases due to enhanced elongation, but jet instability may ensue above a critical voltage. Empirically, for PCL/PVA/Thyme core–shell fibers, raising voltage from 8 kV to 15 kV decreased average diameter from ~750 nm to ~201 nm and promoted stable compound Taylor cone formation [188]. However, excessive voltage disrupts the coaxial structure, causing separate jets and loss of core–shell morphology.

4.1.3 Distance Between Spinneret and Collector

The distance between the coaxial spinneret tip and the collector strongly affects the flight time and solidification of the jet. A typical range is 10–20 cm, though it varies with solution volatility, applied voltage, and ambient conditions. Fibers may not have sufficient time to solidify if the distance is too short, resulting in ribbon-like or fused structures on the collector. Conversely, excessively long distances may reduce the electric field strength, weakening the stretching force on the jet and resulting in thicker, less uniform fibers [189]. The optimal distance ensures that the solvent in both core and shell solutions evaporates adequately, maintaining distinct core–shell morphology without collapsing or mixing the two phases. Additionally, the type of collector (stationary plate, rotating drum, or patterned collector) also influences fiber alignment and surface morphology [190]. The distance between the coaxial spinneret tip and the collector, typically 10–20 cm, significantly influences jet flight time and solidification in coaxial electrospinning, with optimal distances (e.g., 15 cm for polycaprolactone in chloroform) ensuring complete solvent evaporation to form stable fibers, as noted by Dosunmu et al. [191] and Subbiah et al. [192]. This range varies with solution volatility, applied voltage (10–20 kV for polyethylene oxide), and ambient conditions, such as 50% humidity, as reported by Huang et al. [193]. Short distances (e.g., 5 cm) result in insufficient evaporation, leading to ribbon-like or fused structures (2–3 µm wide for PLA). In contrast, long distances (25 cm) reduce electric field strength (from 0.67 kV/cm to 0.4 kV/cm), resulting in thicker, less uniform fibers (400 nm for PVDF), as reported by Reneker and Yarin et al. [194] and Li and Xia et al. [195]. The optimal distance (12–15 cm for PCL/gelatin) ensures solvent evaporation from both core and shell, maintaining distinct core–shell morphology (100 nm core, 200 nm shell) without phase mixing [179]. Additionally, the collector type affects alignment; rotating drums at 1000 rpm produce highly aligned fibres (within 10° of the axis), whereas stationary plates yield random fibres, as shown by Teo et al. [196].

4.1.4 Flow Rates of Core and Shell Solutions

Flow rates are a critical parameter in coaxial electrospinning, significantly influencing jet stability and fiber morphology, requiring precise adjustment of core and shell flow rates to maintain a stable coaxial jet, as noted by Khalf and Madihally [197], discussing core flow rates of 0.1–0.5 mL/h and shell flow rates of 0.8–2 mL/h for PLGA/Col fibers. The shell flow rate is typically higher than the core to ensure robust encapsulation; for instance, Mickova et al.

[198] reported that a shell flow rate of 1.5 mL/h with a core flow rate of 0.3 mL/h for PVA-core/PCL-shell nanofibers produced uniform core–shell structures with core diameters of ~150 nm and total fiber diameters of ~500 nm. Excessive core flow disrupts the coaxial configuration, causing jet breakup or core exposure, as observed by Yang et al. [199], where increasing the core flow from 0.2 mL/h to 0.6 mL/h (shell at 1.2 mL/h) in a PEO/PVA system led to irregular fibers with diameters up to 600 nm and partial core leakage.

4.2 Emulsion Electrospinning

Emulsion electrospinning is a versatile technique used to fabricate ultrafine core–shell nanofibers by electrospinning an emulsion, typically composed of two immiscible phases, such as oil-in-water (O/W) or water-in-oil (W/O) [200,201]. In this process, the internal dispersed phase (e.g., drugs, proteins, or functional materials) is encapsulated within the continuous polymer solution phase. Under the influence of a high-voltage electric field, the emulsion is stretched into a fine jet. As the solvent evaporates during jet flight, the fibers are deposited onto a collector, with the dispersed droplets entrapped inside the polymer matrix, forming a core–shell structure as shown in **Figure 7(a)** [202,203]. This method enables the encapsulation and protection of sensitive biomolecules while allowing for controlled release, making it particularly useful in drug delivery, tissue engineering, and the development of advanced functional materials [204]. The preparation of core–shell nanofibers by emulsion electrospinning depends on multiple factors, including the nature of the emulsion (type, stability, droplet size), polymer concentration, surfactant selection, applied voltage, solution conductivity, tip–collector distance, and flow rate [205]. Each parameter plays a crucial role in ensuring successful fiber formation and achieving a well-defined core–shell morphology. Confocal laser scanning microscopy (CLSM) images of core-sheath structured nanofibers prepared from a W/O emulsion of PEO-FTIC as core, PEG-PLA as shell nanofiber are shown in **Figure 7(b)** [201].

View Article Online
DOI: 10.1039/D5SE01377A

4.2.1 Emulsion Characteristics and Stability

The success of emulsion electrospinning relies heavily on the stability of the emulsion. Typically, a hydrophilic polymer is dissolved in the aqueous phase, while a hydrophobic polymer is dissolved in the organic solvent phase. Surfactants such as PVA, PEG, or Pluronic F-127 are often added to reduce interfacial tension and stabilize droplet size. Stable emulsions with small, uniformly distributed droplets favour the formation of continuous core channels within nanofibers. If the emulsion is unstable, phase separation may occur before spinning, leading to heterogeneous fibers without a clear core–shell structure [206]. The type of emulsion (O/W vs. W/O) dictates the location of the core; for example, encapsulating hydrophilic drugs requires a W/O emulsion, whereas hydrophobic compounds are better suited for O/W systems. Double emulsions are particularly useful for encapsulating sensitive biomolecules such as proteins or growth factors, as the multiple interfaces protect them from organic solvents [207].

4.2.2 Polymer Concentration and Viscosity

Polymer concentration determines the spinnability of the emulsion. At low concentrations, insufficient chain entanglement results in bead formation or droplet spray, rather than the formation of fibers. At excessively high concentrations, viscosity increases, making it difficult to eject a stable jet. An optimal concentration ensures smooth jet elongation, continuous fiber formation, and proper encapsulation of the dispersed phase. In emulsion electrospinning, shell-forming and core-forming polymers must be optimized [201]. For instance, PCL dissolved in chloroform/DMF mixtures is widely used as a shell polymer due to its hydrophobicity and mechanical strength. In contrast, hydrophilic polymers such as gelatin or PEO are often placed in the dispersed aqueous phase. Proper viscosity matching between the phases helps avoid droplet coalescence and irregular fiber morphologies [208].

DOI: 10.1039/D5SE01377A

4.2.3 Surfactant, Solvent Selection, and Evaporation Rate

Surfactants are indispensable for stabilizing emulsions. The choice of surfactant depends on the emulsion type; hydrophilic surfactants stabilize O/W emulsions, whereas hydrophobic surfactants stabilize W/O emulsions. Surfactant concentration must be carefully tuned: too little surfactant leads to phase separation, while excessive surfactant can migrate to the fiber surface during spinning, affecting fiber smoothness and surface chemistry [209]. Moreover, residual surfactants may influence the biocompatibility of fibers in biomedical applications. Solvent volatility critically affects emulsion stability and fiber morphology. A fast-evaporating solvent (chloroform) promotes rapid solidification of the shell polymer, which traps the dispersed phase inside, thus favouring core–shell structures. If the solvent evaporates too slowly, phase separation can occur during flight, resulting in uneven fiber formation. Often, solvent mixtures are used to balance volatility and polymer solubility [210,211].

4.3 Self-Assembly Methods

Core–shell nanofibers formed by self-assembly represent an elegant bottom-up fabrication route that leverages material properties, such as phase separation, block copolymer architecture, and intermolecular interactions, thereby avoiding the need for complex spinneret setups. This section reviews key self-assembly strategies, parameters influencing morphology, and practical implementations.

4.3.1 Phase Separation via Spontaneous Self-Assembly in Single-Nozzle Electrospinning

Another versatile route is the spontaneous phase separation during electrospinning from blended solutions. Liu et al. [212] produced organic core–shell nanofibers via single-nozzle electrospinning of a PQT-12 and PEO blend. PQT-12 migrated to the fiber surface (forming the shell) during solvent evaporation while PEO formed the core. The shell thickness and overall fiber morphology could be tuned simply by adjusting the PQT-12/PEO mass ratio, as

View Article Online
DOI: 10.1039/D5SE01377A

shown in **Figure 8(a).** Optimizing parameters include composition ratio (semiconductor vs matrix polymer), solvent evaporation rate, polymer miscibility, and dynamics within the jet for homogeneous core-shell nanofibers.

4.3.2 Block Copolymer–Directed Self-Assembly

One compelling method utilizes block copolymer self-assembly. Sanwaria et al. [213] demonstrated a strategy to prepare core–shell polymer–inorganic hybrid nanofibers using a PS-b-P4VP diblock copolymer. Silver nanoparticles (with PS ligands) selectively reside in PS domains, forming the core, while the P4VP matrix remains as the shell. Subsequent selective solvent swelling isolates cylindrical PS core fibers, which can be functionalized with additional nanoparticles (Au, CdS) on the P4VP shell as shown in **Figure 8(b)**. Key parameters include block copolymer composition (block lengths, volume fraction), nanoparticle functionalization and affinity to specific blocks, and solvent selectivity—swelling P4VP without dissolving PS to form ultrafine core-shell nanofibers.

4.3.3. Thermal Self-Organization from Preforms

Although not electrospinning, a notable self-assembly approach has emerged from the thermal drawing of layered preforms. Thermally drawing a composite rod composed of core and shell materials (As_2Se_3 core wrapped with PVDF sheath) produced kilometres-long core–shell nanowires as shown in **Figure 8(c)** [214]. Post-thermal treatment induces transformations to structures such as nano-springs, peapods, and core-shell nanospheres, governed by parameters including diameter, temperature, and heat duration. Control factors include preform layer structure and compatibility, drawing ratios (scale reduction), and treatment temperature and duration.

View Article Online
DOI: 10.1039/D5SE01377A

5. Core–Shell Nanofibers for Magnetoelectric Sensors

ME materials, which couple magnetic and electric order parameters through strain mediation, are at the forefront of research in sensors, energy harvesters, and spintronic devices. In conventional bulk composites or thin films, substrate clamping, poor interfacial bonding, and dimensional constraints often limit the ME coefficient. The core–shell nanofibers geometry provides an exceptionally high surface area, reduced mechanical clamping, and excellent stress transfer across core–shell interfaces, favouring stronger ME interactions than bulk or thin-film counterparts. In these fibers, the magnetostrictive phase (commonly spinel ferrites, hexaferrites, or orthoferrites) forms the core, while the piezoelectric phase (such as PZT, $BaTiO_3$, or lead-free perovskites) forms the shell, or vice versa. The concentric architecture ensures that strain generated in one phase under a magnetic or electric field is efficiently transferred to the other, enabling direct and converse ME effects [215].

The first experimental demonstration of ME interactions in electrospun core–shell nanofibers was reported by Xie et al. (2011), who fabricated $CoFe_2O_4$–PZT fibers using coaxial electrospinning followed by annealing at 600 °C, as shown in the schematic of **Figure 9 (a).** The resulting fibers had diameters of ~200–400 nm, with a uniform concentric architecture confirmed by the TEM micrograph in **Figure 9(b)**. Piezo-response force microscopy under applied magnetic fields revealed strain-mediated ME coupling at the single-fiber level, establishing electrospinning as a viable route to 1D ME nanostructures, as shown in **Figure 9 (c)** [216]. Building on this, Sreenivasulu et al. (2018) synthesized $NiFe_2O_4$–$BaTiO_3$ core–shell fibers via coaxial spinning of sol–gel precursors in PVP, followed by calcination at 700 °C. The nanofibers, with diameters in the 150–300 nm range, exhibited a ME voltage coefficient of ~0.4 mV/cm·Oe at low frequency and demonstrated magnetodielectric effects in mat assemblies [217].

A significant theoretical advance was made by **Petrov et al. (2018)**, who developed a continuum model for ME coupling in coaxial nanofibers. The theory predicted direct ME coefficients of tens to hundreds of mV/cm·Oe and converse ME shifts at ferromagnetic resonance, depending on the core–shell diameter ratio, elastic constants, and magnetostrictive/piezoelectric coefficients of the chosen phases [218]. Experimentally, Liu et al. (2020) validated converse ME coupling in $NiFe_2O_4$–PZT fibers (diameters 200–500 nm) using NSMM as shown in **Figure 9(d)**, observing an electric-field-induced resonance shift with a CME coefficient of –24 Oe.cm/V [219]. Shahzad et al. [2024] fabricated a core-shell nanofiber of CoFe2O4-BaTiO3 nanofibers for magnetic-field-triggered release of doxorubicin, achieving 95 % drug release in 30 minutes under a 4 mT field, and demonstrating ~90 % cytotoxicity against SK-MEL-28 melanoma cells while remaining biocompatible in homolysis assays [220]. After that, Ge et al. (2024) reported hexaferrite–BTO core–shell fibers (average diameter ~300 nm) as shown in **Figure 9(e),** confirm by MFM analysis, prepared by coaxial spinning and high-temperature annealing, which exhibited robust ME voltage responses by measuring the polarization under external magnetic field as shown in **Figure 9(f),** in aligned mats suitable for device-level integration [221].

Beyond spinel and hexaferrite systems, Yadav et al. (2022) demonstrated ME properties in electrospun $NdFeO_3$-PZT fibers, with diameters ~128 nm, confirmed by TEM analysis (**Figure 10(a)**), showing ME coupling by recording polarization under an external magnetic field as shown in **Figure 10(b, c)** at RT [222]. Furthermore, Yadav et al. (2022) developed a hexaferrite-PZT ME-enabled core-shell nanofiber as shown in a TEM micrograph (Figure 9 (d)). They demonstrated direct ME coupling as depicted in **Figure 10(e, f)** [223]**.** A notable step toward environmentally benign systems came from Hadouch et al. (2023), who synthesized lead-free CFO-BCTSn fibers (core and shell ~100–250 nm) by coaxial electrospinning as shown in schematic in **Figure 10(g)** followed by core-shell configuration (**Figure 10(h)**), achieving a giant ME voltage coefficient of ~346 mV/cm·Oe as depicted in **Figure 10(i)** [224]. Later, Yadav et al. (2024) demonstrated sensor-grade $Ba_2Zn_2Fe_{12}O_{22}$-PZT core-shell nanofiber ME responses (650–730 V/T at ~8.3 kHz) suitable for AC/DC field detection [225]. Most recently, Saha et al. (2025) summarized these developments, emphasizing that optimization of electrospinning parameters (solution concentration, applied voltage 10–25 kV, flow rates 0.2–1 mL/h, and post-annealing 500–700 °C) is crucial to achieve uniform diameters, strong interfaces, and enhanced ME coefficients for sensor and harvester applications [215]. Despite these critical milestones, it is clear that research on ME core–shell nanofibers remains very limited compared to bulk composites, thin films, or 2D heterostructures. Fewer than a dozen detailed experimental studies have been reported, and only a handful of material systems—primarily CFO–PZT, NFO–BTO, hexaferrite–BTO, and rare-earth orthoferrites—have been explored. This narrow materials base and the lack of systematic studies on factors such as core–shell ratio, fiber alignment, interfacial strain engineering, and device integration leave significant scope for further research. Exploring lead-free ferroelectrics, integrating flexible polymers with oxide cores, and developing aligned fiber arrays for magnetic sensing or spintronic devices could yield breakthroughs in ME performance. Thus, ME core–shell nanofibers represent a highly promising but underexplored frontier with ample opportunities for innovation. The compilation of ME core–shell nanofiber structures, including diameter, ME coefficients/sensitivities, and application-specific features, is summarized in Table 1.

View Article Online
DOI: 10.1039/D5SE01377A

6. Core–Shell Nanofibers for Fuel Cell Applications

Recent progress in fuel-cell engineering has highlighted the effectiveness of core–shell nanofibers in addressing long-standing challenges related to catalyst stability, mass-transport limitations, and fuel crossover. Compared with traditional carbon blacks or granular ceramic catalysts, 1D nanofibers and core–shell nanofibers enable a continuous conductive framework with high porosity, improved catalyst anchoring, and enhanced electron/ion mobility. Iskandarani et al. [226] demonstrated that P(VDF-TrFE)/Pt/C/S-SiO_2 nanofiber cathodes maintain high performance and exceptional durability under low-humidity PEMFC operation due to their interconnected fiber network and enhanced Pt–ionomer interfacial contact. Complementary mechanistic insights from Kabir et al. [227] and Khandavalli et al. [228] demonstrate that optimized polymer–particle interactions and controlled ionomer distribution within nanofibers significantly enhance Pt accessibility, oxygen-reduction kinetics, and catalyst utilization, underscoring the critical role of ink microstructure and spinnability in producing high-quality nanofiber catalyst layers. Beyond electrodes, Liu et al. [229] reported that electrospun nanofiber-reinforced polymer electrolyte membranes offer superior mechanical stability, proton-transport pathways, and humidification tolerance, indicating that nanofiber engineering can also enhance membrane function. In parallel, Kallina et al. [230] demonstrated that humidity-robust nanofiber cathode layers can be realized through the use of tailored ionomer content and multilayer designs, thereby mitigating mass-transport resistance during PEMFC operation. This section provides a brief review and discussion of prominent research works on fuel cells employing 1D nanofibers, core–shell nanofiber structures, highlighting their design strategies, functional advantages, and performance enhancements in energy conversion applications. Li et al. [231] developed core–shell TiO_2/C nanofibers as catalyst supports for fuel cells, where uniformly dispersed Pt nanoparticles (~2 nm) enhanced

View Article Online
DOI: 10.1039/D5SE01377A

methanol oxidation activity and stability. SEM and TEM micrograph of TiO_2/C is shown in **Figures 11 (a) and (b)**, respectively. The system exhibited 7 times higher current density and a 2.5 times boost under UV light, highlighting a synergistic photo-electrocatalytic effect that is beneficial for fuel cell efficiency. Singh and Dempsey et al. [232] synthesized Pt-decorated functionalized carbon nanofibers (fCNFs) for fuel cell applications, achieving uniform Pt dispersion inside and outside the fibers as shown in **Figure 11 (c)**. This design improved Pt utilization, CO tolerance, and long-term durability, outperforming commercial Pt/C catalysts and offering a cost-effective route for high-performance fuel cells, as shown in **Figure 11(d).**

Karuppannan et al. [233] present a highly durable Pt–C core–shell catalyst supported on carbon nanofibers (CNFs) for a proton exchange membrane fuel cell, as shown in the TEM image of **Figure 11 (e)**. The core–shell structure refers to individual Pt nanoparticles, each consisting of a Pt core encapsulated by a thin (~1 nm) nitrogen-doped carbon shell, which are uniformly dispersed on the CNF surface, serving as a stable and conductive support. Using a simple Pt–aniline complex coating followed by heat treatment, the researchers obtained 3–4 nm Pt nanoparticles with excellent uniformity and strong protection against aggregation or dissolution. The optimized catalyst (heat-treated at 900 °C) exhibited superior oxygen reduction reaction (ORR) activity and exceptional durability, maintaining nearly constant performance for 30,000 accelerated stress test cycles with negligible voltage loss at 0.8 A cm^{-2}, as displayed in **Figure 11 (f)**. Its performance exceeded the U.S. DOE 2020 stability targets, demonstrating strong potential for ultra-low Pt loading and long-lasting PEM fuel cells. Senthilkumar et al. [234] report the direct growth of hierarchical Co_3O_4@NiO and Co_3O_4@MnO_2 core–shell nanostructures on carbon fibers for bifunctional catalysis in direct urea fuel cells (DUFCs). SEM and TEM micrographs of Co_3O_4@NiO nanofiber are shown in

View Article Online
DOI: 10.1039/D5SE01377A

Figure 12(a) and 12(b), respectively. The engineered architecture enhances both urea oxidation and oxygen reduction kinetics while reducing charge-transfer resistance. The DUFC achieved a high-power density of 33.8 mW/cm² using urea and 23.2 mW/cm² with human urine, maintaining stable performance over 120 hours, as depicted in **Figure 12(c).** The robust 3D structure offers superior durability, efficient electron/ion pathways, and potential for wastewater-to-energy conversion. Lee et al. [235] developed a novel SiO_2@C core–shell nanofiber via coaxial electrospinning for use as a microporous layer (MPL) in PEM fuel cells. SEM and TEM micrographs of SiO_2@C core–shell nanofiber are shown in **Figures 12(d)** and **12(e)**, respectively. The hydrophilic silica core regulates water retention, while the hydrophobic conductive carbon shell ensures efficient electron transport and prevents flooding. The composite exhibits a higher surface area, strength, and conductivity than pure carbon fibers. When used in PEMFCs, it enhanced power density by 66–302% under varied humidity and temperature conditions, offering an effective strategy for improved water management and stable fuel cell operation, as displayed in **Figure 12(f).** In solid oxide fuel cells (SOFCs), Choi et al. [236] developed $La_{0.75}Sr_{0.25}Cr_{0.5}Mn_{0.5}O_3$@$Sm_{0.2}Ce_{0.8}O_{1.9}$ (LSCM@SDC) core–shell nanofiber anodes via a simple electrospinning route, achieving outstanding coking resistance and ultra-low polarization resistance (~0.11 Ω cm^2 at 800 ℃) under methane fuel, owing to the SDC shell that improved oxygen-ion transport and prevented carbon buildup.

Similarly, Yang et al. [237] fabricated $YCo_{0.5}Fe_{0.5}O_3$–$Gd_{0.1}Ce_{0.9}O_{1.95}$ core–shell cathodes for intermediate-temperature SOFCs (IT-SOFCs), where the GDC shell facilitated oxygen-ion diffusion and charge transfer, yielding a low area-specific resistance of 0.66 Ω.cm^2 and a peak power density of 426.5 mW.cm^{-2} at 550 °C. Extending the concept to direct methanol fuel cells (DMFCs), Lee et al. [238] synthesized Pt–C core–shell catalysts supported on carbon nanofibers (Pt@CS/CNF), in which a graphitized carbon shell selectively blocked methanol while allowing O_2 access to Pt sites. The optimised Pt@CS/CNF900 catalyst demonstrated superior methanol tolerance, oxygen reduction reaction (ORR) activity, and stability over 30,000 cycles, outperforming commercial Pt/C catalysts. Collectively, these works highlight the versatility of core–shell nanofiber designs as a unifying strategy for developing high-efficiency, durable, and fuel-flexible fuel cell electrodes. Delikaya et al. [239] developed a porous electrospun carbon nanofiber network that acts as an integrated electrode and gas diffusion layer (GDE@GDL) for high-temperature polymer electrolyte membrane fuel cells (HT-PEMFCs). This design enhanced oxygen transport, reduced mass-transport resistance, and achieved a 21% higher Pt-normalised power density compared to conventional GDL-based cells. Symillidis et al. [240] fabricated conductive PANI–based core–shell polymer nanofibers supporting Pd and Pd–M (Ag, Bi, Cu) catalysts for direct ethanol fuel cells (DEFCs). The PANI shell improved conductivity, CO tolerance, and catalyst stability, while Pd–Ag and Pd–Bi combinations showed the highest ethanol oxidation activity with lower activation energies than monometallic Pd. Sanna et al. [241] studied $Ce_{0.9}Gd_{0.1}O_{1.95}$–core/Cu-doped $La_{0.6}Sr_{0.4}MnO_3$–shell nanofiber cathodes for intermediate-temperature solid oxide fuel cells (IT-SOFCs). Electrochemical impedance spectroscopy revealed polarisation resistances as low as $1.7\ \Omega\ cm^2$ at 650 °C, significantly lower than those of conventional composite cathodes, with a stable nanofiber morphology after testing. Collectively, these results confirm that core–shell nanofiber engineering enhances mass transport, electrocatalytic activity, and long-term durability across multiple fuel cell technologies, from HT-PEMFCs to DEFCs and SOFCs. An overview of reported core–shell nanofiber systems for fuel cell applications, highlighting structural parameters (fiber diameter, core diameter, shell thickness), device type, and key electrochemical performance metrics, is provided in Table 2.

View Article Online
DOI: 10.1039/D5SE01377A

7. Core–Shell Nanofibers for Drug Delivery Applications

Controlled drug delivery has long been a challenge in biomedicine, where achieving precise dosage, sustained release, and protection of fragile biomolecules is crucial. Electrospun core–shell nanofibers offer a unique solution by providing a high surface-to-volume ratio, tunable porosity, and the ability to encapsulate drugs within the fiber core while protecting them with a polymer shell. This architecture not only prolongs release kinetics but also prevents premature degradation of sensitive molecules such as proteins, peptides, and nucleic acids. Therefore, core–shell nanofibers prepared by coaxial or emulsion electrospinning have emerged as promising carriers for drug delivery, tissue engineering, and wound healing.

7.1 Establishing Encapsulation and Release Control

The concept of drug-loaded core–shell fibers was first rigorously demonstrated by Jiang et al. (2006), who fabricated BSA-dextran as the core and PCL (with PEG modification) as the shell via coaxial electrospinning, as shown in **Figure 13 (a)**. The resulting fibers had diameters of approximately 200–500 nm, as shown in **Figure 13 (b)**. They demonstrated tunable release rates by modifying the inner feed rates and PEG concentration in the shell, allowing BSA to be released gradually over periods ranging from one week to more than one month, with markedly reduced burst release compared to blend spinning [242]**.** Maleki et al. (2013) fabricated a PLGA/PLA shell and a TCH core using the coaxial electrospinning method, with a nanofiber diameter of ~200–800 nm, as confirmed by TEM analysis (**Figure 13(c)**). This analysis demonstrates that the shell thickness can be precisely controlled to regulate the release duration [243].

View Article Online
DOI: 10.1039/D5SE01377A

7.2 Biopolymers and protein stability

After 2016, the literature broadened: Kalwar et al. [2016] used chitosan–PCL and Ovideo et al. [2021] core–shell nanofiber systems, which were explicitly fabricated by coaxial electrospinning, confirming that PCL core/chitosan shell geometries are practicable for biomedical cargo, as illustrated in **Figure 13(d)** [244] and wound-care uses [245], respectively. Emulsion and aqueous coaxial methods improved compatibility with biologics, allowing for the loading of growth factors, enzymes, and peptides with reduced burst release from 2017 to 2024. Recent reviews [246-248] highlight advances in electrospun systems, such as triaxial structures, responsive shells, nanoparticle-hybrid cores, and solvent strategies that preserve protein activity. Yet, proteins loaded core–shell fibers still represent a small fraction of studies, leaving a broad scope for quantitative bioactivity metrics, systematic stabilization research, and translation-oriented efforts in sterilization, scale-up, and regulatory pathways.

7.3 Tissue Engineering and Wound Healing

Hou et al. (2017) fabricated biodegradable, bioactive core–shell fibrous mats via coaxial electrospinning using a PCL shell and PGS core system with surface-immobilized heparin, yielding scaffolds with favorable chemical, mechanical, and biological characteristics for broad tissue-engineering applications [249]. Silva et al. [2020] report the development of aligned core–shell nanofibers composed of a PGS (core) and a PCL (shell), engineered to mimic the anisotropic architecture of articular cartilage while enhancing mechanical strength as illustrated in **Figure 13(e)** [250]. Kartogenin, a small chondrogenic molecule, was encapsulated within the PGS core, allowing for sustained release over a period of up to 21 days. This controlled delivery promoted proliferation and chondrogenic differentiation of human mesenchymal stem/stromal cells without the need for exogenous growth factors such as TGF-β3, highlighting

View Article Online
DOI: 10.1039/D5SE01377A

the potential of KGN-loaded coaxial nanofibers as promising scaffolds for cartilage tissue engineering. Al Fahad et al. (2024) developed a small-diameter vascular graft using coaxial electrospun micro-nanofibers with a PCL/gelatin shell loaded with heparin and VEGF and a PCL core—demonstrating sustained release (~79% heparin; ~86% VEGF over 25 days), as shown in **Figure 13(f)** excellent mechanical performance, full endothelialization, smooth muscle regeneration, and 100% patency in rat aorta implants [251]. Kharaghani et al. (2019) designed core–shell PVA/PAN nanofibers via coaxial electrospinning for dual-drug delivery as depicted in **Figure 13(g),** enabling the simultaneous release of water- and organic-solvent–soluble drugs for tailored therapeutic applications [252]. Li et al. (2021) reported a core–shell GelMA-PDLLA nanofiber-hydrogel composite scaffold with enhanced porosity, water retention, and angiogenic activity, which accelerates chronic diabetic wound healing in vivo, as shown in **Figure 14 (a)** [253]. Guo et al. (2022) developed a core–shell coaxial fiber membrane loaded with CTG in the core and CIP in the shell, achieving controlled release, antibacterial performance, and improved fibroblast proliferation, as well as enhanced scald wound repair in rats [254], as illustrated in **Figure 14(b)**.

Abadi et al., (2025) engineered core–shell PCL–CS/PVA nanofibers via coaxial electrospinning to co-deliver PIO-NEs and GEM over 14 days as shown in schematic of **Figure 14(c),** achieving sustained and controlled release (~80% of PIO, ~77% of GEM), which significantly inhibited proliferation and induced apoptosis in A375 melanoma cells via P53 and PPARγ pathways [255]. Furthermore, Mosallanezhad et al. (2025) developed core–shell chitosan-PCL nanofibers loaded with curcumin for controlled wound therapy. These fibers demonstrated a favorable morphology, enhanced structural and release properties, and strong antimicrobial performance, indicating their promise for infection-resistant wound dressings, as shown in **Figure 14(d)** [256]. Together, these studies emphasize the versatility of core–shell architectures in controlled drug delivery, tissue regeneration, and wound management. A

View Article Online
DOI: 10.1039/D5SE01377A

summary of core–shell nanofiber systems used in drug-delivery applications, including fiber diameters, core and shell dimensions, therapeutic payloads, and corresponding release behaviours, is provided in Table 3. Furthermore, Table 4 summarizes details of parameters involved in the preparation of core-shell nanofiber fabrication techniques.

8. Challenges, Limitations, and Future Directions of Core–Shell Nanofibers

Despite significant progress, the development and deployment of core–shell nanofibers in magnetoelectric sensors, fuel-cell systems, and drug-delivery platforms still encounter several critical challenges that prevent their transition from laboratory research to practical use. One major issue is scalability. Although coaxial and emulsion electrospinning are excellent for producing uniform fibers on a laboratory scale, they suffer from low throughput and high sensitivity to process variations, making it difficult to produce large-area, industrial-scale fibers with consistent core–shell structures. Ensuring reproducibility—especially uniform core diameters, shell thicknesses, and concentricity—requires precise control over solution viscosity, voltage, flow rates, humidity, and solvent evaporation. These factors become more difficult to regulate during scale-up, often leading to structural inconsistencies and batch-to-batch differences. Furthermore, many high-performance materials involve costly precursors or require multiple steps of annealing and calcination, which increase fabrication costs, especially for metal oxides, perovskites, and noble-metal catalysts used in fuel cells.

Another key concern is toxicity and environmental safety, particularly for lead-based piezoelectric systems, such as PZT and PMN-PT. While these materials offer strong magnetoelectric coupling, their inherent lead content limits their use in biomedical devices, wearable technology, and environmentally regulated commercial products. Restrictions from standards such as RoHS and REACH greatly limit their real-world application, highlighting the need for lead-free options like BCTSn, $BaTiO_3$, KNN, and zinc- or barium-based

View Article Online
DOI: 10.1039/D5SE01377A

hexaferrites. However, matching the magnetoelectric performance of lead-based systems while maintaining processability and long-term stability remains an ongoing research challenge.

Device integration and long-term stability are also critical issues. Arranging core–shell nanofibers into ordered arrays and incorporating them into multilayer device architectures require advanced assembly methods that are not yet standardized. In magnetoelectric sensors, defects at the core–shell interface, inadequate strain transfer, or microcracking from repeated magnetic and electric cycling can reduce coupling efficiency. In fuel cells, durability issues such as catalyst detachment, carbon corrosion, ionomer redistribution, or shell degradation in humid, acidic, or high-temperature environments can compromise performance. Drug-delivery fibers must also sustain structural integrity during storage and implantation, prevent uncontrolled burst release, and ensure the biocompatibility of both organic and inorganic elements. These challenges emphasize the importance of robust interfacial engineering, better encapsulation techniques, and stronger mechanical reinforcement of core–shell structures.

Looking ahead, several opportunities can help advance core–shell nanofiber technologies. New fabrication methods—like real-time controlled coaxial electrospinning, 3D-assisted fiber patterning, and hybrid printing-electrospinning platforms—offer promising paths for scalable and precise structural control. Innovations in interface engineering, defect reduction, and domain alignment can further improve coupling efficiency and stability. For biomedical use, creating stimuli-responsive shells that react to pH, temperature, or magnetic/electric fields will be essential for enabling personalized or on-demand therapies. For fuel cells, enhancing ionomer distribution, controlling shell porosity, and stabilizing catalyst–support interactions are crucial for high performance under low-humidity conditions. Using computational tools, such as AI-based material design and Multiphysics simulations, can speed up optimization and predict long-term behavior in vivo or under operational stresses. Ultimately, collaboration across disciplines—materials science, chemical engineering, electronics, and biomedicine—is

View Article Online
DOI: 10.1039/D5SE01377A

vital to transforming core–shell nanofibers from laboratory prototypes into reliable, scalable, and commercially viable solutions technologies.

8. Conclusion

Core–shell nanofibers represent a transformative class of one-dimensional architectures, whose tunable interfaces, high aspect ratios, and multifunctional compositions enable superior performance in magnetoelectric sensing, fuel cell catalysis, and drug delivery applications. Despite significant progress, several critical research gaps must be addressed before these systems can advance toward technologically relevant devices and scalable commercialization. First, optimizing interfacial coupling remains a major challenge across all areas. In magnetoelectric systems, inadequate strain transfer, interfacial defects, and uncontrolled core–shell ratios greatly limit ME coefficients and device sensitivity. Similarly, fuel-cell nanofibers need improved catalyst–support interactions and controlled ionomer distribution to achieve durable and efficient electrochemical performance. For drug-delivery fibers, ensuring long-term shell stability and preventing burst release are key obstacles. Second, there is an urgent need for reliable, lead-free alternatives to traditional high-performance piezoelectric materials, such as PZT and PMN-PT. Although promising candidates—such as BCTSn, $BaTiO_3$, KNN, and Zn- or Ba-based hexaferrites—have been developed, their electromechanical response and long-term reliability still fall short of lead-based systems. Bridging this gap is crucial for enabling sustainable, biocompatible magnetoelectric devices, particularly in biomedical and wearable applications that require strict regulatory standards. Third, flexible and integrated device architectures are a promising yet underdeveloped area. For magnetoelectric sensing, integrating aligned or woven coaxial nanofibers into soft substrates could support wearable or implantable devices. In fuel cells, multilayer nanofiber electrodes and microporous layers need to be engineered for mechanical durability under varying humidity and temperature conditions. For biomedical uses, seamless integration with hydrogels, scaffolds, and tissue-mimicking

View Article Online
DOI: 10.1039/D5SE01377A

platforms will be vital for clinical translation. Lastly, commercialization challenges persist throughout the field. Coaxial electrospinning faces issues with low throughput and batch variability. Maintaining uniform core–shell morphology at an industrial scale is difficult due to sensitivities to viscosity, flow rate, voltage, and humidity. Material costs—especially for noble metals, rare-earth ferrites, and high-purity polymers—further limit scalability. Moreover, the lack of standardized testing protocols for ME performance, drug release kinetics, mechanical stability, and long-term degradation complicates cross-study comparisons. Overall, while core–shell nanofibers offer exceptional multifunctionality and potential, realizing their broader use depends on overcoming these challenges through interdisciplinary advances in interface engineering, scalable manufacturing, predictive modeling, and device integration. With ongoing innovation, core–shell nanofibers are positioned to drive the next generation of sensing, energy, and biomedical technologies.

Credit authorship contribution statement:

Sandeep Kumar Yadav: Visualization, Resources, Methodology, Investigation, Formal analysis, Conceptualization, Writing – original draft. **Vishwa Prakash Jha**: Theoretical Analysis, Conceptualization, Writing – review & editing. **Durga Prasad Pabba, Arun Thirumurugan**: Supervision, Resources, Project administration, Methodology.

Declaration of competing interest:

The authors declare that they have no known competing financial interests or personal relationships that could have appeared to influence the work reported in this paper.

Data availability:

No data was used for the research described in the article.

Figures

View Article Online
DOI: 10.1039/D5SE01377A

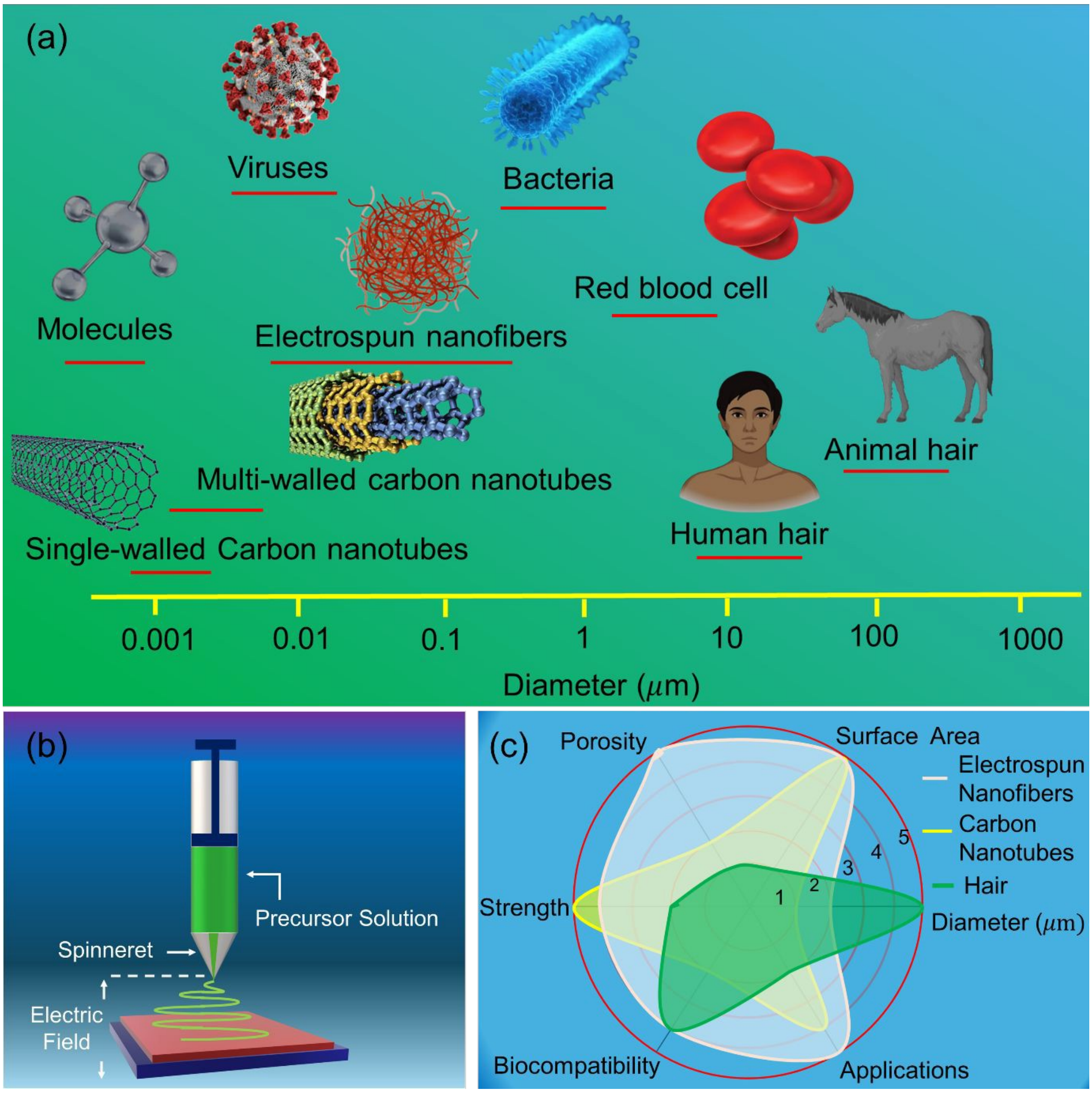

Figure 1. Comparison of the diameters of nanofibers with biological, technological objects, (b) Illustration of electrospinning setup for preparation of nanofibers, and (c) Comparison of biocompatibility, strength, porosity, surface area, diameter, and potential applications of electrospun nanofibers with CNTs and human hairs.

View Article Online
DOI: 10.1039/D5SE01377A

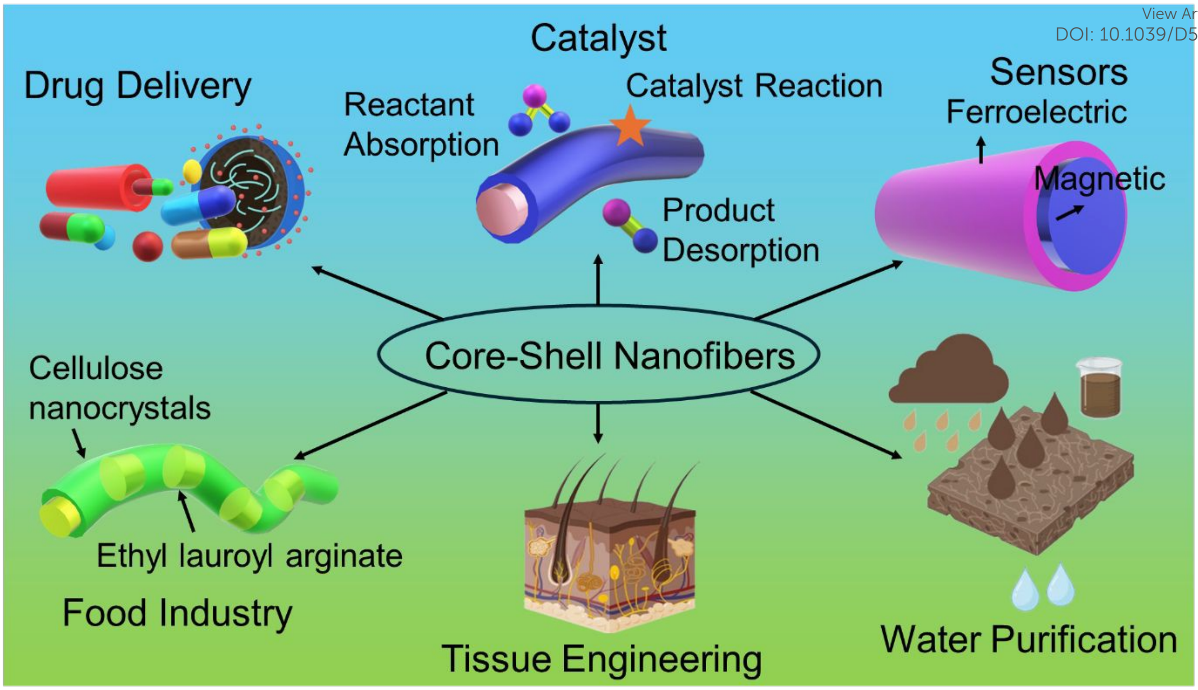

Figure 2. Schematic representation of core–shell nanofiber applications, including drug delivery, catalysis, sensors, food industry, tissue engineering, and water purification.

View Article Online
DOI: 10.1039/D5SE01377A

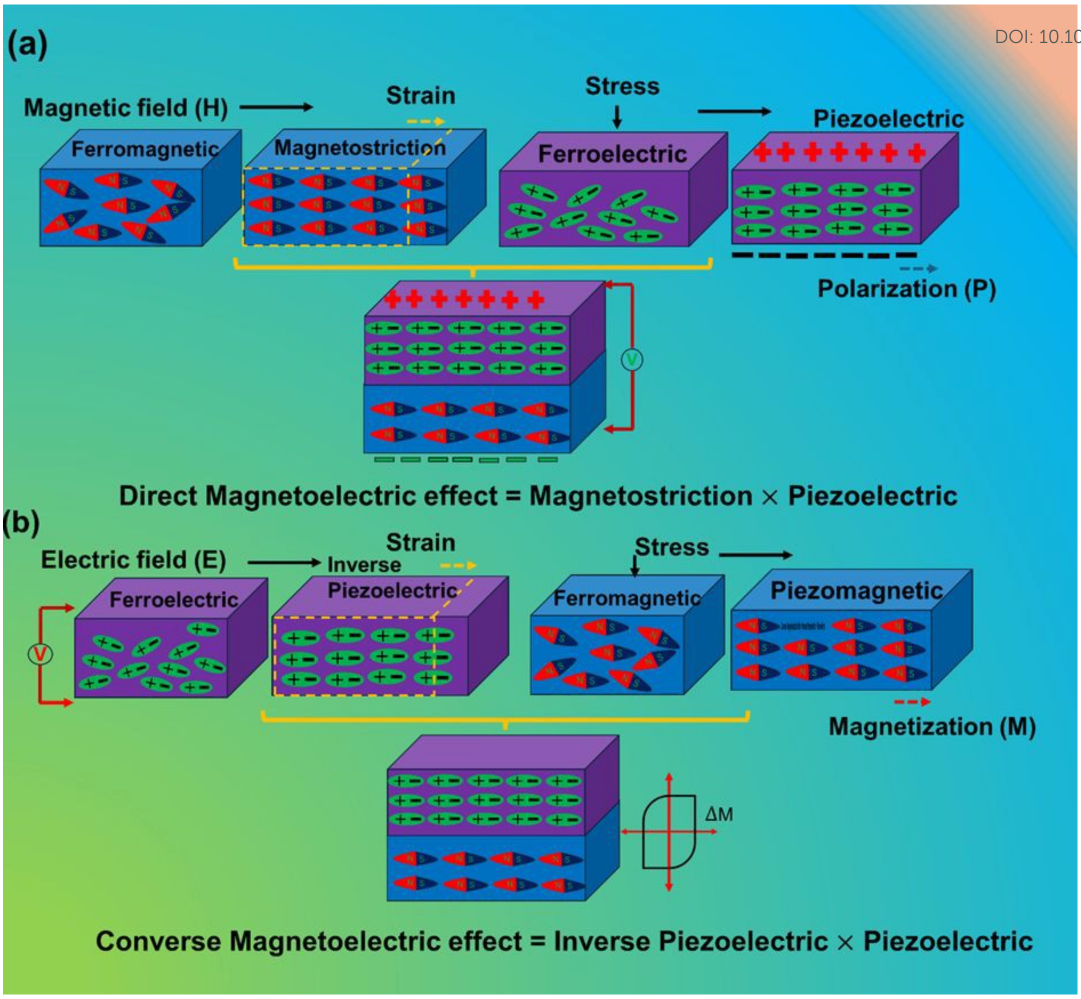

Figure 3. Schematic illustration of strain-mediated ME effect in a composite system (a) Direct ME effect and (b) Converse ME effect.

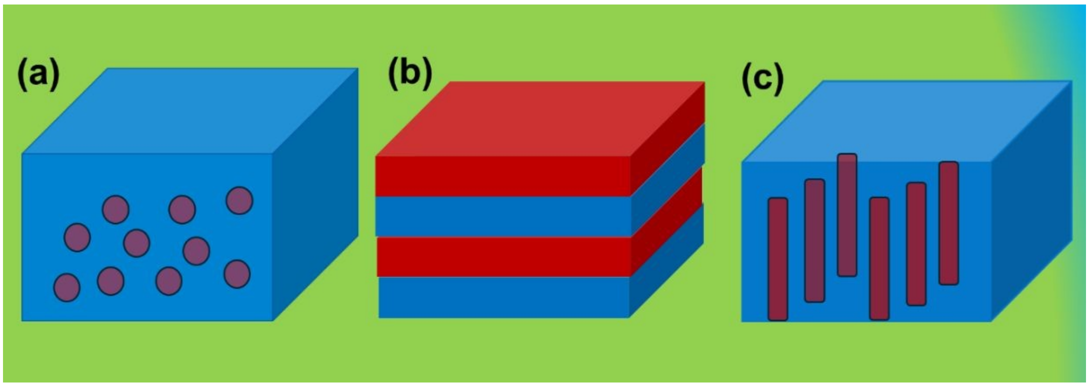

Figure 4. Schematic illustration of core–shell nanostructure functionality in (a) fuel-cell catalysis and (b) drug-delivery systems.

View Article Online
DOI: 10.1039/D5SE01377A

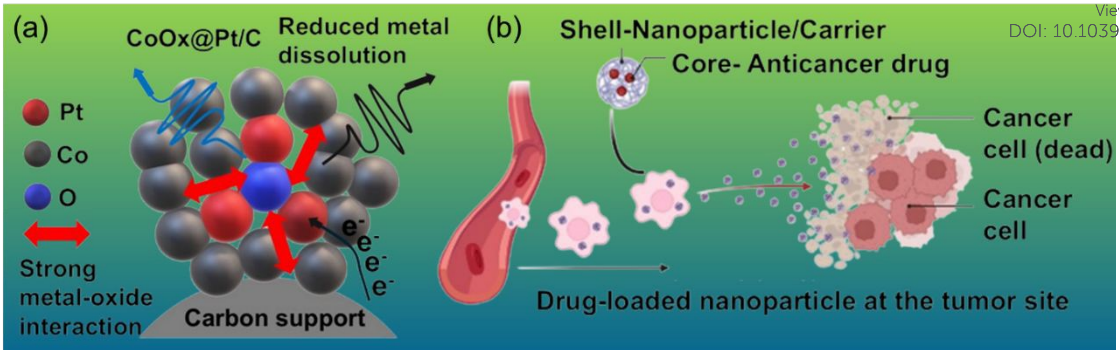

Figure 5. Schematic illustration of core–shell nanostructure functionality in (a) fuel-cell catalysis and (b) drug-delivery systems.

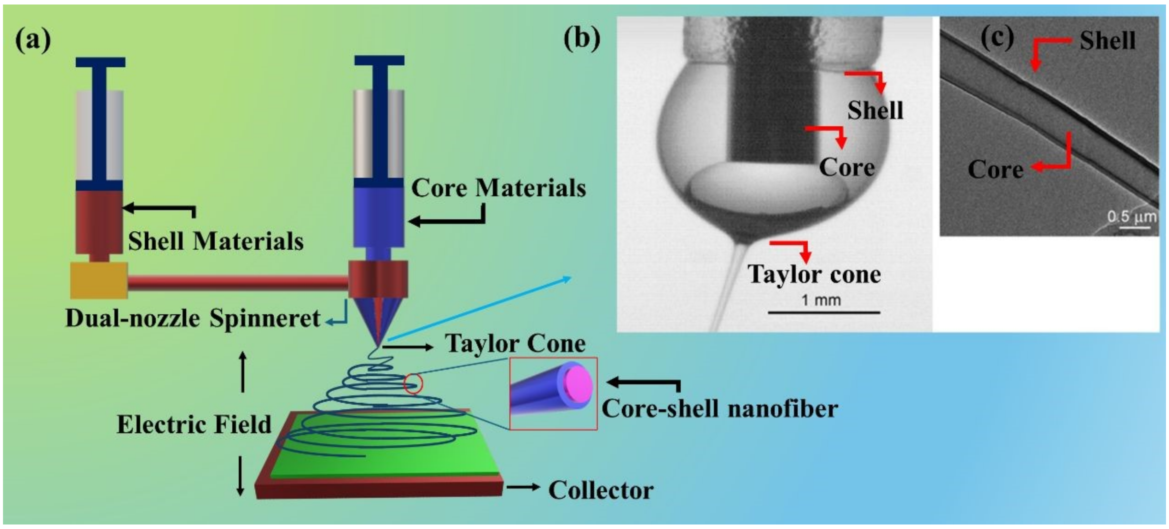

Figure 6. (a) Schematic of electrospinning setup for preparation of core-shell nanofibers, (b) Optical image of core–shell droplets on the nozzles of an apparatus for coaxial electrospinning. (c) SEM image of core–shell fibers of PVDF (core) and PC (shell) produced by coaxial electrospinning. Figure 6 (b,c) adopted from ref. [162]. Copyright© 2007 WILEY-VCH Verlag GmbH & Co. KGaA, Weinheim.

View Article Online
DOI: 10.1039/D5SE01377A

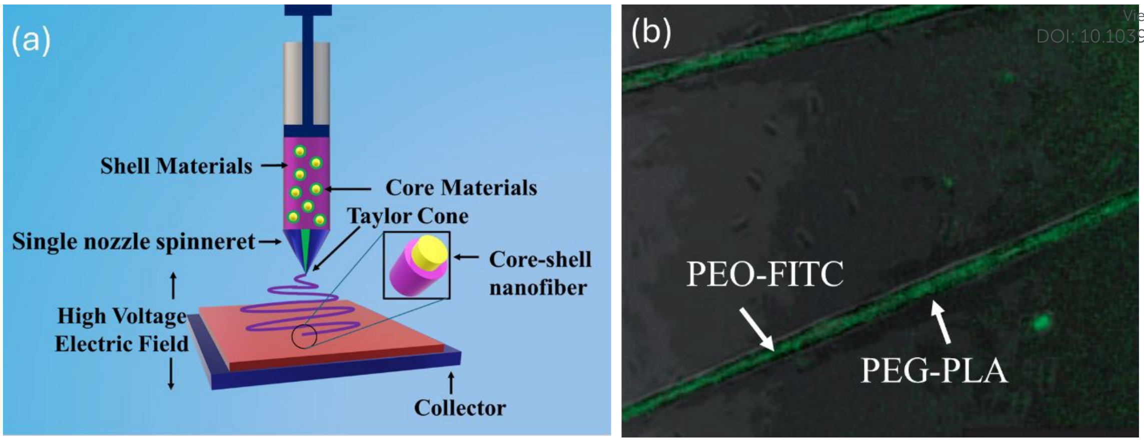

Figure 7. (a) Schematic of preparation of core-shell nanofibers by emulsion technique and (b) CLSM images of core-sheath structured nanofibers prepared from W/O emulsion of PEO-FTIC as core, PEG-PLA as shell nanofibers. Figure 7(b) adopted from ref. [201]. Copyright© 2006 WILEY-VCH Verlag GmbH & Co. KGaA, Weinheim.

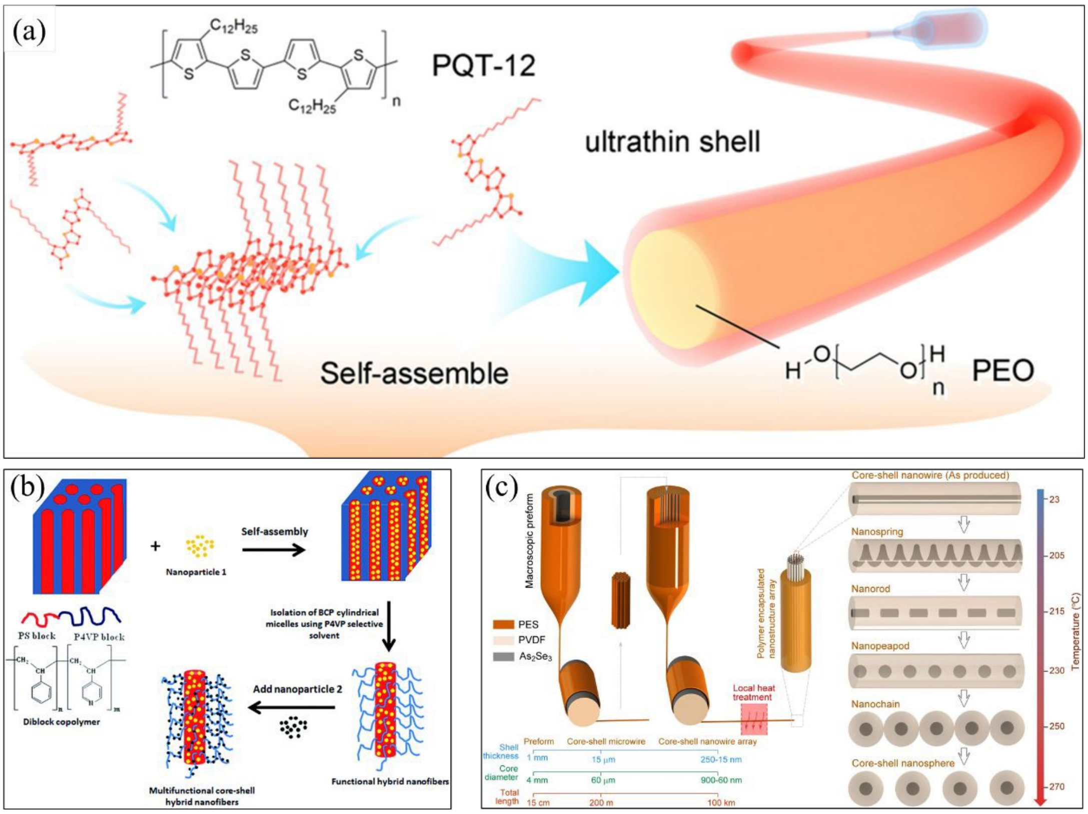

View Article Online
DOI: 10.1039/D5SE01377A

Figure 8. (a) Chemical structure of PQT-12 and PEO and the formation of a core-shell structure by self-assembling induced phase separation, adopted from ref. [212], (b) Schematic illustration for the preparation of multifunctional core–shell nanofibers functionalized with two different types of nanoparticles loaded in the core and in the shell from a self-assembled block copolymer template via a selective solvent approach, adopted from ref. [213], Copyright© The Royal Society of Chemistry 2015, (c) Low temperature, multimaterial fiber drawing method used for the iterative size reduction of a macroscopic layered rod down to core-shell nanowires, adopted from ref. [214], Copyright© Springer Nature 2014.

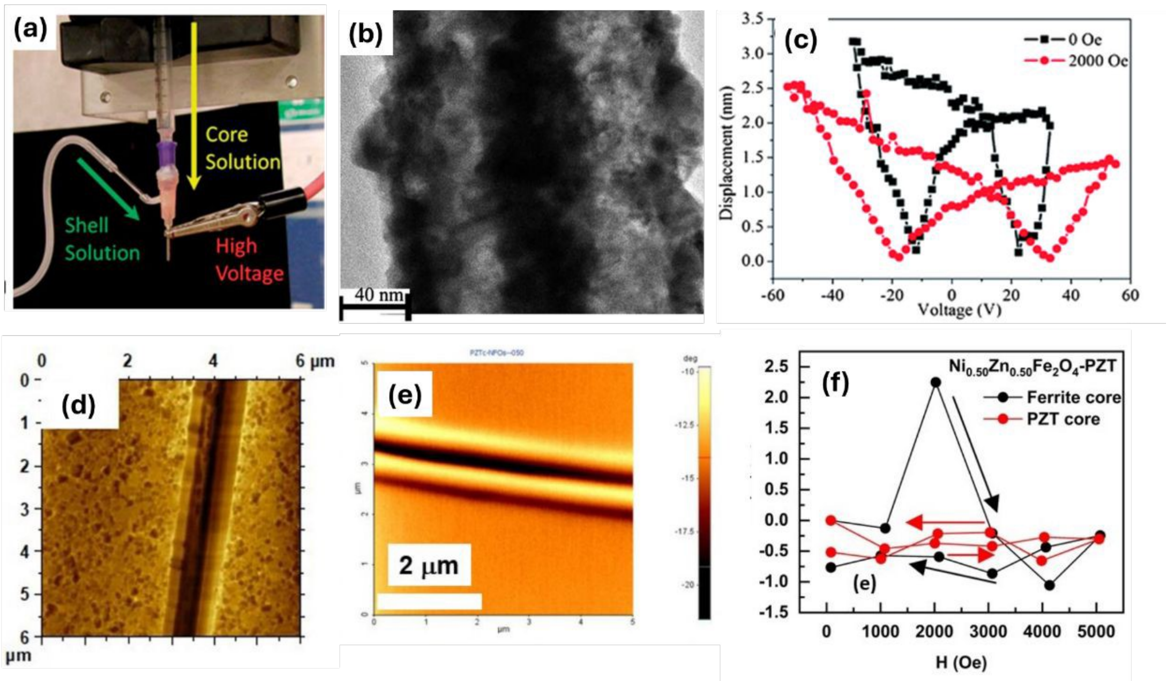

Figure 9. (a) Digital photo of actual coaxial spinneret in electrospinning setup, (b) TEM micrograph of CFO-PZT core-shell nanofiber, (c) The switching characteristics of piezo response in a CFO-PZT core-shell nanofiber before and after the application of external magnetic field by variable field module (VFM), Figure 9 (a, b, c) adopted from ref. [216], Copyright©-The Royal Society of Chemistry 2011, (d) NSMM image of NFO-PZT core-shell nanofibers, adopted from ref. [219], (e) MFM for a fiber of NFO shell–PZT core nanofibers, adopted from ref. [221], (f) Fractional change in the remnant polarization (Pr) as a function of magnetic field (H), adopted from ref. [221].

View Article Online
DOI: 10.1039/D5SE01377A

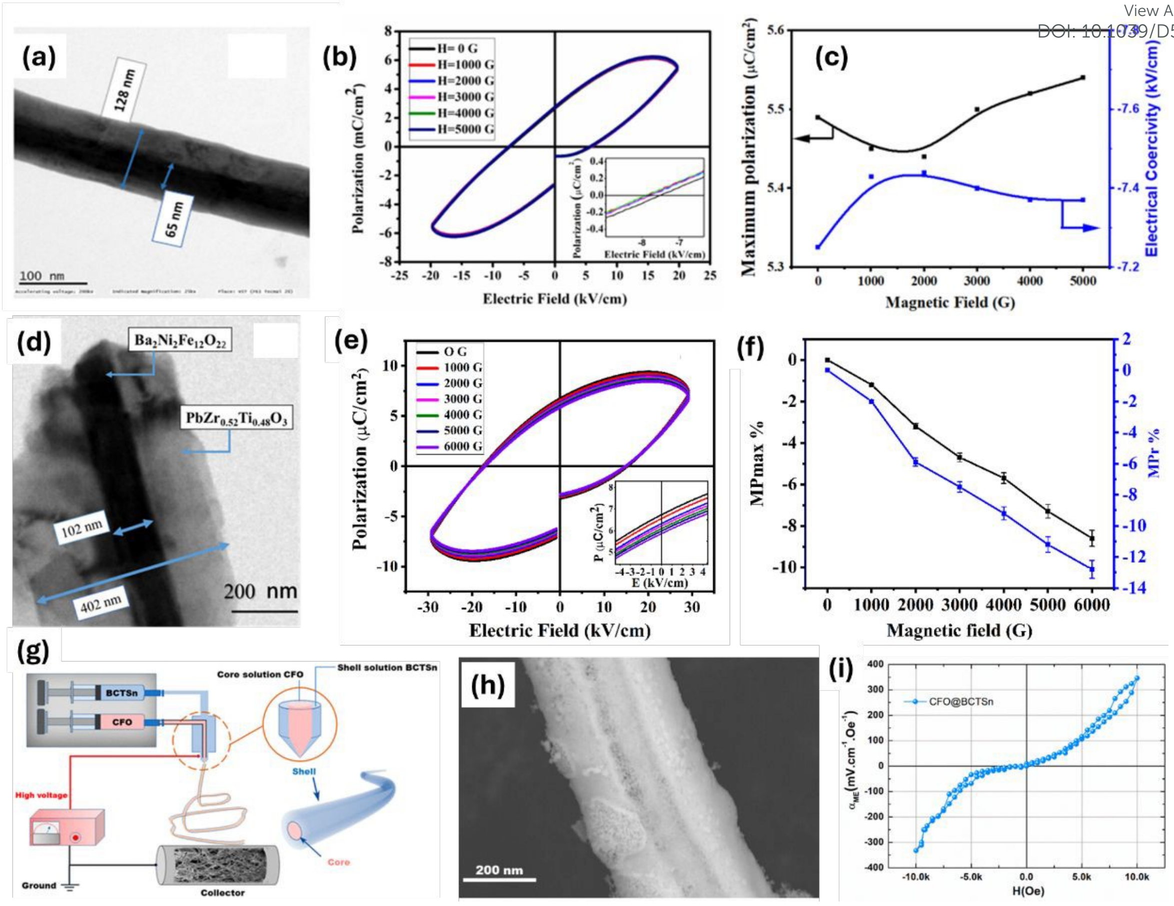

Figure 10. (a) TEM images of the core–shell $NdFeO_3$–$PbZr_{0.52}Ti_{0.48}O_3$ nanofibers, (b) P-E loops of the core–shell NF–PZT nanofibers under various magnetic fields, (c) variations in maximum polarization and electric coercivity with respect to the applied magnetic field, Figure 10 (a, b, c) adopted from ref. [222], Copyright© Elsevier-(2022), (d) TEM micrograph, (e) Variations in the P–E loop, (f) variations in MPmax% and MPr% with respect to magnetic field. Figure 10 (d, e, f) adopted from ref. [223], Copyright© Elsevier-(2022), (g) Coaxial electrospinning of core−shell nanofibers: setup schematics, (h) Annealed CFO-BCTSn core-shell nanofibers, (i) Dependence of the magnetoelectric coefficient of CFO-BCTSn NFs on the DC magnetic field at RT, Figure 10 (g, h, i) adopted from ref. [224], Copyright© 2023 American Chemical Society

View Article Online
DOI: 10.1039/D5SE01377A

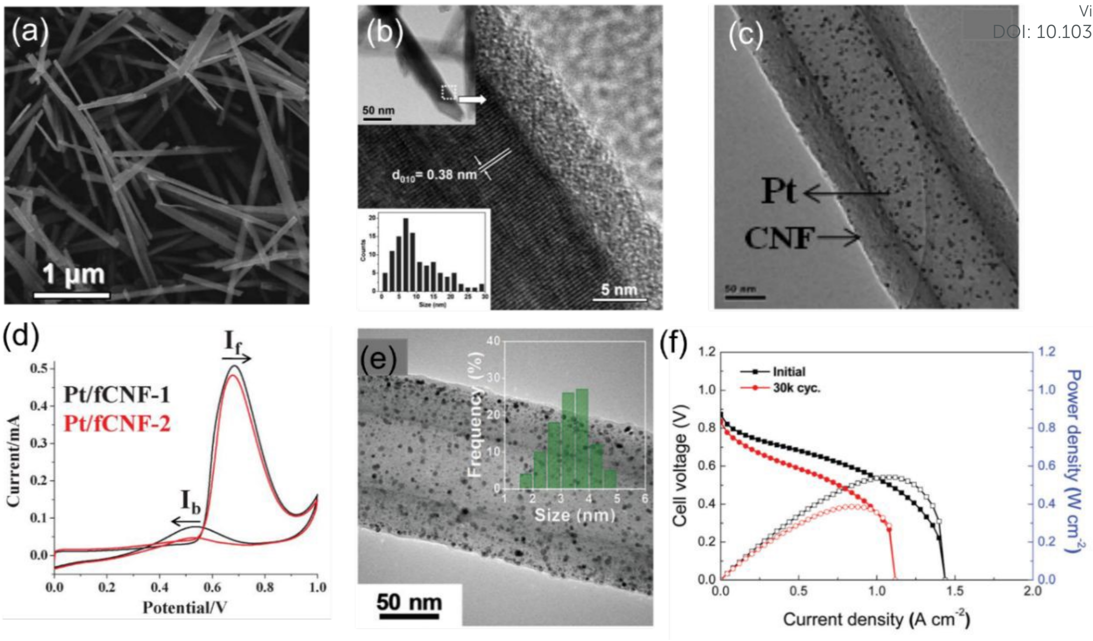

Figure 11. (a) SEM image of TiO_2 nanofibers, (b) TEM images of TiO_2/C. Upper inset: low-magnification TEM image of several fibers; lower inset: distribution of carbon thickness over different regions and fibers, Figure 11 (a, b) adopted from ref. [231], Copyright© Royal Society of Chemistry-(2012), (c) TEM image of Pt/fCNF-1 core-shell nanofibers, (d) Cyclic voltametric responses for methanol electro-oxidation by Pt/fCNF-1 (response after 60 min) and Pt/fCNF-2 (response after 63 min) modified electrodes (labelled) in acidic conditions (1 M methanol + 0.5 M H_2SO_4) at a scan rate of 0.01 V vs. Ag/AgCl. Figure 11 (c, d) adopted from ref. [232], Copyright© Royal Society of Chemistry-(2013). (e) TEM images of Pt@CS/CNF600 core-shell nanofibers, (f) Polarization curves of (a) Pt/C, before and after 30k AST cycles. Solid and open symbols represent the cell voltage and power density, respectively. Figure 11 (e, f) adopted from ref. [233], Copyright© Royal Society of Chemistry-(2019).

View Article Online
DOI: 10.1039/D5SE01377A

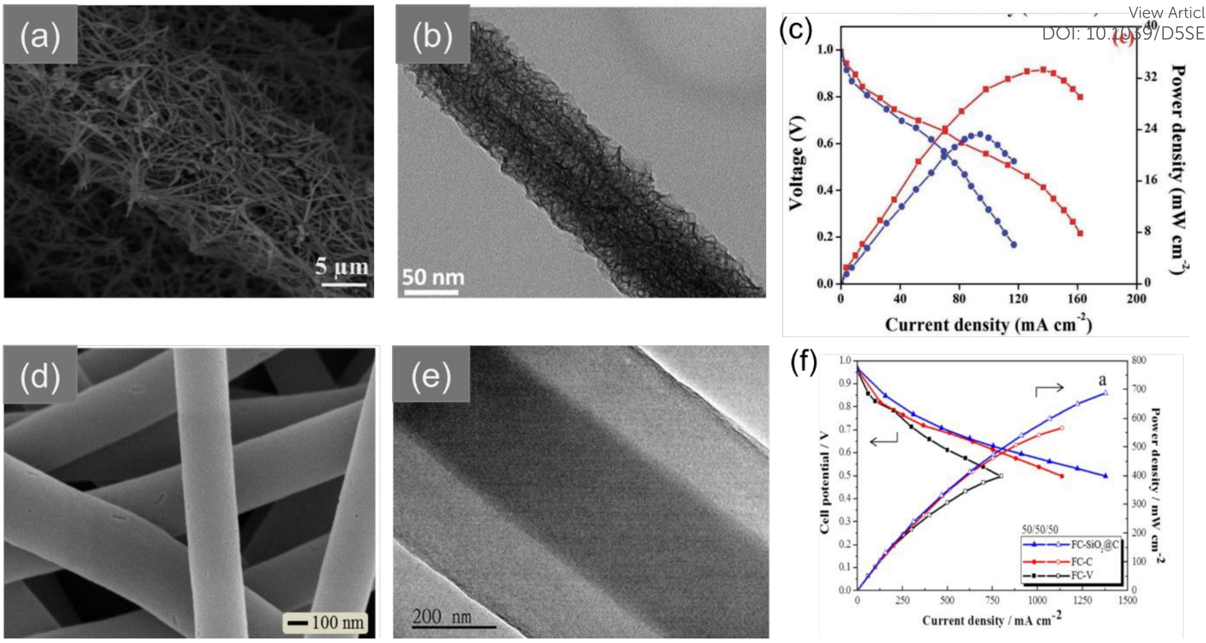

Figure 12. (a) SEM (b) TEM images of Co_3O_4@NiO nanofibers, (c) Polarization of the DUFCs with 50×10^{-3} m urea at RT. Figure 12 (a, b, c) adopted from ref. [234], Copyright© John Wiley and Sons- (2018). (d) SEM and (e) TEM image of SiO2@C core-shell nanofiber, (f) Polarization curves (I-V curves) and power density curves (I-P curves) of FC-V, FC-C, and FC-SiO_2@C under different operating cell at 50 °C. Figure 12 (d, e, f) adopted from ref. [235], Copyright© Springer- (2018).

View Article Online
DOI: 10.1039/D5SE01377A

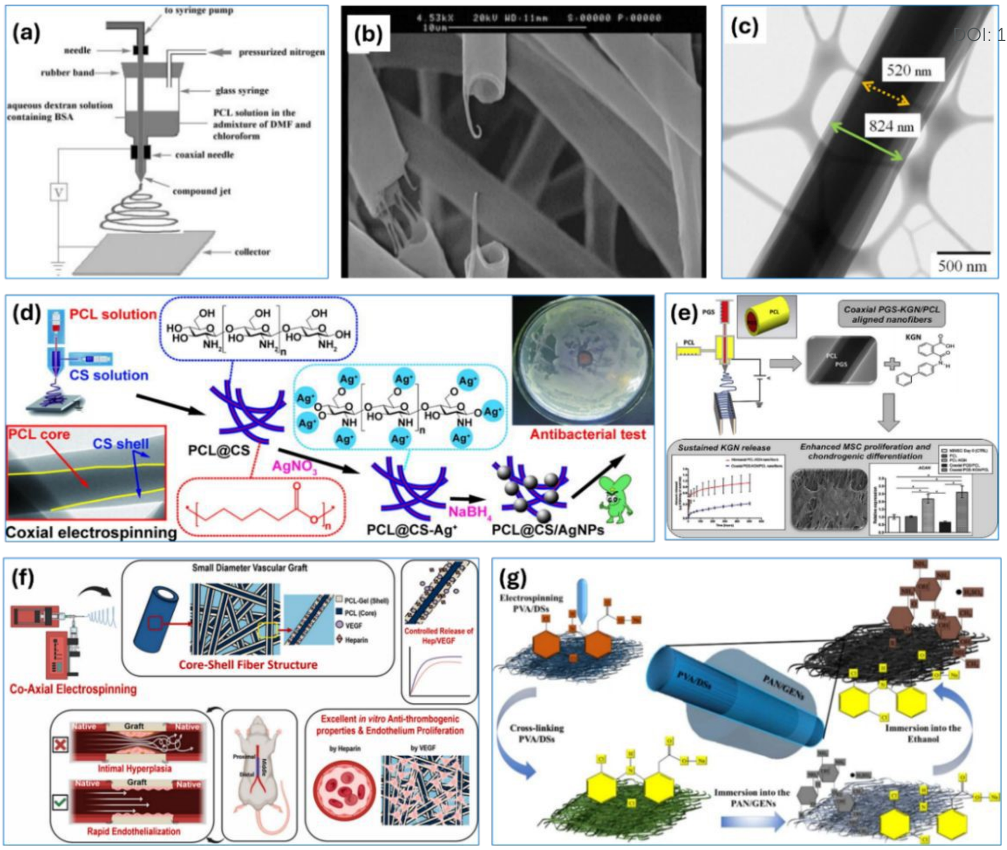

Figure 13. (a) Configuration of the coaxial electrospinning setup used for preparing core–shell structured fibers composed of PCL as shell and dextran containing BSA as core, (b) The morphology changes of the core–shell structured fibers during BSA release after 21 days. Figure 13 (a, b) adopted from ref. [242], Copyright© 2006 Wiley Periodicals, Inc., (c) TEM images of dual nanofibers (scale bar was 500 nm), Core solution: [PLGA, 0.5 wt%, chloroform (8): DMF (2)] (67%) + [TCH 5.94 wt%, methanol] (33%), 0.3 ml/h, shell solution: [PLGA, 2 wt%, chloroform (8): DMF (2)], 3 ml/h, 10 kV, 15 cm, adopted from ref. [243], Copyright© Society of Plastics Engineers-2013, (d) Coaxial electrospinning of polycaprolactone-chitosan for antibacterial activity, adopted from ref. [244], Copyright© 2016 Elsevier B.V. All rights reserved, (e) Kartogenin-loaded coaxial PGS/PCL aligned nanofibers for cartilage tissue engineering, adopted from ref. [250], Copyright© 2019 Elsevier B.V. All rights reserved. (f) Small-diameter vascular graft composed of core-shell structured micro-nanofibers for neointimal hyperplasia, adopted from ref. [251], Copyright© 2024 Elsevier Ltd. All rights reserved, (g) Illustration skims of core-shell nanofiber for dual simultaneous drug delivery, adopted from ref. [252].

View Article Online
DOI: 10.1039/D5SE01377A

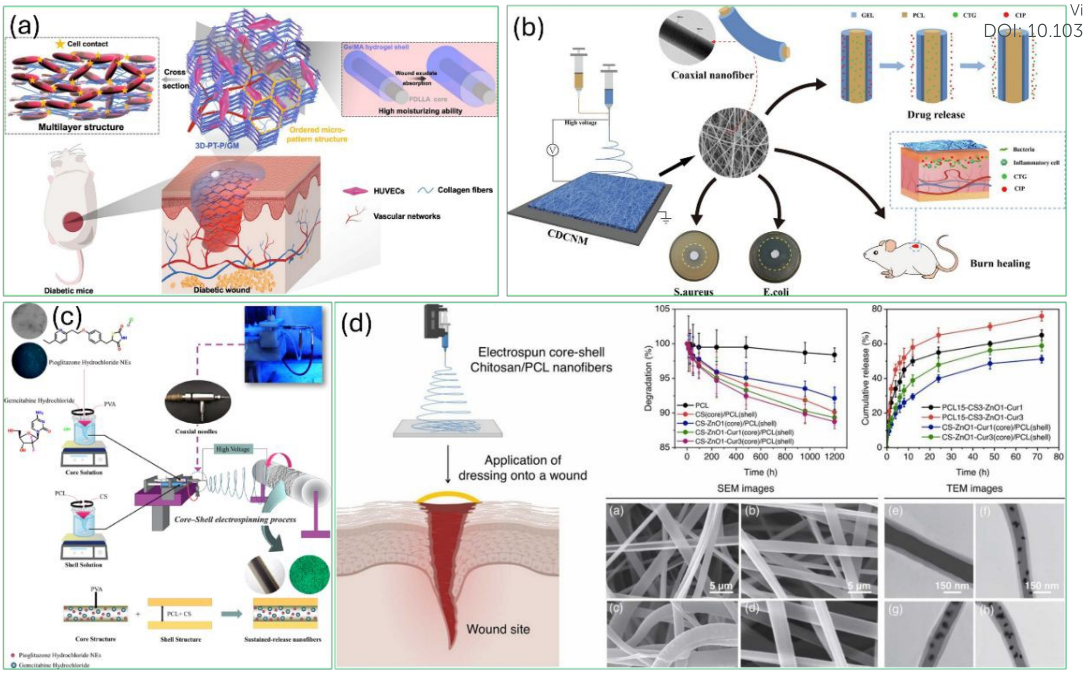

Figure 14. (a) Nanofiber/hydrogel core–shell scaffolds with three-dimensional multilayer patterned structure for accelerating diabetic wound healing, adapted from ref. [231], (b) Dual drug-loaded nanofiber membranes based on coaxial electrostatic spinning technology adopted from ref. [254], Copyright© 2022 Elsevier B.V. All rights reserved, (c) The schematic of nanofibers preparation for localized melanoma therapy delivering Pioglitazone nano emulsions and gemcitabine dual-loaded system, adopted from ref. [255], Copyright © 2025, Springer Nature, (d) Core-shell chitosan-polycaprolactone nanofibers for controlled curcumin release, adopted from ref. [256], Copyright© 2025 Elsevier B.V. All rights are reserved.

View Article Online
DOI: 10.1039/D5SE01377A

Table 1. Compilation of ME core–shell nanofiber structure, including diameter, ME coefficients/sensitivities, and application-specific characteristics.

Core–Shell System	Fiber Diameter	Core Diameter	Shell Thickness	ME Coefficient / Response	Notes	Ref. No.
$CoFe_2O_4$/PZT	200–400 nm	120–260 nm	40–140 nm	Demonstrated strain-mediated ME coupling via PFM	First experimental demonstration of electrospun ME core–shell fibers	[216]
$NiFe_2O_4/BaTiO_3$	150–300 nm	90–200 nm	40–100 nm	αME = 0.4 mV/cm·Oe; Magnetodielectric response	Prepared via coaxial sol–gel electrospinning	[217]
$NiFe_2O_4$/PZT	200–500 nm	150–350 nm	50–150 nm	CME coefficient = −24 Oe·cm/V (electric-field-induced FMR shift)	Validated converse ME effect via NSMM	[219]
Hexaferrite/$BaTiO_3$	300 nm	200–240 nm	40–80 nm	Strong ME voltage response under a magnetic field	Aligned mats exhibit device-scale ME coupling	[221]
$NdFeO_3$/PZT	128 nm	80–100 nm	20–40 nm	Direct ME coupling shown via P–E loop shift	Ultra-thin orthoferrite–PZT fibers	[222]
$CoFe_2O_4/BaTiO_3$	180–320 nm	120–220 nm	40–100 nm	αME = 346 mV/cm·Oe	Lead-free system; strong ME voltage peak	[224]
Hexaferrite ($Ba_2Zn_2Fe_{12}O_{22}$)/PZT	300 nm	200–260 nm	40–80 nm	ME sensitivity 650–730 V/T at ~8.3 kHz	Sensor-grade ME fibers; strong AC/DC ME response	[225]

View Article Online
DOI: 10.1039/D5SE01377A

Table 2. Overview of reported core–shell nanofiber systems for fuel-cell applications, highlighting structural parameters (fiber diameter, core diameter, shell thickness), device type, and key electrochemical performance metrics.

Core–Shell System	Fiber Diameter	Core Diameter	Shell Thickness	Fuel-Cell Type	Key Performance Highlights	Ref. No.
TiO_2 core – Carbon shell (TiO_2@C)	200–400 nm	~150–300 nm	~20–80 nm	DMFC / Methanol oxidation	7× higher oxidation current; strong photo-electrocatalytic enhancement	[231]
Functionalized CNF core – Pt shell nanoparticles (Pt/f-CNF)	250–400 nm	CNF core with uniformly anchored Pt	Thin f-C shell around CNF	DMFC	High CO tolerance; enhanced durability vs. Pt/C	[232]
Pt core – N-doped carbon shell on CNF support (Pt@C/CNF600)	Pt particles 3–4 nm; shell ~1 nm	3–4 nm Pt	1 nm N-doped carbon	PEMFC (cathode)	Excellent stability (30,000 AST); surpasses DOE targets; improved ORR	[233]
Co_3O_4 core – NiO shell (Co_3O_4@NiO)	100–250 nm	80–150 nm	20–60 nm	Direct Urea Fuel Cell (DUFC)	Power density: 33.8 mW cm^{-2} (urea), 23.2 mW cm^{-2} (urine); 120 h stability	[234]
Co_3O_4 core – MnO_2 shell (Co_3O_4@MnO_2)	120–260 nm	90–160 nm	~30–100 nm	DUFC	Enhanced bifunctional activity (OER/ORR); strong chemical stability	[234]
SiO_2 core – Carbon shell (SiO_2@C)	300–600 nm	200–350 nm	80–150 nm	PEMFC (Microporous Layer, MPL)	Strong hydrophilicity; improved water management; better conductivity	[235]
$Ce_{0.9}Gd_{0.1}O_{1.95}$ core – Cu-doped LSM shell (CGO@LSM)	150–300 nm (from SOFC cathode NF synthesis)	100–200 nm	30–80 nm	SOFC (Cathode)	Very low polarization resistance (1.7 Ωcm² @ 650°C)	[241]
PANI core – Pd/Pd–Ag/Pd–Bi catalyst shell polymer nanofibers	200–450 nm (PANI NF)	Conductive PANI	Pd, Pd–Ag, Pd–Bi nanoparticle shells	DEFC	Highest ethanol oxidation with Pd–Ag & Pd–Bi; high CO tolerance	[240]
Porous carbon network (GDE@GDL) with core–shell-like graded layers	Micro–nano hybrid	—	—	HT-PEMFC	21% higher Pt-normalized power density; improved O_2 diffusion	[239]

View Article Online
DOI: 10.1039/D5SE01377A

Table 3. Summary of core–shell nanofiber systems used in drug-delivery applications, including fiber diameters, core and shell dimensions, therapeutic payloads, and corresponding release behaviours.

Core–Shell System	Fiber Diameter	Core Diameter	Shell Thickness	Drug / Payload	Release Behavior	Ref.
PCL core – SF shell	200–450 nm	120–250 nm	50–150 nm	Clindamycin	Sustained release for wound healing	[163]
PCL/PVA or PCL/Col core–shell	200–600 nm	120–350 nm	80–150 nm	Biomedical drugs	Controlled/sustained	[165]
BSA–Dextran core – PCL-PEG shell	200–500 nm	120–300 nm	50–200 nm	BSA protein	Release adjustable (1 week – 1 month)	[242]
TCH core – PLGA/PLA shell	200–600 nm	150–350 nm	50–200 nm	Tetracycline	Sustained antibiotic release	[243]
CTG core – CIP shell	300–700 nm	200–450 nm	80–200 nm	Ceftazidime + Ciprofloxacin	Controlled dual-drug release; improved wound healing	[254]
PCL–CS/PVA core–shell	250–550 nm	150–300 nm	50–150 nm	PIO + GEM	Sustained (14 days)	[255]
Chitosan-PCL core–shell	250–600 nm	150–350 nm	50–200 nm	Curcumin	Antimicrobial; wound healing	[256]

View Article Online
DOI: 10.1039/D5SE01377A

Table 4. Comparison of Core-Shell Nanofiber Fabrication Techniques and Their Parameters

Parameters	**Coaxial electrospinning**	**Emulsion electrospinning**	**Self-assembly methods**		
			Single-nozzle phase-separation	**Block Copolymer self-assembly**	**Thermal Self-Organization**
Material loading	Core/Shell- 8–20 wt% each (independent solutions; need viscosity matching)	Total polymer -8–20 wt% (continuous phase); dispersed phase fraction 5–30% depending on core	- 8–20 wt% (Polymer solution for ES)	0.5–5 wt% (micelles); up to 10–20 wt% (gels)	Bulk preforms (100% solids)
Blend / block design.	Independent choice of core (magnetostrictive, drug, NP) and shell (piezo/structural polymer)	Core encapsulated via immiscible emulsion droplet; surfactant stabilizes phase boundaries	30–70% minor phase. Viscosity for shell/core ≳ 1–2	Volume fraction of the minority block = 0.2–0.35. $\chi N \gtrsim 10–15$	Pre-stacked core/shell glass or polymer with viscosity-matched layers
Operating field/force	Dual nozzle. High-voltage (HV)- 10–25 kV; Tip–collector 10–20 cm; Flow rate balance 0.2–1.0 mL/h	Single-nozzle. HV (10–25 kV); 10–20 cm; flow rate 0.2–1.0 mL/h (continuous phase dominates)	HV- 10–30 kV; tip–collector 10–20 cm; 0.2–1.0 mL/h	Ambient assembly; selective swelling; RT–80 °C	Thermal draw above softening/glass-T; ~180–230 °C (PVDF shell); higher for silica cores
Evaporation/ consolidation	Solvent evaporation for both streams; annealing removes the porosity and improves crystallinity	Solvent evaporation fixes the shell first; dispersed droplets lock in; annealing may remove surfactant.	Fast-evaporating solvent favours shell localization; anneal 60–500 °C (inorganics)	Solvent selectivity + drying drives segregation; optional NP incorporation.	No solvent; thermal relaxation after draw sets nano-geometry
Output geometry	Continuous fibers, typically 150–800 nm in diameter, with transparent concentric shells	Continuous mats; diameter. 100–700 nm; core domain size follows droplet size	Random mats; diameter. 100–800 nm typical nanofibers	Extracted nanofibers (discrete); morphology depends on χN	Kilometre-long arrays, 50 nm to 1 µm diameter.
Best for	Precise core–shell alignment, tunable diameter ratio, multifunctional innovative fibers for sensors	Encapsulation of bioactive proteins, or drugs, in scalable mats with phase-separation-driven shells for medical	Thin reactive shells, sensing, and simple tooling for biomedicals	Functional shells/cores; multi-NP hybrids and biomedical	Ultrahigh uniformity, photonics, scalable optical/electrical arrays for industry

View Article Online
DOI: 10.1039/D5SE01377A

References

1. B. A. Grzybowski, W. T. S. Huck, The nanotechnology of life-inspired systems, The nanotechnology of life-inspired systems. Nature Nanotech 11 (2016) 585–592. https://doi.org/10.1038/nnano.2016.116
2. M.T. Bohr, Nanotechnology goals and challenges for electronic applications, TNANO, 1 (2002) 56-62. https://doi.org/10.1109/TNANO.2002.1005426
3. M.-C. Daniel, D. Astruc, Gold Nanoparticles: Assembly, Supramolecular Chemistry, Quantum-Size-Related Properties, and Applications toward Biology, Catalysis, and Nanotechnology, Chem. Rev.,104(1) (2004) 293–346. https://doi.org/10.1021/cr030698+
4. C. P. Bean, J. D. Livingston, Superparamagnetism, J. Appl. Phys. 30 (1959) S120–S129. https://doi.org/10.1063/1.2185850
5. B. Bhushan, Nanotribology and nanomechanics of MEMS/NEMS and BioMEMS/BioNEMS materials and devices, Microelectron. Eng., 84(3) (2007) 387-412. https://doi.org/10.1016/j.mee.2006.10.059
6. U. Boudriot, R. Dersch, A. Greiner, J. H. Wendorff, Electrospinning Approaches Toward Scaffold Engineering—A Brief Overview, 30(10) (2006) 785-792. https://doi.org/10.1111/j.1525-1594.2006.00301.x
7. D. S. Katti, K. W. Robinson, F. K. Ko, C. T. Laurencin, Bioresorbable nanofiber-based systems for wound healing and drug delivery: Optimization of fabrication parameters, 70B(2) (2004) 286-296. https://doi.org/10.1002/jbm.b.30041
8. F. Mustafa, S. Andreescu, Nanotechnology-based approaches for food sensing and packaging applications, RSC Adv., 10 (2020) 19309-19336. https://doi.org/10.1039/D0RA01084G
9. J. Horne, L. McLoughlin, B. Bridgers, E. K. Wujcik, Recent developments in nanofiber-based sensors for disease detection, immunosensing, and monitoring, Sensors and Actuators Reports, 2 (2020) 100005. https://doi.org/10.1016/j.snr.2020.100005
10. G. T. V. Prabu, B. Dhurai, A Novel Profiled Multi-Pin Electrospinning System for Nanofiber Production and Encapsulation of Nanoparticles into Nanofibers, Sci Rep 10 (2020) 4302. https://doi.org/10.1038/s41598-020-60752-6
11. J.A. Nairn, Aspect ratio requirements for nanotube-reinforced, polymer–matrix composites, Compos Part A Appl Sci Manuf, 42 (2011) 1850-1855. https://doi.org/10.1016/j.compositesa.2011.08.012
12. S. Iwamoto, S.Lee, T. Endo, Relationship between aspect ratio and suspension viscosity of wood cellulose nanofibers, Polym. J., 46 (2014) 73–76 (2014). https://doi.org/10.1038/pj.2013.64
13. A. Frenot, I. S. Chronakis, Polymer nanofibers assembled by electrospinning, Curr. Opin. Colloid Interface Sci., 8 (2003) 64-75. https://doi.org/10.1016/S1359-0294(03)00004-9
14. J. Doshi, D. H. Reneker, Electrospinning process and applications of electrospun fibers, J. Electrost., 35 (1995) 151-160. https://doi.org/10.1016/0304-3886(95)00041-8
15. N. Bhardwaj, S. C. Kundu, Electrospinning: A fascinating fiber fabrication technique, Biotechnol Adv, 28 (2010) 325-347. https://doi.org/10.1016/j.biotechadv.2010.01.004
16. Y. Sun, S. Cheng, W. Lu, Y. Wang, P. Zhang, Q. Yao, Electrospun fibers and their application in drug-controlled release, biological dressings, tissue repair, and enzyme

immobilization, RSC Adv., 9 (2019) 25712-25729. https://doi.org/10.1039/C9RA05012D

17. M. K. Gaydhane, C. S. Sharma, S. Majum, Electrospun nanofibres in drug delivery: advances in controlled release strategies, RSC Adv., 13 (2023) 7312-7328. https://doi.org/10.1039/D2RA06023J
18. B. G. DJ, G. J. J. Wessley, A study on EMI shielding in aircraft: introduction, methods and significance of using electrospun nanocomposites, J. Space Saf. Eng., 11 (2024) 150-160. https://doi.org/10.1016/j.jsse.2024.01.001
19. M.S. Nisha, D. Singh, Manufacturing of Smart Nanomaterials for Structural Health Monitoring (SHM) in Aerospace Application Using CNT and CNF, J. Nano Res, 37 (2015) 42-50. https://doi.org/10.4028/www.scientific.net/JNanoR.37.42
20. M. Jurić, G. Goksen, F. Donsì, S. Jurić, Innovative Applications of Electrospun Nanofibers Loaded with Bacterial Cells Towards Sustainable Agri-Food Systems and Regulatory Compliance, Food Eng. Rev., 16 (2024) 270–303. https://doi.org/10.1007/s12393-024-09369-3
21. D. Martins, V. P. Scagion, R. Schneider, A. C. C. Lemos, J. Oliveira, D. S. Correa, Biodegradable Polymer Nanofibers Applied in Slow Release Systems for Agri-Food Applications. In: Gutiérrez, T. (eds) Polymers for Agri-Food Applications, 2019, Springer, Cham. https://doi.org/10.1007/978-3-030-19416-1_15
22. J. B. Moreira, S. G. Kuntzler, B. P. Vargas, A. A. Comitre, J. A. V. Costa, M. G. de Morais, Nanofiber-Reinforced Bionanocomposites in Agriculture Applications. In: Muthukumar, C., Thiagamani, S.M.K., Krishnasamy, S., Nagarajan, R., Siengchin, S. (eds) Polymer Based Bio-nanocomposites. Composites Science and Technology, 2022, Springer, Singapore. https://doi.org/10.1007/978-981-16-8578-1_17
23. T. Wang, Z. Chen, W. Gong, F. Xu, X. Song, X. He, M. Fan, Electrospun Carbon Nanofibers and Their Applications in Several Areas, ACS Omega, 8(25), 2023, 22316–22330. https://doi.org/10.1021/acsomega.3c01114
24. J. Xue, T. Wu, Y. Dai, Y. Xia, Electrospinning and Electrospun Nanofibers: Methods, Materials, and Applications, Chem. Rev., 119(8) (2019) 5298–5415. https://doi.org/10.1021/acs.chemrev.8b00593
25. I. G. Loscertales, A. Barrero, I. Guerrero, R. Cortijo, M. Marquez, A. M. Ganan-Calvo, Micro/Nano Encapsulation via Electrified Coaxial Liquid Jets, Science, 295(5560) (2002) 1695-1698. https://doi.org/10.1126/science.1067595
26. M. Yousefzadeh, F. Ghasemkhah, Design of Porous, Core-Shell, and Hollow Nanofibers. In: Barhoum, A., Bechelany, M., Makhlouf, A. (eds) Handbook of Nanofibers. Springer, Cham. https://doi.org/10.1007/978-3-319-42789-8_9-2
27. M. Yousefzadeh, S. Ramakrishna, Modeling performance of electrospun nanofibers and nanofibrous assembles. In: Ashanti M (ed) Electrospun nanofibers. Woodhwad Publishing, Cambridge, 2017, 303–337.https://doi.org/10.1016/B978-0-08-100907-9.00013-1
28. Seeram Ramakrishna, Kazutoshi Fujihara, Wee-Eong Teo, Thomas Yong, Zuwei Ma, Ramakrishna Ramaseshan, Electrospun nanofibers: solving global issues, Mater. Today., 9(3) 2006, 40-50. https://doi.org/10.1016/S1369-7021(06)71389-X
29. Y. Zhang, Z. Huang, X. Xu, C. T. Lim, Seeram Ramakrishna, Preparation of Core−Shell Structured PCL-r-Gelatin Bi-Component Nanofibers by Coaxial

Electrospinning, Chem. Mater., 16(18) (2004) 3406–3409. https://doi.org/10.1021/cm049580f

30. Y. Liu, X. Chen, Y. Gao, Y. Liu, D. Yu, P, Liu, Electrospun Core–Sheath Nanofibers with Variable Shell Thickness for Modifying Curcumin Release to Achieve a Better Antibacterial Performance, Biomolecules, 12 (2022) 1057. https://doi.org/10.3390/biom12081057
31. Y. Jiang, D. Fang, G. Song, J. Nie, B. Chen, G. Ma, Fabrication of core–shell nanofibers by single capillary electrospinning combined with vapor induced phase separation, New J. Chem., 37 (2013) 2917. https://doi.org/10.1039/c3nj00654a
32. D. Ponnamma, M. M. Chamakh, A. M. Alahzm, N. Salim, N. Hameed, M. Maadeed, Core-Shell Nanofibers of Polyvinylidene Fluoride-based Nanocomposites as Piezoelectric Nanogenerators. Polymers, 12 (2020) 2344. https://doi.org/10.3390/polym12102344
33. S. Taokaew, T. Chuenkaek, Developments of Core/Shell Chitosan-Based Nanofibers by Electrospinning Techniques: A Review, Fibers, 12 (2024) 26. https://doi.org/10.3390/fib12030026
34. L. Zhu, Y. Zheng, J. Fan, Y. Yao, Z. Ahmad, M.-W. Chang, A novel core-shell nanofiber drug delivery system intended for the synergistic treatment of melanoma, Eur. J. Pharm. Sci., 137 (2019) 105002. https://doi.org/10.1016/j.ejps.2019.105002
35. S. Mallick, K. R. B Singh, V. Nayak, J. Singh, R. P. Singh, Potentialities of core@shell nanomaterials for biosensor technologies, Mater. Lett., 306 (2022) 130912. https://doi.org/10.1016/j.matlet.2021.130912
36. D. Khomskii, Classifying multiferroics: mechanisms and effects, Physics 2 (2009) 20, https://doi.org/10.1103/physics.2.20
37. H. Palneedi, V. Annapureddy, S. Priya, J. Ryu, Status and perspectives of multiferroic magnetoelectric composite materials and applications, Actuators 5 (2016) 9, https://doi.org/10.3390/act5010009
38. J. Mundy, C. Brooks, M. Holtz, D.G. Schlom, Atomically engineered ferroic layers yield a room-temperature magnetoelectric multiferroic, Nature 537 (2016) 523–527, https://doi.org/10.1038/nature19343.
39. Y. Wang, J. Li, D. Viehland, Magnetoelectrics for magnetic sensor applications: status, challenges and perspectives, Mater. Today 17 (2014) 269–275, https://doi.org/10.1016/j.mattod.2014.05.004
40. D.I. Khomskii, Multiferroics: different ways to combine magnetism and ferroelectricity, J. Magn. Magn. Mater. 306 (2006) 1–8, https://doi.org/10.1016/j.jmmm.2006.01.238
41. L.W. Martin, S.P. Crane, Y.H. Chu, M.B. Holcomb, M. Gajek, M. Huijben, C.H. Yang, N. Balke, R. Ramesh, Multiferroics and magnetoelectrics: thin films and nanostructures, J. Phys. Condens. Matter 20 (2008) 434220, https://doi.org/10.1088/0953-8984/20/43/434220
42. H. Liu, X. Yang, A brief review on perovskite multiferroics, Ferroelectrics 507 (2017) 69–85, https://doi.org/10.1080/00150193.2017.1283171
43. W. Prellier, M.P. Singh, P. Murugavel, The single-phase multiferroic oxides: from bulk to thin film, J. Phys. Condens. Matter 17 (2005) R803, https://doi.org/10. 1088/0953-8984/17/30/R01

44. J. Zhang, W. Xue, T. Su, H. Ji, G. Zhou, F. Jiang, Z. Quan, X. Xu, Nanoscale magnetization reversal by magnetoelectric coupling effect in Ga 0.6 Fe 1.4 O 3 multiferroic thin films, ACS Appl. Mater. Interfaces 13 (2021) 18194–18201, https://doi.org/10.1021/acsami.0c21659
45. M. Niu, H. Zhu, Y. Wang, J. Yan, N. Chen, P. Yan, J. Ouyang, Integration-friendly, chemically stoichiometric BiFeO3 films with a piezoelectric performance challenging that of PZT, ACS Appl. Mater. Interfaces 12 (2020) 33899–33907, https://doi.org/10.1021/acsami.0c07155
46. C. Lu, M. Wu, L. Lin, J.M. Liu, Single-phase multiferroics: new materials, phenomena, and physics, Natl. Sci. Rev. 6 (2019) 653–668, https://doi.org/10.1093/ nsr/nwz091
47. H. Schmid, Some symmetry aspects of ferroics and single phase multiferroics, J. Phys. Condens. Matter 20 (2008) 434201, https://doi.org/10.1088/0953-8984/ 20/43/434201z
48. Y. Cheng, B. Peng, Z. Hu, Z. Zhou, M. Liu, Recent development and status of magnetoelectric materials and devices, Phys. Lett. 382 (2018) 3018–3025, https://doi.org/10.1016/j.physleta.2018.07.014.
49. X. Liang, H. Chen, N.X. Sun, Magnetoelectric materials and devices, Appl. Mater. 9 (2021) 41114, https://doi.org/10.1063/5.0044532
50. A. Jaiswal, I. Chakraborty, K. Roy, Energy-Efficient Memory Using Magneto-Electric Switching of Ferromagnets, IEEE Magnetics Letters, 8 (2017) 4306905. https://doi.org/10.1109/LMAG.2017.2712685
51. K. L. Wang, H. Lee, P. K. Amiri, Magnetoelectric Random Access Memory-Based Circuit Design by Using Voltage-Controlled Magnetic Anisotropy in Magnetic Tunnel Junctions, IEEE Transactions on Nanotechnology, 14 (2015) 992-997. https://doi.org/10.1109/TNANO.2015.2462337
52. Z. Fang, J. Jiao, H. Wu, T. Jiang, S. Fu, J. Cheng, O. Sokolov, S. Ivanov, M. Bichurin, F. Li, Y. Wang, Crafting very low frequency magnetoelectric antenna via piezoelectric and electromechanical synergic optimization strategy, Journal of Materiomics, 11(3) (2025) 100900. https://doi.org/10.1016/j.jmat.2024.05.010
53. T. Nan, H. Lin, Y. Gao, A. Matyushov, G. Yu, H. Chen, N. Sun, S. Wei, Z. Wang, M. Li, X. Wang, A. Belkessam, R. Guo, B. Chen, J. Zhou, Z. Qian, Y. Hui, M. Rinaldi, M. E. McConney, B. M. Howe, Z. Hu, J. G. Jones, G. J. Brown, N. X. Sun, Acoustically actuated ultra-compact NEMS magnetoelectric antennas, Nat Commun 8 (2017) 296. https://doi.org/10.1038/s41467-017-00343-8
54. C. Dong, C. Sun, L. Chen, Y. He, Y. Liu, B. Luo, N. X. Sun, Ultra-compact magnetoelectric sensor for femto-Tesla VLF signal reception, Mater. Today Electron., 11 (2025) 100135. https://doi.org/10.1016/j.mtelec.2025.100135
55. X. Hu, L. Zhang, Z. Wang, Y. Xiang, X. Chen, Z. Xue, Wireless driven and self-sensing flexible gripper based on piezoelectric elastomer/high-entropy alloy magnetoelectric composite, Chem. Eng. J., 498 (2024) 155415. https://doi.org/10.1016/j.cej.2024.155415
56. P. Yang, X. Hu, R. Li, Z. Zhou, Y. Gui, R. Sun, D. Wu, X. Wang, X. Bian, Flexible magnetoelectric sensors with enhanced output performance and response time for parking spaces detection systems, Sens. Actuators A: Phys., 382 (2025) 116161. https://doi.org/10.1016/j.sna.2024.116161
57. E. Spetzler, B. Spetzler, D. Seidler, J. Arbustini, L. Thormählen, E. Elzenheimer, M. Höft, A. Bahr, D. Meyners, J. McCord, On the Origin of Signal and Bandwidth of

View Article Online
DOI: 10.1039/D5SE01377A

Converse Magnetoelectric Magnetic Field Sensors, 4 (2025) 2400109. https://doi.org/10.1002/adsr.202400109

58. L. Zimoch, S. Schröder, E. Elzenheimer, S. Kaps, T. Strunskus, F. Faupe, M. Höft, R. Adelung, Electret integrated magnetic field sensor based on magnetostrictive polymer composite with nT resolution, Sci Rep 15 (2025) 1561. https://doi.org/10.1038/s41598-024-85069-6
59. Y. Qiu, Q. Zhong, Y. Zhou, J. An, Y. Li, A. Song, J. Wang, G. Yu, M. Zhu, Y. Wu, H. Zhou, A Low Conductivity Medium Detection Module Based on Magnetoelectric Sensors, IEEE TRANSACTIONS on Instrumentation and measurement, 4 (2025) 6007509. https://doi.org/10.1109/TIM.2025.3561443
60. X. Xu, W. Wu, T. Zhu, M. Pei, X. Zhang, Q. Han, High-performance magnetoelectric composite with low DC bias magnetic field for detecting ultra-weak magnetic field, Compos. Commun., 56 (2025) 102371. https://doi.org/10.1016/j.coco.2025.102371
61. J. Shen, J. Cong, D. Shang, Y. Chai, S. Shen, K. Zhai, Y. Sun, A multilevel nonvolatile magnetoelectric memory, Sci Rep, 6 (2016) 34473. https://doi.org/10.1038/srep34473
62. N. Rangarajan, S. Patnaik, J. Knechtel, O. Sinanoglu, S. Rakheja, SMART: A Secure Magnetoelectric Antiferromagnet-Based Tamper-Proof Non-Volatile Memory, IEEE Access, 8 (2020) 76130 – 76142. https://doi.org/10.1109/ACCESS.2020.2988889
63. M. Müller, Y.-Lin Huang, S. Vélez, R. Ramesh, M. Fiebig, M. Trassin, Training the Polarization in Integrated La0.15Bi0.85FeO3-Based Devices, Advanced Materials, 33 (2021) 2104688. https://doi.org/10.1002/adma.202104688
64. J. Ma, J. Hu, Z. Li, C.-W. Nan, Recent Progress in Multiferroic Magnetoelectric Composites: from Bulk to Thin Films, Advanced Materials, 23 (2011) 1035-1165. https://doi.org/10.1002/adma.201003636
65. N. A. Spaldin, R. Ramesh, Advances in magnetoelectric multiferroics, Advances in magnetoelectric multiferroics. Nature Mater 18 (2019) 203–212 (2019). https://doi.org/10.1038/s41563-018-0275-2
66. C. A. F. Vaz, J. Hoffman, C.H. Ahn, R. Ramesh, Magnetoelectric Coupling Effects in Multiferroic Complex Oxide Composite Structures, 22 (2010) 2900-2918. https://doi.org/10.1002/adma.200904326
67. C.-hong Lin, Y.-Chuan Lin, Magnetoelectric coupling in nonlinear three-phase composites: A micromechanical study, International Journal of Mechanical Sciences, 299 (2025) 110425. https://doi.org/10.1016/j.ijmecsci.2025.110425
68. Y. Li, Z. Wang, J. Yao, T. Yang, Z. Wang, J.-Mian Hu, C. Chen, R. Sun, Z. Tian, J. Li, L.-Qing Chen, D. Viehland, Magnetoelectric quasi-(0-3) nanocomposite heterostructures, Nat Commun, 6 (2015) 6680. https://doi.org/10.1038/ncomms7680
69. A. Kumar, D. Kaur, Magnetoelectric heterostructures for next-generation MEMS magnetic field sensing applications, Journal of Alloys and Compounds, 897 (2022) 163091. https://doi.org/10.1016/j.jallcom.2021.163091
70. D. K. Pradhan, S. Kumari, R. K. Vasudevan, E. Strelcov, V. S. Puli, D. K. Pradha, A. Kumar, J. M. Gregg, A. K. Pradhan, Sergei V. Kalinin, R. S. Katiyar, Exploring the Magnetoelectric Coupling at the Composite Interfaces of FE/FM/FE Heterostructures, Sci Rep 8, 17381 (2018). https://doi.org/10.1038/s41598-018-35648-1
71. S. Ryu, J. H. Park, H. M. Jang, Magnetoelectric coupling of [00l]-oriented $Pb(Zr_{0.4}Ti_{0.6})O_3$-$Ni_{0.8}Zn_{0.2}Fe_2O_4$ multilayered thin films, Appl. Phys. Lett. 91 (2007) 142910. https://doi.org/10.1063/1.2798054

72. G.-Liang Yu, H.-Wu Zhang, F.-Ming Bai, Y.-Xun Li, J. Li, Theoretical investigation of magnetoelectric effect in multilayer magnetoelectric composites, Compos. Struct., 119 (2015) 738-748. https://doi.org/10.1016/j.compstruct.2014.09.049
73. A. C. Lima, N. Pereira, R. Policia, C. Ribeiro, V. Correia, S. Lanceros-Mendez, P. Martins, All-printed multilayer materials with improved magnetoelectric response, J. Mater. Chem. C, 7 (2019) 5394-5400. https://doi.org/10.1039/C9TC01428D
74. G. Srinivasan, E. T. Rasmussen, J. Gallegos, R. Srinivasan, Yu. I. Bokhan, V. M. Laletin, Magnetoelectric bilayer and multilayer structures of magnetostrictive and piezoelectric oxides, Phys. Rev. B 64 (2001) 2144080. https://doi.org/10.1103/PhysRevB.64.214408
75. Y. Wang, J. Xu, Y. Shen, C.-ai Wang, Z. Zhang, F. Li, J. Cheng, Y. Ye, R. Shen, Fabrication of energetic aluminum core/hydrophobic shell nanofibers via coaxial electrospinning, Chem. Eng. J., 427 (2022) 132001. https://doi.org/10.1016/j.cej.2021.132001
76. J. Hu, Y. Liu, S. Zhang, B. Tang, Novel designed core–shell nanofibers constituted by single element-doped BaTiO3 for high-energy–density polymer nanocomposites, Chem. Eng. J., 428 (2022) 131046. https://doi.org/10.1016/j.cej.2021.131046
77. A. Almasian, M. Giahi, G. C. Fard, S.A. Dehdast, L. Maleknia, Removal of heavy metal ions by modified PAN/PANI-nylon core-shell nanofibers membrane: Filtration performance, antifouling and regeneration behavior, Chem. Eng. J., 351 (2018) 1166-1178. https://doi.org/10.1016/j.cej.2018.06.127
78. J. Zhang, S. Li, D.-D. Ju, X. Li, J.-C. Zhang, X. Yan, Y.-Z Long, F. Song, Flexible inorganic core-shell nanofibers endowed with tunable multicolor upconversion fluorescence for simultaneous monitoring dual drug delivery, Chem. Eng. J., 349 (2018) 554-561. https://doi.org/10.1016/j.cej.2018.05.112
79. Y. Liu, G. Sreenivasulu, P. Zhou, J. Fu, D. Filippov, W. Zhang, T. Zhou, T. Zhang, Piyush Shah, M. R. Page, Gopalan Srinivasan, S. Berweger, T. M. Wallis, P. Kabos, Converse magneto-electric effects in a core–shell multiferroic nanofiber by electric field tuning of ferromagnetic resonance, Sci Rep 10 (2020) 20170. https://doi.org/10.1038/s41598-020-77041-x
80. L. F. Henrichs, X. Mu, T. Scherer, U. Gerhards, S. Schuppler, P. Nagel, M. Merz, C. Kübel, M. H. Fawey, T. C. Hansen, H. Hahn, First-time synthesis of a magnetoelectric core–shell composite via conventional solid-state reaction, Nanoscale, 12, (2020) 15677. https://doi.org/10.1039/d0nr02475a
81. G. Schileo, Recent developments in ceramic multiferroic composites based on core/shell and other heterostructures obtained by sol-gel routes, Progress in Solid State Chemistry, 41 (2013) 87-98. https://doi.org/10.1016/j.progsolidstchem.2013.09.001
82. V. J. Folen, G. T. Rado, E. W. Stalder, Anisotropy of the Magnetoelectric Effect in Cr_2O_3, Phys. Rev. Lett. 6 (1961) 607. https://doi.org/10.1103/PhysRevLett.6.607
83. J. Wang, J. B. Neaton, H. Zheng, V. Nagarajan, S. B. Ogale, B. Liu, D. Viehland, V. Vaithyanathan, D. G. Schlom, U. V. Waghmare, N. A. Spaldin, K. M. Rabe, M. Wuttig, R. Ramesh, Epitaxial BiFeO3 Multiferroic Thin Film Heterostructures, Science, 299 (2003) 1719-1722. https://doi.org/10.1126/science.1080615
84. C.-Y. Kuo, Z. Hu, J.C. Yang, S.-C. Liao, Y.L. Huang, R.K. Vasudevan, M.B. Okatan, S. Jesse, S.V. Kalinin, L. Li, H.J. Liu, C.-H. Lai, T.W. Pi, S. Agrestini, K. Chen, P.

Ohresser, A. Tanaka, L.H. Tjeng, Y.H. Chu, Single-domain multiferroic $BiFeO_3$ films, Nat Commun 7 (2016) 12712. https://doi.org/10.1038/ncomms12712
85. A. M. Kadomtseva, S. S. Krotov, Yu. F. Popov, G. P. Vorob'ev, Features of the magnetoelectric behavior of the family of multiferroics RMn_2O_5 at high magnetic fields (Review), Low Temp. Phys. 32 (2006) 709–724. https://doi.org/10.1063/1.2219494
86. B. Kh. Khannanov, V. A. Sanina, E. I. Golovenchits, M.P. Scheglov, Electric polarization induced by phase separation in magnetically ordered and paramagnetic states of RMn_2O_5 (R=Gd, Bi), J. Magn. Magn. Mater., 421 (2017) 326-335. https://doi.org/10.1016/j.jmmm.2016.08.040
87. T. Kimura, G. Lawes, T. Goto, Y. Tokura, A. P. Ramirez, Magnetoelectric phase diagrams of orthorhombic RMnO$_3$ (R=Gd, Tb, and Dy), Phys. Rev. B, 71 (2005) 224425. https://doi.org/10.1103/PhysRevB.71.224425
88. G.E. Tongue Magne, R.M. Keumo Tsiaze, A.J. Fotué, N.M. Hounkonnou, L.C. Fai, Cumulative effects of fluctuations and magnetoelectric coupling in two-dimensional $RMnO_3$ (R = Tb, Lu and Y) multiferroics, Phys. Lett. A, 400 (2021) 127305. https://doi.org/10.1016/j.physleta.2021.127305
89. R. Ramesh, Making metallic memories, Nature Nanotech 5 (2010) 761–762. https://doi.org/10.1038/nnano.2010.218
90. S. A. Wolf, J. Lu, M. R. Stan, E. Chen, D. M. Treger, The Promise of Nanomagnetics and Spintronics for Future Logic and Universal Memory, Proceedings of the IEEE, 98 (2010) 2155-2168. https://doi.org/10.1109/JPROC.2010.2064150
91. J. Atulasimha, S. Bandyopadhyay, Bennett clocking of nanomagnetic logic using multiferroic single-domain nanomagnets, Appl. Phys. Lett. 97 (2010) 173105. https://doi.org/10.1063/1.3506690
92. N A Pertsev, H Kohlstedt, Resistive switching via the converse magnetoelectric effect in ferromagnetic multilayers on ferroelectric substrates, Nanotechnology, 21 (2010) 475202. https://doi.org/10.1088/0957-4484/21/47/475202
93. C. Nan, M. I. Bichurin, S. Dong, D. Viehland, G. Srinivasan, Multiferroic magnetoelectric composites: Historical perspective, status, and future directions, J. Appl. Phys. 103 (2008) 031101. https://doi.org/10.1063/1.2836410
94. J. Ma, J. Hu, Z. Li, C. Nan, Recent Progress in Multiferroic Magnetoelectric Composites: from Bulk to Thin Films, Adv. Mater., 23 (2011) 1062-1087. https://doi.org/10.1002/adma.201003636
95. Y. F. Popov, A. M. Kadomtseva, G. P. Vorob'ev, A. K. Zvezdin, Discovery of the linear magnetoelectric effect in magnetic ferroelectric $BiFeO_3$ in a strong magnetic field. Ferroelectrics, 162(1) (1994) 135–140. https://doi.org/10.1080/00150199408245098
96. W. Eerenstein, N. D. Mathuar, J. F. Scott, Multiferroic and magnetoelectric materials, Nature, 442 (2006) 759–765. https://doi.org/10.1038/nature05023
97. S. K. Yadav, P. D. Prasad, A. Soosairaj, K. Divya, A. A. Arunmozhi, L. R. Asirvatham, V S. Manikandan, M. Navaneethan, A. Thirumurugan, Study on the Structural, Magnetic, and Magnetodielectric Properties of M-type $BaFe_{12}O_{19}$ and $SrFe_{12}O_{19}$ Hexaferrite Nanoparticles, Surf. Interfaces. 52 (2024) 104956. https://doi.org/10.1016/j.surfin.2024.104956
98. S. K. Yadav, P. D. Prasad, A. Soosairaj, K. Divya, A. A. Arunmozhi, L. R. Asirvatham, V S. Manikandan, M. Navaneethan, A. Thirumurugan, Investigation of Magnetocapacitance and Magnetoconductivity in Single-Phase Y-Type Hexaferrite

$Ba_2Co_2Fe_{12}O_{22}$ Nanoparticles, Surf. Interfaces. 54 (2024) 105162. https://doi.org/10.1016/j.surfin.2024.105162

99. M. I. Bichurin, V. M. Petrov, Theory of low-frequency magnetoelectric coupling in magnetostrictive-piezoelectric bilayers, Physical Review B, 68 (2003) 054402. https://doi.org/10.1103/PhysRevB.68.054402
100. G.-L. Yu, H.-W. Zhang, F.-M. Bai, Y.-X. Li, J. Li, Theoretical investigation of magnetoelectric effect in multilayer magnetoelectric composites, Compos. Struct., 119 (2015) 738-748. https://doi.org/10.1016/j.compstruct.2014.09.049
101. I. A. Osaretin, R. G. Rojas, Theoretical model for the magnetoelectric effect in magnetostrictive/piezoelectric composites, Phys. Rev. B, 82 (2010) 174415. https://doi.org/10.1103/PhysRevB.82.174415
102. Y. Wang, D. Hasanyan, M. Li, J. Gao, J. Li, D. Viehland, H. Luo, Theoretical model for geometry-dependent magnetoelectric effect in magnetostrictive/piezoelectric composites, J. Appl. Phys. 111 (2012) 124513. https://doi.org/10.1063/1.4729832
103. N. Pakam, A. Arockiarajan, An analytical model for predicting the effective properties of magneto-electro-elastic (MEE) composites, Comput. Mater. Sci., 65 (2012) 19-28. https://doi.org/10.1016/j.commatsci.2012.07.003
104. H. Hong, K. Bi, Y.G. Wang, Magnetoelectric performance in Ni/Pb(Zr,Ti)O_3/FeCo trilayered cylindrical composites, J. Alloys Compd., 545 (2012) 182-185. https://doi.org/10.1016/j.jallcom.2012.08.048
105. X. H. Ge, H. Ji, Y. Li, J. K. Chen, Y. G. Wang, Diameter and sequence effects on magnetoelectric effect in FeCo/Pb(Zr,Ti)O_3/Ni trilayered long cylindrical composite structures, J. Alloys Compd., 752 (2018) 303-307. https://doi.org/10.1016/j.jallcom.2018.04.153
106. H .Q. Shen, Y. G. Wang, D. Xie, J. H. Cheng, Magnetoelectric effect in FeCo/PMN-PT/FeCo trilayers prepared by electroless deposition of FeCo on PMN-PT crystals with various orientations, J. Alloys Compd., 610 (2014) 11-14. https://doi.org/10.1016/j.jallcom.2014.04.221
107. J. Shi, M. Wu, W. Hu, C. Lu, X. Mu, J. Zhu, A study of high piezomagnetic (Fe-Ga/Fe-Ni) multilayers for magnetoelectric device, J. Alloys Compd., 806 (2019) 1465-1468. https://doi.org/10.1016/j.jallcom.2019.07.265
108. S. U. Jen, Y. C. Chen, Field annealing effect on magnetostriction and sensitivity of the ferromagnetic $Fe_{60}Co_{18}Ga_{22}$/Si(100) film, J. Magn. Magn. Mater., 466 (2018) 55-59. https://doi.org/10.1016/j.jmmm.2018.05.092
109. S. W. Meeks, J. C. Hill, Piezomagnetic and elastic properties of metallic glass alloys $Fe_{67}CO_{18}B_{14}Si_1$ and $Fe_{81}B_{13.5}Si_{3.5}C_2$, J. Appl. Phys. 54 (1983) 6584–6593. https://doi.org/10.1063/1.331893
110. D. A. Petrov, V. S. Leontiev, G. A. Semenov, S. N. Ivanov, O. V. Sokolov, A. I. Kozonov, K. A. Syrovarova, K. V. Semenova, M. I. Bichurin, The study of the Metglas/GaAs/Metglas magnetostrictive-piezo-semiconductive structure for practical application, J. Phys.: Conf. Ser. 2052 (2021) 012032. https://doi.org/10.1088/1742-6596/2052/1/012032
111. T. Deng, Z. Chen, W. Di, B. Fang, H. Luo, Enhancement magnetoelectric effect in Metglas-Fe by annealing, Appl. Phys. A 127 (2021) 899. https://doi.org/10.1007/s00339-021-05045-z

112. D. Davino, A. Giustiniani, C. Visone, The piezo-magnetic parameters of Terfenol-D: An experimental viewpoint, Physica B: Condensed Matter, 407 (2012) 1427-1432. https://doi.org/10.1016/j.physb.2011.05.059

113. Chien-hong Lin, Ying-Zhao Lin, Analysis of nonlinear piezomagnetism for magnetostrictive terfenol-D composites, J. Magn. Magn. Mater., 540 (2021) 168490. https://doi.org/10.1016/j.jmmm.2021.168490

114. Z. Chen, Y. Su, S. A. Meguid, The effect of field-orientation on the magnetoelectric coupling in Terfenol-D/PZT/Terfenol-D laminated structure, J. Appl. Phys. 116 (2014) 173910. https://doi.org/10.1063/1.4901069

115. G. Jian, F. Xue, C. Zhang, C. Yan, N. Zhao, C.P. Wong, Orientation dependence of elastic and piezomagnetic properties in $NiFe_2O_4$, JJ. Magn. Magn. Mater., 442 (2017) 141-144. https://doi.org/10.1016/j.jmmm.2017.06.103

116. A. Aubert, V. Loyau, F. Mazaleyrat, M. LoBue, Investigation of Piezomagnetism in Nickel Ferrite, IEEE Sens. J., 23 (2023) 5660–5669. https://doi.org/10.1109/JSEN.2023.3237910

117. A. D. Sheikh, V. L. Mathe, Effect of the piezomagnetic $NiFe_2O_4$ phase on the piezoelectric $Pb(Mg_{1/3}Nb_{2/3})_{0.67}Ti_{0.33}O_3$ phase in magnetoelectric composites, Smart Mater. Struct. 18 (2009) 065014. https://doi.org/10.1088/0964-1726/18/6/065014

118. K. V. Siva, S. Sudersan, A. Arockiarajan, Bipolar magnetostriction in $CoFe_2O_4$: Effect of sintering, measurement temperature, and prestress, J. Appl. Phys. 128 (2020) 103904. https://doi.org/10.1063/5.0021796

119. M. V. Reddy, A. Lisfi, S. Pokhare, D. Das, Colossal piezomagnetic response in magnetically pressed Zr^{+4} substituted cobalt ferrites, Sci Rep 7, (2017) 7935. https://doi.org/10.1038/s41598-017-08160-1

120. Z. Gubinyi, C. Batur, A. Sayir, F. Dynys, Electrical properties of PZT piezoelectric ceramic at high temperatures, J Electroceram 20 (2008) 95–105. https://doi.org/10.1007/s10832-007-9364-3

121. N. Izyumskaya, Y.-I. Alivov, S.-J. Cho, H. Morko¸ H. Lee, Y. S. Kang, Processing, Structure, Properties, and Applications of PZT Thin Films, Critical Reviews in Solid State and Materials Sciences, 32 (2007) 111–202. https://doi.org/10.1080/10408430701707347

122. G. L. Smith, J. S. Pulskamp, L. M. Sanchez, D. M. Potrepka, R. M. Proie, T. G. Ivanov, R. Q. Rudy, W. D. Nothwang, S. S. Bedair, C. D. Meyer, R. G. Polcawich, PZT-Based Piezoelectric MEMS Technology, J. Am. Ceram. Soc., 95(6) (2012) 1777–1792. https://doi.org/10.1111/j.1551-2916.2012.05155.x

123. J.-M. Kiat, Y. Uesu, B. Dkhil, M. Matsuda, C. Malibert, G. Calvarin, Monoclinic structure of unpoled morphotropic high piezoelectric PMN-PT and PZN-PT compounds, Phys. Rev. B 65 (2002) 064106. https://doi.org/10.1103/PhysRevB.65.064106

124. S. Xu, Y.-W. Yeh, G. Poirier, M. C. McAlpine, R. A. Register, N. Yao, Flexible Piezoelectric PMN–PT Nanowire-Based Nanocomposite and Device, Nano Lett. 13(6) (2013) 2393–2398. https://doi.org/10.1021/nl400169t

125. A. Hall, M. Allahverdi, E.K. Akdogan, A. Safari, Piezoelectric/electrostrictive multimaterial PMN-PT monomorph actuators, Journal of the European Ceramic Society, 25(12) (2005) 2991-2997. https://doi.org/10.1016/j.jeurceramsoc.2005.03.196

126. T. Kobayashi, M Ichiki, R Kondou, K Nakamura, R Maeda, Fabrication of piezoelectric microcantilevers using LaNiO3 buffered Pb(Zr,Ti)O3 thin film, J. Micromech. Microeng. 18 (2018) 035007. https://doi.org/10.1088/0960-1317/18/3/035007

127. P. W. Jaschin, R. Bhimireddi, K. B. R. Varma, Enhanced Dielectric Properties of $LaNiO_3$/$BaTiO_3$/PVDF: A Three-Phase Percolative Polymer Nanocrystal Composite, ACS Appl. Mater. Interfaces,10(32) (2018) 27278–27286. https://doi.org/10.1021/acsami.8b07786

128. Y. Wang, H. Cheng, Y. Shi, T. Nishikado, I. Kanno, High performance $LaNiO_3$-buffered, (001)-oriented PZT piezoelectric films integrated on (111) Si, Appl. Phys. Lett. 121 (2022) 182902. https://doi.org/10.1063/5.0107526

129. M. Acosta, N. Novak, V. Rojas, S. Patel, R. Vaish, J. Koruza, G. A. Rossetti, Jr., J. Rödel, $BaTiO_3$-based piezoelectrics: Fundamentals, current status, and perspectives, Appl. Phys. Rev. 4 (2017) 041305. https://doi.org/10.1063/1.4990046

130. D. Ghosh, A. Sakata, J. Carter, P.A. Thomas, H. Han, J. C. Nino, J. L. Jones, Domain Wall Displacement is the Origin of Superior Permittivity and Piezoelectricity in $BaTiO_3$ at Intermediate Grain Sizes, Adv. Funct. Mater., 24(7) (2014) 885-896. https://doi.org/10.1002/adfm.201301913

131. A. Iqbal, F. M.-Yasin, Reactive Sputtering of Aluminum Nitride (002) Thin Films for Piezoelectric Applications: A Review, Sensors, 18(6) (2018) 1797. https://doi.org/10.3390/s18061797

132. C. M. Lueng, H. L. W. Chan, C. Surya, C. L. Choy, Piezoelectric coefficient of aluminum nitride and gallium nitride, J. Appl. Phys. 88 (2000) 5360–5363. https://doi.org/10.1063/1.1317244

133. S. T. Haider, M. A. Shah, D.-G. Lee, S. Hur, A Review of the Recent Applications of Aluminum Nitride-Based Piezoelectric Devices, IEEE Access, 11 (2023) 58779 – 58795. https://doi.org/10.1109/ACCESS.2023.3276716

134. S. Mohammadpourfazeli, S. Arash, A. Ansari, S. Yang, K. Mallick, R. Bagherzadeh, Future prospects and recent developments of polyvinylidene fluoride (PVDF) piezoelectric polymer; fabrication methods, structure, and electro-mechanical properties, RSC Adv., 13 (2023) 370-387. https://doi.org/10.1039/D2RA06774A

135. Z. Feng, Z. Zhao, Y. Liu, Y. Liu, X. Cao, D.-G. Yu, K. Wang, Piezoelectric Effect Polyvinylidene Fluoride (PVDF): From Energy Harvester to Smart Skin and Electronic Textiles, Adv. Mater. Technol., 8(11) (2023) 2300021. https://doi.org/10.1002/admt.202300021

136. Y. Fu, E. C Harvey, M. K Ghantasala, G. M Spinks, Design, fabrication and testing of piezoelectric polymer PVDF microactuators, Smart Mater. Struct. 15 (2006) S141. https://doi.org/10.1088/0964-1726/15/1/023

137. D. P. Pabba, N. Ram, J. Kaarthik, V. R. Bhaviripudi, S. K. Yadav, A. Soosairaj, N. K. Pabba, V. Annapureddy, A. Thirumurugan, H.S. Panda, R. Aepuru, assessing mechanical and stray magnetic field energy harvesting capabilities in lead-free

PVDF/BCT-BZT composites integrated with Metglas, Ceram. Int., 50 (2024) 33009-33017. https://doi.org/10.1016/j.ceramint.2024.06.115

138. D. Viehland, M. Wuttig, J. McCord, E. Quandt, Magnetoelectric magnetic field sensors, MRS Bulletin 43 (2018) 834–840. https://doi.org/10.1557/mrs.2018.261

139. D. Saveliev, D. Chashin, L. Fetisov, M. Shamonin, Y. Fetisov, Ceramic-Heterostructure-Based Magnetoelectric Voltage Transformer with an Adjustable Transformation Ratio, Materials, 2020, 13(18) (2020) 3981. https://doi.org/10.3390/ma13183981

140. F. Narita, M. Fox, A Review on Piezoelectric, Magnetostrictive, and Magnetoelectric Materials and Device Technologies for Energy Harvesting Applications, Adv. Eng. Mater., 20(5) (2018) 1700743. https://doi.org/10.1002/adem.201700743

141. S. Dong, J. Zhai, Z. Xing, J.-F. Li, D. Viehland, Extremely low frequency response of magnetoelectric multilayer composites, Appl. Phys. Lett., 86 (2005) 102901-102905. https://doi.org/10.1063/1.1881784

142. J. Zhai, Z. Xing, S. Dong, J. Li, D. Viehland, Detection of pico Tesla magnetic fields using magneto electric sensors at room temperature, Appl. Phys. Lett., 88 (2006) 062510-062520. https://doi.org/10.1063/1.2172706

143. M. Li, A. Matyushov, C. Dong, H. Chen, H. Lin, T. Nan, Z. Qian, M. Rinaldi, Y. Lin, N. X. Sun, Ultra-sensitive NEMS magnetoelectric sensor for picotesla DC magnetic field detection, Appl. Phys. Lett. 110, (2017) 143510. https://doi.org/10.1063/1.4979694

144. D.T. H. Giang, N.H. Duc, Magnetoelectric sensor for microtesla magnetic fields based on $(Fe_{80}Co_{20})_{78}Si_{12}B_{10}$/PZT laminates, Sens. Actuator A Phys., 149 (2009) 229–232. https://doi.org/10.1016/j.sna.2008.12.003

145. Z. Chu, C. Dong, C. Tu, X. Liang, H. Chen, C. Sun, Z. Yu, S. Dong, N.-X. Sun, A low power and high sensitivity magnetic field sensor based on converse magnetoelectric effect, Appl. Phys. Lett., 115 (2019) 162901-162910. https://doi.org/10.1063/1.5122774

146. R. Carvalho, S. Lanceros-Mendez, P. Martins, Tailoring polymer-based magnetoelectrics for spintronics: Evaluating the converse effect, Appl. Mater. Today, 38 (2024) 102216. https://doi.org/10.1016/j.apmt.2024.102216

147. Y.-M. Jia, F.-F. Wang, X.-Y. Zhao, H.-S. Luo, S. W. Or, H. L. W. Chan, Converse magnetoelectric effects in piezoelectric–piezomagnetic layered composites, Compos Sci Technol, 68(6) (2008) 1440-1444. https://doi.org/10.1016/j.compscitech.2007.10.046

148. G. Srinivasan, Y. K. Fetisov, Microwave Magnetoelectric Effects and Signal Processing Devices, Integr. Ferroelectr., 83 (2006) 89-98. https://doi.org/10.1080/10584580600949105

149. W. Kleemann, Multiferroic and magnetoelectric nanocomposites for data processing, Phys. D: Appl. Phys. 50 92017) 223001. https://doi.org/10.1088/1361-6463/aa6c04

View Article Online
DOI: 10.1039/D5SE01377A

150. W. Yinan, E. Song, Y. Wang, D. Su, X. Guo, Z. Ma, Dual-drive DC magnetic sensor based on converse magnetoelectric coupling effect, J. Appl. Phys. 137 (2025) 124505. https://doi.org/10.1063/5.0260874

151. Y. Chen, T. Fitchorov, A. L. Geiler, J. Gao, C. Vittoria, V. G. Harris, Dynamic response of converse magnetoelectric effect in a PMN-PT-based multiferroic heterostructure, Appl Phys A, 100 (2010) 1149–1155. https://doi.org/10.1007/s00339-010-5726-9

152. Y. Jia, S. W. Or, H. L. W. Chan, X. Zhao, H. Luo, Converse magnetoelectric effect in laminated composites of PMN–PT single crystal and Terfenol-D alloy, Appl. Phys. Lett. 88 (2006) 242902. https://doi.org/10.1063/1.2212054

153. S. Wongprasod, N. Tanapongpisit, P. Laohana, T. M. Huyen Nguyen, H. Q. Van, S. Kim, S. Srikam, S. Sonsupap, N. Chanlek, M. Horprathum, A. Khamkongkaeo, S. Maensiri, W. Meevasana, C. Wung Bark, W. Saenrang, Porous Electrospun Carbon Nanofibers Bearing TiO2 Hollow Nanospheres for Supercapacitor Electrodes, ACS Appl. Nano Mater., 7(6) (2024) 6712–6721. https://doi.org/10.1021/acsanm.4c00922

154. A. Mamun, M. Kiari, L. Sabantina, Recent Review of Electrospun Porous Carbon Nanofiber Mats for Energy Storage and Generation Applications. Membranes. 13(10) (2023) 830. https://doi.org/10.3390/membranes13100830

155. S. Shin, Y. Yoon, S. Park, M. W. Shin, Fabrication of core-shell structured cobalt nanoparticle/carbon nanofiber as a bifunctional catalyst for the oxygen reduction/evolution reactions, J. Alloy. Compd., 939 (2023) 168731. https://doi.org/10.1016/j.jallcom.2023.168731

156. Jinghe Bai, Defeng Zhou, Xiaofei Zhu, Ning Wang, Ruyi Chen, Bolin Wang, New SOFC Cathode: 3D Core–Shell-Structured La0.6Sr0.4Co0.2Fe0.8O3−δ@PrO2−δ Nanofibers Prepared by Coaxial Electrospinning, ACS Appl. Energy Mater., 5(9) (2022) 11178–11190. https://doi.org/10.1021/acsaem.2c01782

157. Malihe Ghazalian, Shahnoosh Afshar, Amir Rostami, Shiva Rashedi, Seyed Hajir Bahrami, Fabrication and characterization of chitosan-polycaprolactone core-shell nanofibers containing tetracycline hydrochloride, Colloids Surf. A Physicochem. Eng. Asp., 636 (2022) 128163. https://doi.org/10.1016/j.colsurfa.2021.128163

158. Shiva Rashedi, Shahnoosh Afshar, Amir Rostami, Malihe Ghazalian, Hossein Nazockdast, Co-electrospun poly(lactic acid)/gelatin nanofibrous scaffold prepared by a new solvent system: morphological, mechanical and in vitro degradability properties, Int. J. Polym. Mater. Polym. Biomater., 70(8) (2021) 545–553. https://doi.org/10.1080/00914037.2020.1740987

159. Elham Hajiani, Shahriar Osfouri, Reza Azin, Sasan Zaeri, Amir Rostami, Sustained release of phenytoin from jellyfish collagen-based electrospun nanofibers: A wound dressing candidate with promising cell compatibility, J Drug Deliv Sci Tec, 112 (2025) 107183. https://doi.org/10.1016/j.jddst.2025.107183

160. Ruiliang Ge, Yuexin Ji, Yanfei Ding, Chang Huang, Hua He, Deng-Guang Yu, Electrospun self-emulsifying core-shell nanofibers for effective delivery of paclitaxel, Front. Bioeng. Biotechnol., 11 (2023). https://doi.org/10.3389/fbioe.2023.1112338

161. Yongzhen Li, 1, Jia Du, Xuejiao Sun, Dawei Lan, Jinlong Cui, Hu Zhao, Yongqiang Zhang, Wenxiu He, Preparation of TiO2/nitrogen-doped CNF composites as high-performance lithium-ion battery anodes by electrospinning, J. Cryst. Growth, 624 (2023) 127417. https://doi.org/10.1016/j.jcrysgro.2023.127417

View Article Online
DOI: 10.1039/D5SE01377A

162. A. Greiner, J. H. Wendorff, Electrospinning: A Fascinating Method for the Preparation of Ultrathin Fibers, Angew. Chem. Int. Ed., 46(30) (2007) 5670-5703. https://doi.org/10.1002/anie.200604646

163. N. R. Tanha, M. Nouri, Core-shell Nanofibers of Silk Fibroin/Polycaprolactone-Clindamycin: Study on Nanofibers Structure and Controlled Release Behavior, Polym. Sci. Ser. A 61 (2019) 85–95 (2019). https://doi.org/10.1134/S0965545X19010085

164. C. Jiang, J. Nie, G. Ma, A polymer/metal core–shell nanofiber membrane by electrospinning with an electric field, and its application for catalyst support, RSC Adv., 6 (2016) 22996. https://doi.org/10.1039/c5ra27687j

165. P. Moradipour, M. Limoee, S. Janfaza, L. Behbood, Core‑Shell Nanofibers Based on Polycaprolactone/Polyvinyl Alcohol and Polycaprolactone/Collagen for Biomedical Applications, J. Pharm. Innov., 17 (2022) 911–920. https://doi.org/10.1007/s12247-021-09568-z

166. Y. Liu, P. Zhou, B. Ge, J. Liu, J. Zhang, W. Zhang, T. Zhang, G. Srinivasan, Strain-Mediated Magneto-Electric Effects in Coaxial Nanofibers of Y/W-Type Hexagonal Ferrites and Ferroelectrics, J. Compos. Sci. 5 (2021) 268. https://doi.org/10.3390/jcs5100268

167. M. Abasalta, A. Asefnejad, M. T. Khorasani, A. R. Saadatabadi, M. Irani, Adsorption and sustained release of doxorubicin from N-carboxymethyl chitosan/polyvinyl alcohol/poly(ε-caprolactone) composite and core-shell nanofibers, J. Drug. Deliv. Sci. Technol., 67 (2022) 102937. https://doi.org/10.1016/j.jddst.2021.102937

168. E. Korina, O. Stoilova, N. Manolova, I. Rashkov, Polymer fibers with magnetic core decorated with titanium dioxide prospective for photocatalytic water treatment, J. Environ. Chem. Eng., 6(2) 2018 2075-2084. https://doi.org/10.1016/j.jece.2018.03.016

169. J. K. Park, O.-V. P.-Nguyen, H. S. Yoo, Coaxial Electrospun Nanofibers with Different Shell Contents to Control Cell Adhesion and Viability, ACS Omega, 5(43) (2020) 28178–28185. https://doi.org/10.1021/acsomega.0c03902

170. M. Zhang, C. Liu, B. Li, Y. Shen, H. Wang, K. Ji, X. Mao, L. Wei, R. Sun, F. Zhou, Electrospun PVDF-based piezoelectric nanofibers: materials, structures, and applications, Nanoscale Adv., 5 (2023) 1043-1059. https://doi.org/10.1039/D2NA00773H

171. R. Singh, F. Ahmed, P. Polley, J. Giri, Fabrication and Characterization of Core–Shell Nanofibers Using a Next-Generation Airbrush for Biomedical Applications, ACS Appl. Mater. Interfaces, 10(49) (2018) 41924–41934. https://doi.org/10.1021/acsami.8b13809

172. M.-R. Norouzi, L. G.-Mobarakeh, F. Itel, J. Schoeller, H. Fashandi, A. Borzi, A. Neels, G. Fortunato, R. M. Rossi, Emulsion electrospinning of sodium alginate/poly(ε-caprolactone) core/shell nanofibers for biomedical applications, Nanoscale Adv., 4 (2022) 2929-2941. https://doi.org/10.1039/D2NA00201A

173. M. Naeimirad, A. Zadhoush, R. Kotek, R. E. Neisiany, S. N. Khorasani, S. Ramakrishna, Recent advances in core/shell bicomponent fibers and nanofibers: A review, Journal of Applied Polymer Science, 135 (2018) 46265. https://doi.org/10.1002/app.46265

174. K. Jalaja, D. Naskar, S. C. Kundu, N. R. James, Potential of electrospun core–shell structured gelatin–chitosan nanofibers for biomedical applications, Carbohydr. Polym., 136 (2016) 1098-1107. https://doi.org/10.1016/j.carbpol.2015.10.014

175. A. L. Yarin, Coaxial electrospinning and emulsion electrospinning of core–shell fibers, Polymers for Advanced Technologies, 22 (2011) 310-317. https://doi.org/10.1002/pat.1781

176. B. Abadi, N. Goshtasbi, S. Bolouria, J. Tahsili, M. A.-Sardou, H. Forootanfar, Electrospun hybrid nanofibers: Fabrication, characterization, and biomedical applications, Front. Bioeng. Biotechnol., 10 (2022). https://doi.org/10.3389/fbioe.2022.986975

177. B. Rezaei, M. Ghani, M. Askari, A. M. Shoushtari, R. M. A. Malek, Fabrication of Thermal Intelligent Core/Shell Nanofibers by the Solution Coaxial Electrospinning Process, Adv. Polym. Technol., 2015. https://doi.org/10.1002/adv.21534

178. S. N. Reznik, A. L. Yarin, E. Zussman, L. Bercovici, Evolution of a compound droplet attached to a core-shell nozzle under the action of a strong electric field, Phys. Fluids., 18 (2006) 062101. https://doi.org/10.1063/1.2206747

179. A. K. Moghe, B. S. Gupta, Co-axial Electrospinning for Nanofiber Structures: Preparation and Applications, Polym Rev, 48 (2008) 353-377. https://doi.org/10.1080/15583720802022257

180. N. E. Zander, Hierarchically Structured Electrospun Fibers, Polymers, 5(1) (2013) 19-44. https://doi.org/10.3390/polym5010019

181. D. Han, A. J. Steckl, Coaxial Electrospinning Formation of Complex Polymer Fibers and their Applications, ChemPlusChem, 84(10) (2019) 1453-1497. https://doi.org/10.1002/cplu.201900281

182. N. R. Tanha, M. Nouri, An experimental study on the coaxial electrospinning of silk fibroin/poly(vinyl alcohol)–salicylic acid core-shell nanofibers and process optimization using response surface methodology, Journal of Industrial Textiles, 48(5) (2017) 884-903. https://doi.org/10.1177/1528083717747334

183. A. S. Motamedi, H. Mirzadeh, F. Hajiesmaeilbaigi, S. B.-Khoulenjani, M. Al. Shokrgozar, Effect of electrospinning parameters on morphological properties of PVDF nanofibrous scaffolds. Prog Biomater 6 (2017) 113–123. https://doi.org/10.1007/s40204-017-0071-0

184. M. Kashif, S. Rasul, M. M. Mohideen, Y. Liu, Advancing Electrochemical Energy Storage: A Review of Electrospinning Factors and Their Impact, Energies, 18(9) (2025) 2399. https://doi.org/10.3390/en18092399

185. C. Li, Q. Li, X. Ni, G. Liu, W. Cheng, G. Han, Coaxial Electrospinning and Characterization of Core-Shell Structured Cellulose Nanocrystal Reinforced PMMA/PAN Composite Fibers, Materials, 10(6) (2017) 572. https://doi.org/10.3390/ma10060572

186. G. I. Taylor, Electrically driven jets, Proc. R. Soc. Lond. A313453–475. http://doi.org/10.1098/rspa.1969.0205

187. W. E. Teo, S. Ramakrishna, A review on electrospinning design and nanofibre assemblies, Nanotechnology, 17 (2006) R89. http://doi.org/10.1088/0957-4484/17/14/R01

188. P. Koushki, S. H. Bahrami, M. R.-Mohammadi, Coaxial nanofibers from poly(caprolactone)/ poly(vinyl alcohol)/Thyme and their antibacterial properties,

View Article Online
DOI: 10.1039/D5SE01377A

Journal of Industrial Textiles. 47(5) (2016) 834-852. http://doi.org/10.1177/1528083716674906

189. J. Hu, S. Zhang, B. Tang, Rational design of nanomaterials for high energy density dielectric capacitors via electrospinning, Energy Stor. Mater., 37 (2021) 530-555. https://doi.org/10.1016/j.ensm.2021.02.035

190. H. Fong, I. Chun, D. H. Reneker, Beaded nanofibers formed during electrospinning, Polymer, 40 (1999) 4585-4592. https://doi.org/10.1016/S0032-3861(99)00068-3

191. O. O. Dosunmu, G. G. Chase, W. Kataphinan, D. H. Reneker, Electrospinning of polymer nanofibres from multiple jets on a porous tubular surface, Nanotechnology 17 (2006) 1123. https://doi.org/10.1088/0957-4484/17/4/046

192. T. Subbiah, G. S. Bhat, R. W. Tock, S. Parameswaran, S. S. Ramkumar, Electrospinning of nanofibers, J. Appl. Polym. Sci., 96(2) (2005) 557-569. https://doi.org/10.1002/app.21481

193. Z.-M. Huang, Y.-Z. Zhang, M. Kotaki, S. Ramakrishna, A review on polymer nanofibers by electrospinning and their applications in nanocomposites, Compos Sci Technol, 63(15) (2003) 2223-2253. https://doi.org/10.1016/S0266-3538(03)00178-7

194. D. H. Reneker, A. L. Yarin, Electrospinning jets and polymer nanofibers, Polymer 49(10) (2008) 2387-2425. https://doi.org/10.1016/j.polymer.2008.02.002

195. D. Li, Y. Xia, Electrospinning of Nanofibers: Reinventing the Wheel? Adv. Mater., 16(14) (2004) 1151-1170. https://doi.org/10.1002/adma.200400719

196. W. E. Teo, M. Kotaki, X. M. Mo, S. Ramakrishna, Porous tubular structures with controlled fibre orientation using a modified electrospinning method, Nanotechnology 16 (2005) 918. https://doi.org/10.1088/0957-4484/16/6/049

197. A. Khalf, S. V. Madihally, Recent advances in multiaxial electrospinning for drug delivery, Eur. J. Pharm. Biopharm., 112 (2017) 1-17. https://doi.org/10.1016/j.ejpb.2016.11.010

198. A. Mickova, M. Buzgo, O. Benada, M. Rampichova, Z. Fisar, E. Filova, M. Tesarova, D. Lukas, E. Amler, Core/Shell Nanofibers with Embedded Liposomes as a Drug Delivery System, Biomacromolecules, 13(4) (2012) 952–962. https://doi.org/10.1021/bm2018118

199. Y. Lu, J. Huang, G. Yu, R. Cardenas, S. Wei, E. K. Wujcik, Z. Guo, Coaxial electrospun fibers: applications in drug delivery and tissue engineering, WIREs Nanomed Nanobiotechnol, 8 (2016) 654–677. https://doi.org/10.1002/wnan.1391

200. M. Liu, X. Hao, Y. Wang, Z. Jiang, H. Zhang, A biodegradable core-sheath nanofibrous 3D hierarchy prepared by emulsion electrospinning for sustained drug release, J Mater Sci 55 (2020) 16730–16743. https://doi.org/10.1007/s10853-020-05205-1

201. X. Xu, X. Zhuang, X. Chen, X. Wang, L. Yang, X. Jing, Preparation of Core-Sheath Composite Nanofibers by Emulsion Electrospinning, Macromol. Rapid Commun., 27(19) (2006) 1637-1642. https://doi.org/10.1002/marc.200600384

202. G. F. Elfawal, A. O.Šišková, A. E. Andicsová, Electrospinning: A Game-Changer in Fiber Production and Practical Applications, Fibers Polym (2025). https://doi.org/10.1007/s12221-025-01105-w

203. N. Nikmarama, S. Roohinejad, S. Hashemic, M. Koubaa, F. J. Barba, A. Abbaspourrad, R. Greiner, Emulsion-based systems for fabrication of electrospun

nanofibers: food, pharmaceutical and biomedical applications, RSC Adv., 7 (2017) 28951-28964. https://doi.org/10.1039/C7RA00179G

204. C. Zhang, F. Feng, H. Zhang, Emulsion electrospinning: Fundamentals, food applications and prospects, Trends Food Sci. Technol., 80 (2018) 175-186. https://doi.org/10.1016/j.tifs.2018.08.005

205. H. Cheng, X. Yang, X. Che, M. Yang, G. Zhai, Biomedical application and controlled drug release of electrospun fibrous materials, Mater. Sci. Eng. C, 90 (2018) 750-763. https://doi.org/10.1016/j.msec.2018.05.007

206. M. F. Abdullah, T. Nuge, A. Andriyana, B. C. Ang, F. Muhamad, Core–Shell Fibers: Design, Roles, and Controllable Release Strategies in Tissue Engineering and Drug Delivery, Polymers, 11(12) (2019) 2008. https://doi.org/10.3390/polym11122008

207. Y. Wang, D.-Guang Yu, Y. Liu, Y.-Nan Liu, Progress of Electrospun Nanofibrous Carriers for Modifications to Drug Release Profiles, J. Funct. Biomater., 13(4) (2022) 289. https://doi.org/10.3390/jfb13040289

208. Š. Zupančič, Core-shell nanofibers as drug delivery systems, Acta Pharm. 69 (2019) 131-153. https://doi.org/10.2478/acph-2019-0014

209. S. Ghosh, A. K. Yadav, P. M. Gurave, R. K. Srivastava, Unique Fiber Morphologies from Emulsion Electrospinning—A Case Study of Poly(ε-caprolactone) and Its Applications, Colloids Interfaces, 2023, 7(1) (2023) 19. https://doi.org/10.3390/colloids7010019

210. Y. Cho, J. W. Baek, M. Sagong, S.l Ahn, J. S. Nam, Il-Doo Kim, Electrospinning and Nanofiber Technology: Fundamentals, Innovations, and Applications, Adv. Mater., 37(28) (2025) 2500162. https://doi.org/10.1002/adma.202500162

211. J. Hu, M. P. Prabhakaran, X. Ding, S. Ramalrishna, Emulsion electrospinning of polycaprolactone: influence of surfactant type towards the scaffold properties, J. Biomater. Sci. Polym., 26 (2015) 57-75. https://doi.org/10.1080/09205063.2014.982241

212. D. Liu, Q. Shi, S. Jin, Y. Shao, J. Huang, Self-assembled core-shell structured organic nanofibers fabricated by single-nozzle electrospinning for highly sensitive ammonia sensors, InfoMat. 1 (2019) 525–532. https://doi.org/10.1002/inf2.12036

213. S. Sanwaria, S. Singh, A. Horechyy, P. Formanek, M. Stamm, R. Srivastavaa, B. Nandan, Multifunctional core–shell polymer–inorganic hybrid nanofibers prepared via block copolymer self-assembly, RSC Adv., 5 (2015) 89861. https://doi.org/10.1039/c5ra17161j

214. T. Khudiyev, O. Tobail, M. Bayindir, Tailoring self-organized nanostructured morphologies in kilometer-long polymer fiber, Sci Rep, 4 (2014) 4864. https://doi.org/10.1038/srep04864

215. S. Saha, S. Acharya, Y. Liu, P. Zhou, M. R. Page, G. Srinivasan, Review of Magnetoelectric Effects on Coaxial Fibers of Ferrites and Ferroelectrics, Appl. Sci., 15 (2025) 5162. https://doi.org/10.3390/app15095162

216. S. Xie, F. Ma, Y. Liu, J. Li, Multiferroic $CoFe_2O_4$–$Pb(Zr_{0.52}Ti_{0.48})O_3$ core-shell nanofibers and their magnetoelectric coupling, Nanoscale, 3 (2011) 3152. https://doi.org/10.1039/C1NR10288E

View Article Online
DOI: 10.1039/D5SE01377A

217. G. Sreenivasulu, J. Zhang, R. Zhang, M. Popov, V. Petrov, G. Srinivasan, Multiferroic Core-Shell Nanofibers, Assembly in a Magnetic Field, and Studies on Magneto-Electric Interactions, Materials, 11 (2018) 18. https://doi.org/10.3390/ma11010018

218. V. M. Petrov, J Zhang, H Qu, P Zhou, T Zhang, G Srinivasan, Theory of magnetoelectric effects in multiferroic core–shell nanofibers of hexagonal ferrites and ferroelectrics, 2018 J. Phys. D: Appl. Phys., 51 (2018) 284004. https://doi.org/10.1088/1361-6463/aac56f

219. Y. Liu, G. Sreenivasulu, P. Zhou, J. Fu, D. Filippov, W. Zhang, T. Zhou, T. Zhang, Piyush Shah, M. R. Page, G. Srinivasan, S. Berweger, T. M. Wallis, P. Kabos, Converse magneto‑electric effects in a core–shell multiferroic nanofiber by electric field tuning of ferromagnetic resonance, Sci Rep 10 (2020) 20170. https://doi.org/10.1038/s41598-020-77041-x

220. K. Shahzad, M. A. Abbasi, M. H. Rafe, A. Pestereva, F. Ullah, M. Zaman, M. Irfan, M. Afzal, A. Orlova, Doxorubicin-loaded core@shell cobalt ferrite-barium titanate magnetoelectric nanofibers for improved anticancer activity, 2025 Biomed. Mater. 20 015021. https://doi.org/10.1088/1748-605X/ad971e

221. B. Ge, J. Zhang, S. Saha, S. Acharya, C. Kshirsagar, S. Menon, M. Jain, M. R. Page, Gopalan Srinivasan, Evidence for a Giant Magneto-Electric Coupling in Bulk Composites with Coaxial Fibers of Nickel–Zinc Ferrite and PZT, J. Compos. Sci. 8 (2024) 309. https://doi.org/10.3390/jcs8080309

222. S. K. Yadav, J. Hemalatha, Electrospinning, and characterization of magnetoelectric $NdFeO_3$–$PbZr_{0.52}Ti_{0.48}O_3$ Core–Shell nanofibers, Ceram. Int., 48 (2022) 18415-18424. https://doi.org/10.1016/j.ceramint.2022.03.110

223. S. K. Yadav, J. Hemalatha, Direct magnetoelectric and magnetodielectric studies of electrospun $Ba_2Ni_2Fe_{12}O_{22}$–$Pb(Zr_{0.52}Ti_{0.48})O_3$ core–shell nanofibers, J. Magn. Magn. Mater., 564 (2022) 170174. https://doi.org/10.1016/j.jmmm.2022.170174

224. Y. Hadouch, D. Mezzane, M. Amjoud, V. Laguta, K. Hoummada, V. O. Dolocan, M. Jouiad, M. Lahcini, H. Uršič, V. Fišinger, N. Novak, Z. Kutnjak, Y. Gagou, I. Lukyanchuk, M. E. Marssi, Multiferroic $CoFe_2O_4$–$Ba_{0.95}Ca_{0.05}Ti_{0.89}Sn_{0.11}O_3$ Core–Shell Nanofibers for Magnetic Field Sensor Applications, ACS Appl. Nano Mater., 12(6) (2023) 10236–10245. https://doi.org/10.1021/acsanm.3c01101

225. S. K. Yadav, J. Hemalatha, Synthesis and characterization of magnetoelectric $Ba_2Zn_2Fe_{12}O_{22}$–$PbZr_{0.52}Ti_{0.48}O_3$ electrospun core–shell nanofibers for the AC/DC magnetic field sensor application, Appl. Phys. A., 130 (2024) 67. https://doi.org/10.1007/s00339-023-07158-z

226. B. Iskandarani, N. R. Mojarrad, A. Yürüm, S. A. Gürsel, B. Y. Kaplan, Electrospun Nanofiber Electrodes for Boosted Performance and Durability at Lower Humidity Operation of PEM Fuel Cells, Energy Fuels, 36 (2022) 9282−9294. https://doi.org/10.1021/acs.energyfuels.2c01595

227. S. Kabir, T. V. Cleve, S. K. Khandavalli, S. Medina, S. Pylypenko, S. Mauger, M. Ulsh, K.C. Neyerlin, Toward Optimizing Electrospun Nanofiber Fuel Cell Catalyst Layers: Microstructure and Pt Accessibility, ACS Appl. Energy Mater., 4 (2021) 3341−3351. https://doi.org/10.1021/acsaem.0c03073

228. S. K. Khandavalli, N. S.-Nene, S. Kabir, S. Sur, J. P. Rothstein, K. C. Neyerlin, S. A. Mauger, M. Ulsh, Toward Optimizing Electrospun Nanofiber Fuel Cell Catalyst Layers: Polymer−Particle Interactions and Spinnability, ACS Appl. Polym. Mater., 3 (2021) 2374−2384. https://doi.org/10.1021/acsapm.0c01354

229. N. Liu, S. Bi, Y. Zhang, Y. Ou, C. Gong, J. Ran, Y. Chen, Y. Yang, Nanofiber-based polymer electrolyte membranes for fuel cells, Carbon Energy.7 (2025) 7, e677. https://doi.org/10.1002/cey2.677

230. V. Kallina, F. Hasché, M. Oezaslan, Advanced design of electrospun nanofiber cathode catalyst layers for PEM fuel cells at low humidity, Curr Opin Electrochem, 47 (2024) 101559. https://doi.org/10.1016/j.coelec.2024.101559

231. W. Li, Y. Bai, F. Li, C. Liu, K.-Yu Chan, X. Feng, X. Lu, Core–shell TiO2/C nanofibers as supports for electrocatalytic and synergistic photo electrocatalytic oxidation of methanol, J. Mater. Chem., 22 (2012) 4025. https://doi.org/10.1039/c2jm14847a

232. B. Singh, E. Dempsey, Exceptional Pt nanoparticle decoration of functionalised carbon nanofibers: a strategy to improve the utility of Pt and support material for direct methanol fuel cell applications, RSC Advances, 3 (2013) 2279. https://doi.org/10.1039/c2ra21862c

233. M. Karuppannan, Y. Kim, S. Gok, E. Lee, J. Y. Hwang, J.-H. Jang, Y.-H. Cho, T. Lim, Y.-E. Sung, O. J. Kwon, A highly durable carbon-nanofiber-supported Pt–C core–shell cathode catalyst for ultra-low Pt loading proton exchange membrane fuel cells: facile carbon encapsulation, Energy Environ. Sci., 12 (2019) 2820. https://doi.org/10.1039/c9ee01000a

234. N. Senthilkumar, G. G. kumar, A. Manthiram, 3D Hierarchical Core–Shell Nanostructured Arrays on Carbon Fibers as Catalysts for Direct Urea Fuel Cells, Adv. Energy Mater. 8 (2018) 8, 1702207. https://doi.org/10.1002/aenm.201702207

235. H.-Fan Lee, P.-Chin Wang, Y. Whei C.-Yang, An electrospun hygroscopic and electron-conductive core-shell silica@carbon nanofiber for microporous layer in proton-exchange membrane fuel cell, J. Solid State Electrochem., 23 (2019) 971–984. https://doi.org/10.1007/s10008-019-04198-5

236. Y. Choi, H.-Jin Cho, J. Kim, J.-Y. Kang, J. Seo, J. H. Kim, S. J. Jeong, D.-K. Lim, Il-doo Kim, W. Jung, Nanofiber Composites as Highly Active and Robust Anodes for Direct-Hydrocarbon Solid Oxide Fuel Cells, ACS Nano, 16 (2022) 14517−14526. https://doi.org/10.1021/acsnano.2c04927

237. J. Yang, J. Wang, L. Fu, K. Wu, Z. Liu, K.Wu, J. Zhou, Electrospun Core−Shell Fibers for High-Efficient Composite Cathode-Based Solid Oxide Fuel Cells, Energy Fuels, 35 (2021) 1768−1778. https://dx.doi.org/10.1021/acs.energyfuels.0c02953

238. D. Lee, S. Gok, Y. Kim, Y.-E. Sung, E. Lee, J.-H. Jang, J. Y. Hwang, O. J. Kwon, T. Lim, Methanol Tolerant Pt−C Core−Shell Cathode Catalyst for Direct Methanol Fuel Cells, ACS Appl. Mater. Interfaces, 12 (2020) 44588−44596. https://dx.doi.org/10.1021/acsami.0c07812

239. O. Delikaya, N. Bevilacqua, L. Eifert, U. Kunz, R. Zeis, C. Roth, Porous electrospun carbon nanofibers network as an integrated electrode@gas diffusion layer for high temperature polymer electrolyte membrane fuel cells, Electrochim. Acta, 345 (2020) 136192. https://doi.org/10.1016/j.electacta.2020.136192

View Article Online
DOI: 10.1039/D5SE01377A

240. A. Symillidis, S. Georgiadou, W.-F. Lin, Conductive core/shell polymer nanofibres as anode materials for direct ethanol fuel cells, ASEM, 2 (2023) 100070. https://doi.org/10.1016/j.asems.2023.100070

241. C Sanna, P Costamagna, P Holtappels, Electrochemical Impedance Spectroscopy of Core-Shell Nanofiber Cathodes, with $Ce_{0.9}Gd_{0.1}O_{1.95}$ (Core) and Cu-Doped $La_{0.6}Sr_{0.4}MnO_3$ (Shell), for Application in Solid Oxide Fuel Cells, ChemElectroChem, 10 (2023) e202300101. https://doi.org/10.1002/celc.202300101

242. H. Jiang, Y. Hu, P. Zhao, Y. Li, K. Zhu, Modulation of protein release from biodegradable core–shell structured fibers prepared by coaxial electrospinning, J Biomed Mater Res B Appl Biomater., 79B(1) (2006) 50-57. https://doi.org/10.1002/jbm.b.30510

243. M. Maleki, M. Latifi, M. A.-Tehran, S. Mathur, Electrospun core–shell nanofibers for drug encapsulation and sustained release, Polymer Engineering & Science, 53(8) (2013) 1770-1779. https://doi.org/10.1002/pen.23426

244. K. Kalwar, W.-X. Sun, D. Li, X.-Ji Zhang, D. Shan, Coaxial electrospinning of polycaprolactone@chitosan: Characterization and silver nanoparticles incorporation for antibacterial activity, React Funct Polym., 107 (2016) 87-92. https://doi.org/10.1016/j.reactfunctpolym.2016.08.010

245. M. Oviedo, Y. Montoya, W. Agudelo, A. G.-García, J. Bustamante, Effect of Molecular Weight and Nanoarchitecture of Chitosan and Polycaprolactone Electrospun Membranes on Physicochemical and Hemocompatible Properties for Possible Wound Dressing, Polymers, 13 (2021) 4320. https://doi.org/10.3390/polym13244320

246. B. Pant, M. Park, S.-J. Park, Drug Delivery Applications of Core-Sheath Nanofibers Prepared by Coaxial Electrospinning: A Review, Pharmaceutics, 11(7) (2019) 305; https://doi.org/10.3390/pharmaceutics11070305

247. J. Li, Y. Liu, H. E. Abdelhakim, Drug Delivery Applications of Coaxial Electrospun Nanofibres in Cancer Therapy, Molecules, 27 (2022) 1803. https://doi.org/10.3390/molecules27061803

248. N. Rajabifar, A. Rostami, S. Afshar, P. Mosallanezhad, P. Zarrintaj, M. Shahrousvand, H. Nazockdast, Wound Dressing with Electrospun Core-Shell Nanofibers: From Material Selection to Synthesis, Polymers, 16 (2024) 2526. https://doi.org/10.3390/polym16172526

249. L. Hou, X. Zhang, P. E. Mikael, L. Lin, W. Dong, Y. Zheng, Trevor John Simmons, Fuming Zhang, Robert J. Linhardt, Biodegradable and Bioactive PCL−PGS Core−Shell Fibers for Tissue Engineering, ACS Omega, 2(10) (2017) 6321–6328. https://doi.org/10.1021/acsomega.7b00460

250. J. C. Silva, R. N. Udangawa, J. Chen, C. D. Mancinelli, F. F. F. Garrudo, P. E. Mikael, J. M. S. Cabral, F. C. Ferreira, R. J. Linhardt, Kartogenin-loaded coaxial PGS/PCL aligned nanofibers for cartilage tissue engineering, Mater. Sci. Eng. C, 107 (2020) 110291. https://doi.org/10.1016/j.msec.2019.110291

251. M. A. Al Fahad, H.-Y. Lee, S. Park, M. Choi, P. C. Shanto, M. Park, S. H. Bae, B.-T. Lee, Small-diameter vascular graft composing of core-shell structured micro-nanofibers loaded with heparin and VEGF for endothelialization and prevention of neointimal hyperplasia, Biomaterials, 306 (2024) 122507. https://doi.org/10.1016/j.biomaterials.2024.122507

252. D. Kharaghani, P. Gitigard, H. Ohtani, K. Oh Kim, S. Ullah, Y. Saito, M. Qamar Khan, I. S. Kim, Design and characterization of dual drug delivery based on in-situ assembled PVA/PAN core-shell nanofibers for wound dressing application. Sci Rep 9 (2019) 12640. https://doi.org/10.1038/s41598-019-49132-x

253. J. Li, T. Zhang, M. Pan, F. Xue, F. Lv, Q. Ke, H. Xu, Nanofiber/hydrogel core–shell scaffolds with three-dimensional multilayer patterned structure for accelerating diabetic wound healing. J Nanobiotechnol 20 (2022) 28. https://doi.org/10.1186/s12951-021-01208-5

254. J. Guo, T. Wang, Z.Yan, D. Ji, J. Li, H. Pan, Preparation and evaluation of dual drug-loaded nanofiber membranes based on coaxial electrostatic spinning technology, Int. J. Pharm., 629 (2022) 122410. https://doi.org/10.1016/j.ijpharm.2022.122410

255. A. J.-N.-Abadi, H. P.-Toroudi, M. Hadjianfar, Z. Mirjafary, R. F.-Majidi, A, Akbarzadeh, Core–shell nanofibers for localized melanoma therapy delivering Pioglitazone nanoemulsions and gemcitabine dual loaded system, Sci Rep 15 (2025) 28401. https://doi.org/10.1038/s41598-025-14483-1

256. P. Mosallanezhad, N. Rajabifar, A. Rostami, Z. Ahmadi, R. Taghdimi, H. Nazockdast, Preparation and structural analyses of antimicrobial core-shell chitosan-polycaprolactone nanofibers for controlled curcumin release, Colloids Surf. A Physicochem. Eng. Asp., 716 (2025) 136736. https://doi.org/10.1016/j.colsurfa.2025.136736

View Article Online
DOI: 10.1039/D5SE01377A

Data Availability Statement

No experimental data was used for the research described in the article.